AD-A162 766 STUDY OF TRANSPORT PROPERTIES AND STRUCTURE OF EXTENDED-CHAIN POLYMERS· D (U) VIRGINIA UNIV CHARLOTTESVILLE DEPT OF MATERIALS SCIENCE R E BARKER ET AL SEP 85 1/2

UNCLASSIFIED F/G 11/9 NL

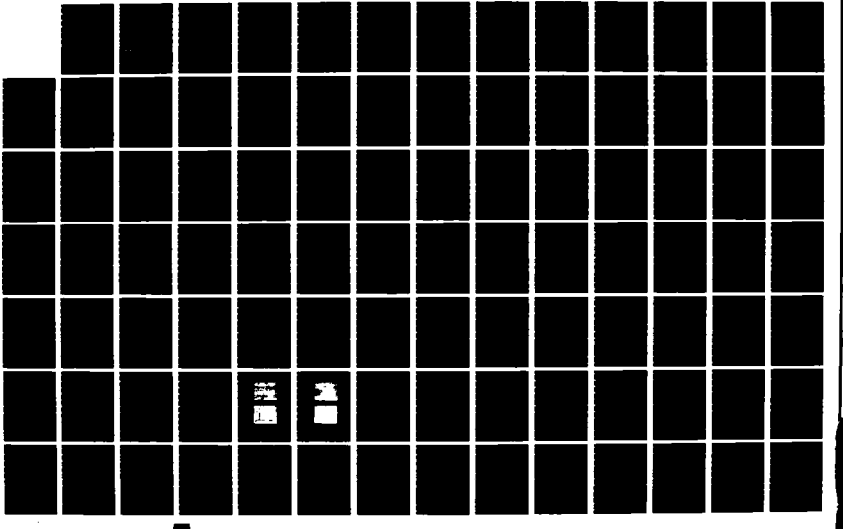

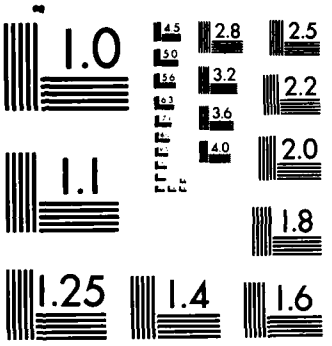

Interim
~~Technical~~ Report

Grant No. 80-0014A,B

STUDY OF TRANSPORT PROPERTIES AND STRUCTURE OF EXTENDED-CHAIN POLYMERS: DIFFUSION AND SOLUBILITY OF GASES

Submitted to:

U.S. Air Force Office of Scientific Research
Bolling Air Force Base
Washington, D.C. 20332-*6448*

Attention: Mr. Donald R. Ulrich
Building 410 NC

Submitted by:

R. E. Barker, Jr.
Professor

W-S. Huang
Research Assistant

Report No. UVA/525631/MS86/101
September 1985

SCHOOL OF ENGINEERING AND APPLIED SCIENCE

DEPARTMENT OF MATERIALS SCIENCE

UNIVERSITY OF VIRGINIA
CHARLOTTESVILLE, VIRGINIA 22901

Interim ~~Technical~~ Report

Grant No. 80-0014A,B

STUDY OF TRANSPORT PROPERTIES AND STRUCTURE OF EXTENDED-CHAIN POLYMERS: DIFFUSION AND SOLUBILITY OF GASES

Submitted to:

U.S. Air Force Office of Scientific Research
Bolling Air Force Base
Washington, D.C. 20332-6448

Attention: Mr. Donald R. Ulrich
Building 410 NC

Submitted by:

R. E. Barker, Jr.
Professor

W-S. Huang
Research Assistant

Department of Materials Science
SCHOOL OF ENGINEERING AND APPLIED SCIENCE
UNIVERSITY OF VIRGINIA
CHARLOTTESVILLE, VIRGINIA

Report No. UVA/525631/MS86/101
September 1985

Copy No. _____

Unclassified
SECURITY CLASSIFICATION OF THIS PAGE (When Data Entered)

REPORT DOCUMENTATION PAGE	READ INSTRUCTIONS BEFORE COMPLETING FORM
1. REPORT NUMBER: AFOSR-TR- 85-1110	2. GOVT ACCESSION NO.: AD-A162 766
	3. RECIPIENT'S CATALOG NUMBER
4. TITLE (and Subtitle): Study of Transport Properties and Structure in Extended Chain Polymers: Diffusion and Solubility of Gases	5. TYPE OF REPORT & PERIOD COVERED: Interim Report 1 Oct 81 - 30 Sep 82
	6. PERFORMING ORG. REPORT NUMBER
7. AUTHOR(s): R. E. Barker, Jr. W-S. Huang	8. CONTRACT OR GRANT NUMBER(s): AFOSR 80-0014
9. PERFORMING ORGANIZATION NAME AND ADDRESS: Department of Materials Science University of Virginia, Thornton Hall Charlottesville, Virginia 22901	10. PROGRAM ELEMENT, PROJECT, TASK AREA & WORK UNIT NUMBERS: 2303/A3 61102F
11. CONTROLLING OFFICE NAME AND ADDRESS: U.S. Air Force Office of Scientific Research Bolling AFB, Washington, D.C. 20332-6448	12. REPORT DATE: September 1985 13. NUMBER OF PAGES: 170
14. MONITORING AGENCY NAME & ADDRESS (if different from Controlling Office)	15. SECURITY CLASS. (of this report): Unclassified 15a. DECLASSIFICATION/DOWNGRADING SCHEDULE

16. DISTRIBUTION STATEMENT (of this Report)

Approved for public release,
distribution unlimited

17. DISTRIBUTION STATEMENT (of the abstract entered in Block 20, if different from Report)

18. SUPPLEMENTARY NOTES

19. KEY WORDS (Continue on reverse side if necessary and identify by block number)

Extended Chain Polymers
Poly Phenylene Benzobisthiazoles (PPBT)
Sorption
Diffusion
Transport Properties
Moisture Permeation

20. ABSTRACT (Continue on reverse side if necessary and identify by block number)

The study of the transport properties in extended chain polymers has added to the understanding of relations between their macroscopic and microscopic properties. There was a need to determine the extent to which a new class of high strength extended chain polymers absorb various vapors and how the vapor moves within the materials, which have a highly anisotropic fibrous morphology. The main polymer
(continued on back)

DD FORM 1 JAN 73 1473 EDITION OF 1 NOV 65 IS OBSOLETE

Unclassified
SECURITY CLASSIFICATION OF THIS PAGE (When Data Entered)

Unclassified

Cont'd

20. ABSTRACT

studied as a representative of the class is poly p-phenylene benzobisthiazole (PPBT). Since PPBT samples were available only in limited quantities as fine fibers (~20 μm in diameter) and thin narrow film (10 ~ 30 μm thick), we developed three techniques for such samples in this work: (1) X-ray energy dispersive analysis; (2) a weighing method with a Cahn electrobalance; and (3) sorption and desorption measurements for a sample suspended on a precision quartz spring in an evacuable chamber. Measurements were sensitive to a few micrograms of mass change. The obtained sorption and desorption curves were non-fickian. Diffusants, such as water, benzene, and ethanol were studied under different temperatures.

An abnormally large heat of sorption (solution) and paradoxical data from two experimental systems with somewhat different conditions are attributed to a large volume fraction of microcavities in PPBT. This hypothesis was shown to be consistent by using the theory of dual sorption. A statistical mechanical model due to diBenedetto was modified to correlate the activation energy with rotation energy and to make possible the prediction of the parallel diffusion coefficient.

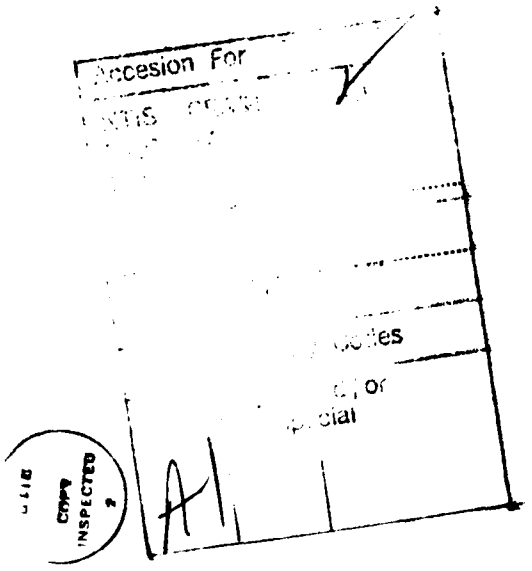

Unclassified

TABLE OF CONTENTS

TABLE OF CONTENTS (Continued)

TABLE OF CONTENTS (Continued)

TABLE OF CONTENTS (Continued)

LIST OF TABLES

LIST OF FIGURES

LIST OF SYMBOLS

A	Area or A Constant Defined by Equation (45)
B	An Effective Chain-Bending Modulus
b	Thickness or Hole Affinity Constant
C	Concentration of Diffusant
C_0, C_1, C_2	Defined by Equation (83), Appendix B
C_d	Ordinary Dissolution
C_f	Final Concentration
C_i	The Initial Internal Concentration
C_j	Concentration of Species j
C_s	Concentration on the Surface
D	Diffusion Coefficient
D_o	Preexponential Factor of Diffusivity
D_d	Diffusion Coefficient of Desorption or Diffusion Coefficient Defined by Equation (45)
D_d'	Diffusivity of Mobile Species in Dual Sorption Theory
D_{eff}	Effective Diffusivity
D_s	Diffusion Coefficient of Sorption
D_x, D_y, D_z	Diffusion Coefficient along X, Y, Z Direction Respectively
$D_{//}$	Parallel Diffusivity
$D_\perp$	Transverse Diffusivity
d	Diameter of Diffusant
d_v	Diffusant Diameter Taken from Gas Viscosity Measurements
E	Activation Energy or Electric Field

E_{ap}	Apparent Activation Energy
E_d	Activation Energy of Diffusion
f	Force
f(z)	Potential Energy per Unit Length of Chain in The Pace-Datyner Model
$\bar{f}_{j,\alpha}$	Average Force of j Species along α Direction
f'	Number of Degrees of Freedom
g	A Geometrical Factor
ΔG^*	Gibbs Activation Free Energy
H_s	Heat (Enthalpy) of Solubility
h	Planck's Constant
ΔH^*	Activation Enthalpy
J	Diffusive Flux Density
J_0	Total Number of Jumps Per Second
J_1	Increased Concentration of Free Molecules in Optical Method
J_2	Flux Going into Trapping Sites between ξ and $\xi + d\xi$ in Optical Method
$J_{j,\alpha}$	Diffusive Flux Density of Species j along X_α direction
j	Current Density
k	Boltzmann's Constant
K_d	Henry's law Solubility Coefficient
$\bar{L}$	The Root Mean Square Displacement ($\bar{L}$) between Jumps of Diffusant
l	Thickness
M_t, M_∞	Mass Uptaken or Loss at Time t, ∞ Respectively
m	A Numerical Factor to Correct for Overlap of Free Volume in Free Volume Theory

m^*	Mass Per Leonard-Jones Center
N	Total Number of Ions in Ionic Conduction
N_A	Avogadro's Number
N_i	The Number of Diffusant Molecules Having Free Volume in the ith Region
n_o	The Concentration of Trapping Sites
n_j	Defined as $C_j N_A$
P	Permeability
P_f	The Probability that f' Degrees of Freedom Will Co-Operate in a Diffusion Step
p	Pressure
p_f	The Final Pressure
p_i	The Initial Pressure
Q_t, Q_∞	The Amount of Diffusant Passing Through a Sheet in Time t, ∞ Respectively
q	Electric Charge of Ions
R	Gas Constant or Resistance or A Constant which Equals bS_h'/kd
r	Crystal Ionic Radius
r_g	Diameter of Diffusant
s	Solubility
S_c	Configurational Entropy
S_h	Hole Saturation Constant
ΔS^*	Activation Entropy
T	Temperature
T_g	Glass Transition Temperature
t	Time

t_o	Time Lag in the Measurement with RG Electrobalance
$t_{1/2}$	Time at $M_t/M_\infty = 1/2$
U	Activation Barriers for Jump Itself
u	Gas Kinetic Velocity
$u_{j,a}$	Speed of j Species along X_a Direction
v	The Effective Volume Per Center
v_a	The Unit Cell Volume in the Activated State
v_f, V_f	Free Volume
v_i	Average Free Volume in ith Region
$\bar{v}_m$	The Mean Molecular Volume over the Temperature Range of Interest
W	The Formation Energy of Sites
α	Mean Value of the Coefficient of Thermal Expansion over the Temperature Range of interest
γ	Activity Coefficient
γ_j	Activity Coefficient of Species j
ε^*	Energy Parameter
λ	Chain Length Per Center Defined by Figure (2) in Molecular Model and one chain in Statistical Mechanical Model
λ'	Jump Distance
ξ	Moving Boundary Defined by Figure (1)
τ	Lag Time in Permeation
ρ_o, ρ_i	Defined as Figure (2)
σ'	The Distance between Centers
σ^*	Distance Parameter
ρ_c^*	Defined by Figure (4)

μ	Chemical Potential
μ_j	Chemical Potential of Species j
$\mu_j^{(0)}$	Chemical Potential of Species j at Absolute Zero Temperature
ν	Thermal Vibration Frequency or Jump Frequency
ϕ	Leonard-Jones 6-12 Potential Function
ϕ_c	Total Interaction Energy Defined by Equation (30)
$\Delta\phi$	An Addition Energy Required to Create a Void, Whose Excess Volume is $2\lambda n(\pi/4)r\hat{g}^2$
ω	Molecular Mobility
ω_j	Molecular Mobility of Species j

Chapter I INTRODUCTION AND LITERATURE SURVEY

A. Introduction

An important development in recent years has been the evolutions of chemical and physical techniques to produce highly ordered polymers. Some of the resulting materials exceed all others in their ratio of tensile strength to density (s/ρ). Because of their potential for applications capitalizing on their large s/ρ value the major portion of research on ordered polymers has dealt with mechanical properties and with methods of synthesis or production. Other subjects, such as transport properties, have received relatively less attention. As pointed out by Barker, Tsai, and Willency,[1] transport properties such as electrical conductivity and the diffusion of various molecular species in polymers not only are of interest in themselves but also provide useful probes to gain a better understanding of the polymer's properties in general. Some of the most recently discovered types of ordered polymers are the extended chain (rigid rod) polymers. The main material studied in this thesis is the trans-isomer of poly (paraphenylene-benzobisthiazole) (PPBT).

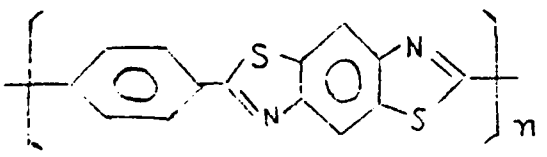

The available PPBT samples were of very small dimensions, (the fibers were only 10 μm - 40 μm in diameter and the films, only 10 μm - 30 μm thick and 6 mm wide). Furthermore, the available samples exhibited considerable internal and external imperfections which may lead to certain difficulties. At this point it is useful to summarize some of the problem areas:

(i) Difficult manipulation due to the small sizes of samples.

(ii) Variable diameter along a fiber and uneven surface and thickness of a film.

(iii) Small total quantity of compounds sorbed by the polymer.

Regarding difficulty (i) the experiments are hard to perform not only because of the small size but also due to a tendency of the samples to fibrilate. Difficulty (ii) will induce experimental error, because diffusion depends strongly on the thickness. Difficulty (iii) requires that the experiments be carried out with highly sensitive instruments.

Since it so ubiquitous and plays such an important role with regard to the electrical properties of polymers, one of the major diffusants studied was water. It exists in the normal atmosphere and affects the properties of PPBT.

The reaction between PPBT and H_2O was assumed to be a protonation effect.[2] From an observed shift of the C=N stretching band in laser Raman spectra from 1481 cm^{-1} (solid) to 1515 cm^{-1} (in methane sulfonic acid (MSA)) the protonation process in MSA was deduced to be expressed by the following equation where P denotes the neutral PPBT chain:

$$P + nCH_3HSO_3 \rightleftarrows H_nP^{n+} + nCH_3SO_3^-.$$

Then for water, the analogous reaction is:

$$P + nH_2O \rightleftarrows H_nP^{n+} + nOH^-.$$

Because of this, moisture affects the electrical conductivity of PPBT in a strong way. This has been extensively studied by D. Y. Chen.[3]

In order to study the diffusion of a given species through PPBT, three methods have been developed: 1. X-ray energy dispersive analysis. 2. Weighing method with a Cahn electrobalance, and 3. Sorption and Desorption for a sample suspended on a quartz spring in an evacuable chamber.

Besides water, ethanol, and benzene also have been studied. Benzene was chosen because its size, shape, and electronic structure relative to these properties of the mer make it of special interest. The polymer has been

studied under different temperatures so that the activation energy E_d, solubility s and the preexponential factor D_0 have been obtained. The data from experiments in the Cahn electrobalance were not consistent with those from experiments using the quartz spring balance. Efforts to resolve this conflict led to the discovery of a useful model based on a distribution of microcavities. A molecular model involving the partial rotation of chain segments has been developed to account for the activation energy. This model is consistent with the chain packing configuration as inferred by X-ray diffraction.

When PPBT was doped using ionic compounds (nitrates and chlorides) to provide trapping sites, the diffusion coefficients of H_2O in doped PPBT vs the charge to radius ratio, q/r of the cations was found to be linear.

Finally, the parallel diffusion in PPBT has been considered from the view points of fibrilar morphology and crystal structure.

For a thorough understanding of the diffusion processes in PPBT, we must be able to represent the mass flow by means of some equations based on different experimental methods and theoretical concepts. The following pages of background discussion will serve this end.

B. Literature Survey

1. Fick's Laws. Approximately a century ago (in 1889) Fick developed a continuum approach to the phenomenon of diffusion which still provides the framework for discussion of the principles.

Assume diffusion only in the +x direction, then consider a thin layer of diffusant between x and x+dx. The number of molecules of diffusant (of type j) per unit volume at any time t is a function only of x. Let $C_j(x,t)$ denote this concentration. The diffusive flux J_j of molecules across a perpendicular plane at x is the net number of molecules of j passing through unit area of the plane in the positive x direction in unit time.

At the molecular level diffusion is a statistical phenomenon which can be related in a useful way to changes in the chemical potential μ_j of the diffusant in the diffusate. The chemical potential may be viewed as the statistical analogy of the potential energy function in classical mechanics. Thus the gradient of μ_j in a given direction x_α corresponds to the average force on a diffusant molecule due to interactions with its molecular surroundings.

$$\bar{f}_{j,\alpha} = - \frac{\partial \mu_j}{\partial x_\alpha} \cdot \frac{1}{N_A} , \quad (\alpha = x,y,z) \qquad (1)$$

The factor of 1/Avogadro's number is included to convert the usual units for chemical potential (J/mol) into energy per molecule, so that $f_{j,\alpha}$ is the α-component of force per molecule of type j. This average force causes a statistical drift of the diffusant with a speed $u_{j,\alpha}$ given by

$$u_{j,\alpha} = \omega_j \bar{f}_{j,\alpha} \tag{2}$$

where ω_j is the molecular mobility of species j. The net diffusive flux density is

$$J_{j,\alpha} = n_j u_{j,\alpha} = n_j \omega_j \bar{f}_{j,\alpha} = -C_j \omega_j (\partial \mu_j / \partial x_\alpha) N_A^{-1} \tag{3}$$

with $C_j = n_j / N_A$ relating the concentration C_j in mol/m^3 to that n_j in $molecules/m^3$. The chemical potential is related to the concentration through the familiar thermodynamical relation

$$\mu_j = \mu_j^o + RT\ln(\gamma_j C_j) \tag{4}$$

from which the usual relation,

$$J_{j,\alpha} = -D_{j,\alpha} (\partial C_j / \partial x_\alpha) \tag{5}$$

Known as Fick's first law is seen to follow as a restricted special case (when the activity coefficient γ_j is not dependent on C_j and when there is no thermal gradient and no interphase boundary).

$$J(x) = -C\omega\frac{\partial u}{\partial x} \quad \text{(omitting the subscript j).} \tag{6}$$

In the absence of chemical reactions, etc. the conservation of component j may be expressed: Accumulation rate = influx rate - outflow rate

$$(Adx)\frac{\partial C}{\partial t} = \frac{A[J(x) - J(x + dx)]dx}{dx}$$

$$\frac{\partial C}{\partial t} = -\frac{\partial J}{\partial x} = \frac{\partial}{\partial x}\left(C\omega\frac{\partial u}{\partial x}\right)$$

$$= C\omega\frac{\partial^2 u}{\partial x^2} + \frac{\partial u}{\partial x}\frac{\partial}{\partial x}(C\omega) \tag{7}$$

or for the conditions appropriate for Fick's first law, we have Fick's second law

$$\frac{\partial C_j}{\partial t} = (\omega_j kT)\frac{\partial^2 C_j}{\partial x^2}, \quad D_j = \omega_j kT \tag{8}$$

2. Experimental Methods.

a. X-Ray Energy dispersive analysis. This method was developed by Barker, Reynolds and Malhotra,[4] and was successfully applied to Hg diffusion in Ag_3Sn Amalgams.

The solution to the on-dimensional diffusion equation for a semi-infinite solid is (Appendix A)

$$C(x,t) = C_s\operatorname{erfc}\left(\frac{x}{\sqrt{4Dt}}\right) + C_i\operatorname{erf}\left(\frac{x}{\sqrt{4Dt}}\right) \tag{9}$$

C_s is the constant concentration on the surface, and C_i is the initial internal concentration. The experimental condition relevant to the present study is $C_i = 0$, then equation (7) becomes

$$C(x,t) = C_s \text{erfc}(x/\sqrt{4Dt})$$

$$= C_s(1 - \text{erf}(x/\sqrt{4Dt})) \tag{9a}$$

Consequently

$$x/\sqrt{4Dt} = \text{erf}^{-1}((C_s - C)/C_s) \tag{9b}$$

where $\text{erf}^{-1}((C_s - C)/C_s)$ denotes the inverse or antierror function. It follows that

$$D = x^2/4t[\text{erf}^{-1}((C_s - C)/C_s)]^2 \tag{9c}$$

If a diffusant were applied to the sample boundary for a time interval t, then, by detecting several concentrations at various distances from the boundary a plot of x vs. $\text{erf}^{-1}(1 - (C/C_s))$ would enable one to compute the diffusion coefficient from the equation:

$$D = (\text{slope})^2/4t \tag{10}$$

b. Time lag (Permeation Method[5,6]). From the instant the diffusant is first admitted to one side of a film and

prior to the establishment of a steady state, both the rate of flow and the concentration at any point within the film vary with time. If the diffusion coefficient is constant, the film is initially completely free of diffusant, and diffusant is continually removed from the low concentration side, the amount of diffusant Q_t which passes through the film of thickness b in time t is given by

$$\frac{Q_t}{AC_2b} = \frac{D}{b^2}t + \frac{1}{6} - \frac{2}{\pi^2}\sum_{\eta=1}^{\infty}\frac{(-1)^\eta}{\eta^2}e^{-D(\frac{\eta\pi}{b})^2 t}. \qquad (11)$$

As $t \to \infty$, the steady state is approached and the exponential terms become negligibly small, so that the graph of Q_t against t tends to the line

$$Q_t/A = (DC_2/b)(t - b^2/6D) \qquad (11a)$$

which has an intercept τ, on the t-axis, given by

$$\tau = b^2/6D. \qquad (12)$$

Therefore

$$D = b^2/6\tau. \qquad (13)$$

The mathematical details are shown in Appendix B.

c. Sorption and Desorption Method.[5] If the concentration just within the surface of a film exposed to

diffusant is maintained constant, then the amount of diffusant M_t, taken up by the film of thickness b in a time t, is given by the equation

$$M_t/M_\infty = 1 - \frac{8}{\pi^2} \sum_{n=0}^{\infty} \frac{1}{(2n+1)^2} \exp[-\frac{D(2n+1)^2\pi^2 t}{b^2}] \qquad (14)$$

Appendix C provides the details.

M_∞ is the equilibrium sorption attained theoretically after infinite time. Assume $t_{1/2}$ is the time at $M_t/M_\infty = 1/2$, the above equation can be written as

$$t_{1/2}/b^2 = -\frac{1}{\pi^2 D} \ln\{\frac{\pi^2}{16} - \frac{1}{9}(\frac{\pi^2}{16})^9\} \qquad (15)$$

Thus, we have

$$D = 0.04919\ b^2/t_{1/2}. \qquad (16)$$

The time $t_{1/2}$ can be found experimentally and thus D can be calculated. Another form of equation (14) is

$$M_t/M_\infty = 4(Dt/b^2)^{1/2}(1/\pi^{1/2} + 2\sum_{n=0}^{\infty}(-1)^n \text{ierfc}(nb/2(Dt)^{1/2})) \qquad (17)$$

where

$$\text{ierf}(nb/2(Dt)^{1/2}) = (1/\sqrt{\pi})e^{-n^2b^2/4Dt} - (nb/2(Dt)^{1/2})\text{erfc}(nb/2(Dt)^{1/2}) \qquad (18)$$

The value of D can be deduced from an observation of the initial gradient of a graph of M_t/M_∞ as a function of $(t/b^2)^{\frac{1}{2}}$.

This kind of analysis has been used by Garrett and Park (1967) (Garrett, 1965)[7] for kinetic and equilibrium sorption measurements. Others, for example Baughan,[8] and Carpenter and Twiss[9] were also working on these kind of methods.

The equations given above are for films. The same approach has been applied to fibers and spherical particles. For fibers the diffusion coefficient D was determined from the slope of the linear relationship obtained when plotting $(M_t/M_\infty)^{\frac{1}{2}}$ against t using the following equation

$$D = (\pi r^2/16t)(M_t/M_\infty)^{\frac{1}{2}} \qquad (19)$$

d. An Optical Method.[10] This method was applied to diffusion in which the diffusant made a visible border in polymers. There are two known situations in which sharp borders occur. The first is the most widely known. Namely swelling of the polymer by the diffusant creates an advancing zone between the swollen phase and the unswollen phase. To get such an effect $D_{swollen} > D_{unswollen}$. The second situation occurs when there are colored trapping sites which change color or refractive index when a diffusant molecule

is trapped. J. J. Hermans[11] proposed a mechanism in which the boundary line indicates the abrupt change from "all holes filled" to all holes empty. Figure (1) gives diagramatic representation to the situation.

Barker[10] used this idea and derived an equation that is very practical. He assumed the shaded area in Figure 1.b. has approximately the area of a triangle, then from equation

$$\bar{J} = J_1 + J_2$$

He obtained the equation

$$-D\partial C/\partial x \cong n_0(d\xi/dt) + (C_s/2)(d\xi/dt) \cong DC_s/\xi \qquad (20)$$

Here, $\bar{J}$ is the amount of diffusant entering the polymer in unit time. J_1 corresponds to the increased concentration of free molecules, J_2 represents the flux going into traps between ξ and $\xi+d\xi$, and n_0 is the concentration of traps. The concentration maintained just inside the surface of the polymer is denoted by C_s.

If C_s and n_0 are constants

$$D \cong (\xi^2/2t)(n_0/C_s + \tfrac{1}{2}) \qquad (21)$$

later on, Barker found from experiments for O_2 diffusion in polycarbonate that better agreement is obtained by replacing the $\frac{1}{2}$ by 0.32.

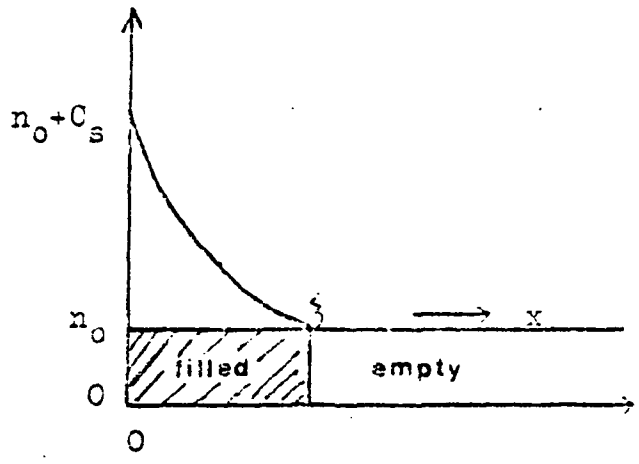

(a) Diffusion of particles which are trapped in non-diffusible holes

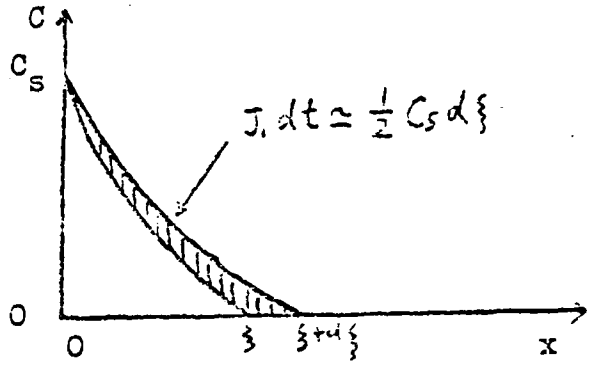

(b) Untrapped scavenger concentration

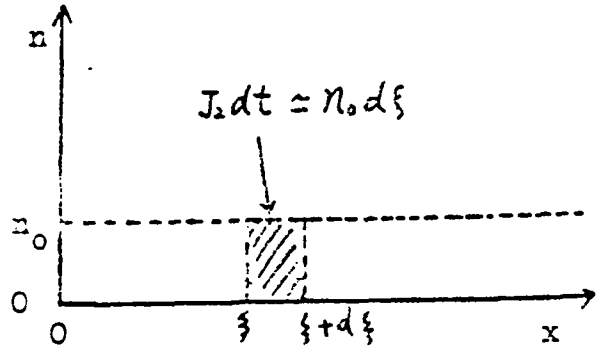

(c) Concentration of trapping sites

Fig.1 Schematic representation of the concentrations of diffusant and trapping radicals.[10]

e. Other Methods. Certain other methods can detect concentrations at a particular distance from a boundary, for example certain refractive index techniques, radiation absorption methods (spectrophotometric methods),[12] etc. According to the equation

$$C(x,t) = (C_s/(\pi Dt)^{\frac{1}{2}})\exp(-x^2/4Dt) \qquad (22)$$

which represents the concentration profile at time t subsequent to an initial highly localized concentration on a planar interface. On plotting $\log C(x,t)$ vs. x^2, a straight line having the slope $1/(4Dt)$ should be obtained from which D may be calculated if t is known.

3. Some Other Effects Related to Diffusion.

a. Relations between D, s, and P. The diffusive transport through homogeneous, nonporous polymer membranes was quite generally treated as if the membrane were ideal so that the flow could be described by Fick's laws based on the concentration of the permeant. In such a case the current density J through the membrane is the product of the negative concentration gradient and the diffusion coefficient (Fick's first law of diffusion)

$$J = -D\partial C/\partial x$$

In a planar membrane of uniform material properties, the steady state concentration gradient is constant so that the flux per unit area of the membrane is given by

$$J = -D\Delta C/\Delta x = D(C_1 - C_2)/b. \tag{23}$$

where the membrane has a thickness b which is uniform and D is independent of C. The subscript 1 relates to the upstream and the subscript 2 to the downstream boundary of the membrane.

In case of an "ideal gas-membrane pair" one has the simple relationship for an isothermal sorption process

$$C = sp \tag{24}$$

which defines s and which is just Henry's law if s, the sorption coefficient, is a constant independent of pressure p, then from equation (23),

$$J = -Ds\Delta p/\Delta x = Ds(p_1 - p_2)/b = -P\Delta p/\Delta x \tag{25}$$

so that the constant permeability coefficient is given by

$$P = Ds, \tag{26}$$

although there usually is an extra constant factor to handle various mixtures of unit systems.

b. Concentration Dependent Diffusion Coefficients. Usually organic vapor diffusion is concentration-dependent. Crank introduced a mean value $\bar{D}$, which is the average of the diffusion coefficients for a number of different surface concentrations. Calculations have shown that for any one experiment, $\bar{D}$ provides a reasonable approximation to

$$1/C_f \int_0^{C_f} D \, dC \tag{27}$$

where 0 to C_f is the concentration range existing in the sheet during that experiment.[13] If D_s is calculated from the initial gradient for sorption and D_d from the gradient for desorption, then $\frac{1}{2}(D_s + D_d)$ is a better approximation to

$$(1/C_f) \int_0^{C_f} D \, dC$$

c. Temperature Effect. Under ideal conditions, diffusion follows the Arrhenius equation

$$D = D_0 e^{-E_d/kT} \tag{28}$$

over sufficiently restricted temperature ranges. The pre-exponential factor D_0 includes entropic terms.

d. Gas or Vapor Properties that Affect Diffusion. Usually, larger gas molecules need larger holes in the polymer for diffusion to proceed. Accordingly, the smaller the molecules are, the smaller the activation energy will be and

consequently the larger the diffusivity will be. If the molecular size is large, the effects of molecular shape and flexibility become important. Branched compounds usually have much lower values of E_d than nonbranched compounds of the same size.[14-17]

e. Nature of the Polymer. From the hole theory of diffusion, the rate of diffusion depends on (a) the number and size distribution of pre-existing holes, and (b) the ease of hole formation. It is physically obvious that increased crystallinity will reduce D. Also, if cross linking increases, the diffusion constant decreases and the activation energy of diffusion will increase. It is also relevant to mention that both of these processes would be expected to decrease the configurational entropy of the polymer S_c and that the correlated decreases in D would be qualitatively consistent with Barker's entropy correlation theory,[18] according to which any structural change which reduces the configurational entropy S_c of a complex molecular system (the polymer) will lead to an approximately equal increase in the activation entropy ΔS^* for structurally controlled rate processes. The addition of plasticizer to a polymer decreases the cohesive forces between the chains, resulting in an increase in segmental mobility. It is clear that the rate of diffusion will increase when plasticizer is present.

f. Glass Transition Temperature. Most of the polymers show a sharp change of Arrhenius slope at their glass transition temperatures. Above the glass temperature there is a greatly increased segmental mobility allowing for a larger zone of activation, leading to the observed increases in both energy and entropy of activation.[19] Often, below the glass temperature diffusion becomes anomalous. Sorption curves may show Non-Fickian character. D may show time and thickness dependence.

g. Fickian Characteristics. The mathematical solution mentioned in section I.B.2.c. (Sorption and Desorption Method) in this thesis is based on Fick's law. Sorption curves having characteristics expected from the specified solutions are customarily called Fickian (or normal) type sorption. The following is a summary of important Fickian sorption features that have been made available by the mathematical studies of Crank and associates.

(a) Both absorption and desorption curves are linear in the initial stage. For absorption, the linear region extends to over 60% or more of M_∞, where (M_∞ / M_O) is the amount of vapor absorbed per gram of dry polymer until the sorption equilibrium is reached. For D(C) increasing with C the absorption curve is linear almost up to the final sorption equilibrium.

(b) Above the linear portions both absorption and desorption curves are concave toward the abscissa axis, irrespective of the form of D(C).

(c) When the initial concentration C_i and the final concentration C_f are fixed, a series of absorption curves for films of different thicknesses are superposable to a single curve if each curve is replotted in the form of a reduced curve, i.e. (M_t/M_o) is plotted against $t^{\frac{1}{2}}/b$. This also applies to the corresponding series of desorption curves.

(d) The reduced absorption curve so obtained always lies above the corresponding reduced desorption curve if D is an increasing function of C between C_i and C_f. Both reduced curves coincide over the entire range of t when D is constant in this concentration interval. The divergence of the two curves becomes more marked as D increases more strongly with C in the concentration range considered.

(e) For absorptions from a fixed C_i to different C_f's, the initial slope of the reduced curve becomes larger as the concentration increment C_f-C_i becomes larger, provided that D increases monotonocally with C in the range considered. This also applies to the reduced desorption curves which start from different C_i's to a fixed C_f.

Chapter II THEORIES

In this chapter a number of theories, which have been considered in the analysis of the experiments, are outlined. Although each of the theories discussed provides some useful qualitative insights, a self-consistent combination of the theories (mainly the DiBenedetto-Paul theory and the dual sorption theory) has been adopted for quantitative use with the data. It also should be mentioned that there is considerable overlap of the concepts in the various theoretical models.

A. Molecular and Statistical Mechanical Models

1. Molecular Model. DiBenedetto and Paul[20] assumed the sorbed gas in an ordered region of a polymer is contained within a cell composed of four parallel segments containing n structural units per segment. The activation energy for diffusion is related to the variation in the average potential energy of a molecular interaction which accompanies a volume change of $\lambda n(\pi/4)r_g^2$, where r_g is the diameter of diffusant and λ is defined in Fig. 2. First they applied the Leonard-Jones 6-12(Mie) potential function

$$\phi = \epsilon^*[(\rho^*/\rho')^{12} - 2(\rho^*/\rho')^6] \qquad (29)$$

to this system using a model in which a single center

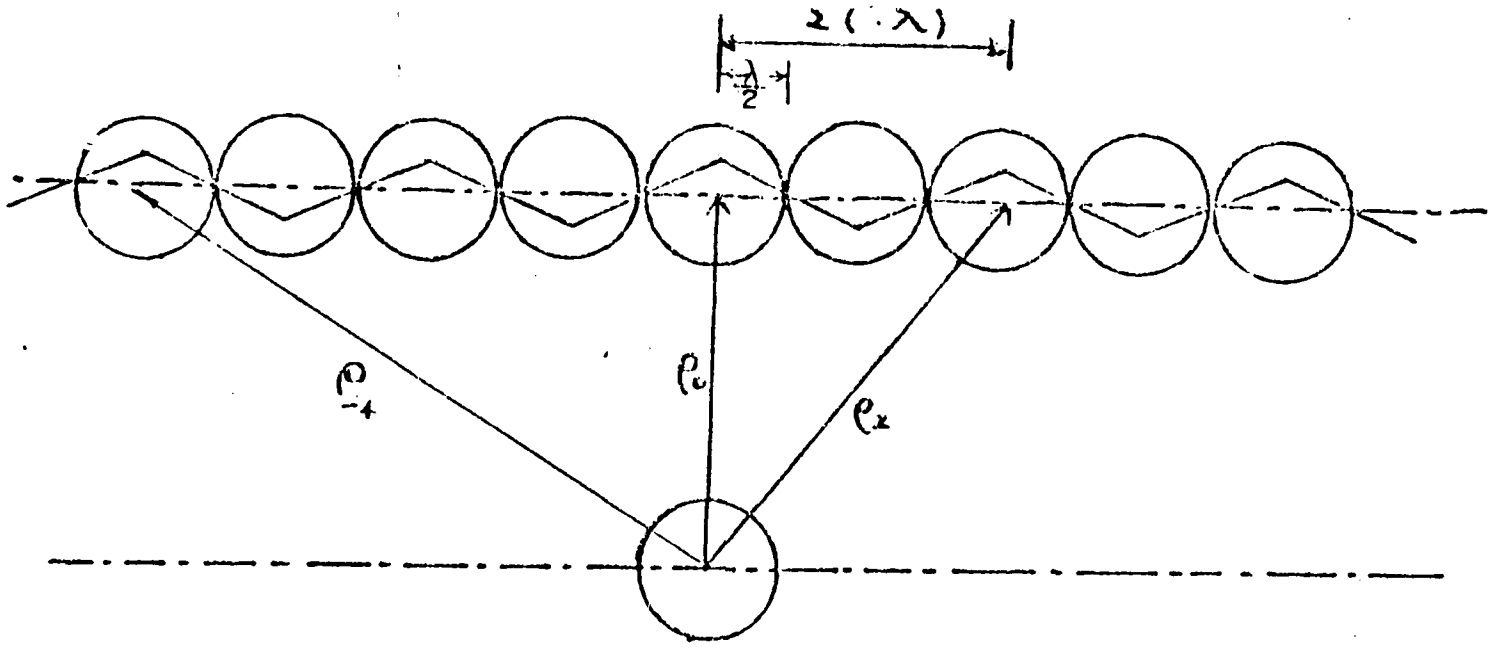

Fig. 2 Model for chain interaction.[20]

interacts with its neighboring chain of 21 centers (arbitrary) to give the total interaction energy ϕ_c as below

$$\phi_c = \varepsilon^* \sum_{i=-10}^{10} [(\rho^*/\rho_i')^{12} - 2(\rho^*/\rho_i')^6] \tag{30}$$

where ε^* and ρ^* are energy and distance parameters respectively; and ρ' is the distance between centers.

Figure (2) gives

$$\rho_i^2 = \rho_o^2 + i^2(\lambda)^2, \quad i = (0,\pm1,\pm2,\ldots) \tag{31}$$

where λ is again the chain length per center (twice the value of λ in ref. 20) and ρ_o is the nearest neighbor distance. Substitution into equation (30) gives

$$\phi_c = \varepsilon^*[C(\rho^*/\rho_o')^{12} - 2D(\rho^*/\rho_o')^6] \tag{32}$$

where

$$C = 1 + 2 \sum_{i=1}^{i=10} [1 + i^2(\lambda/\rho_o')^2]^{-6}$$

$$D = 1 + 2 \sum_{i=1}^{i=10} [1 + i^2(\lambda/\rho_o')^2]^{-3}$$

Now

$$\phi_c = (\varepsilon^*/\lambda)[0.77(v^*/v)^{11/2} - 2.32(v^*/v)^{5/2}], \tag{33}$$

where $v = \lambda(\rho_o')^2$ is the effective volume per center, which

came from the assumption that each center is constrained to move in plane perpendicular to the chain axis and $v^* = \lambda\rho^{*2}$.

Diffusion is assumed to occur when an extra volume of $\lambda n(\pi/4)r_g^2$ added to the normal effective volume nv.

$$nv_a = \lambda n(\pi/4)r_g^2 + nv. \tag{34}$$

The activation energy is given by

$$\Delta E_d = N_A(\Delta\phi). \tag{35}$$

with $\Delta\phi$ equal to four times the change in Eq. 33 corresponding to the volume change. Equation (33) is multiplied by 4 because of the interaction between four segments of this hypothetical cell. The final result of DiBenedetto and Paul is

$$\Delta E_d = (4nN_A\varepsilon^*/\lambda) \cdot \rho^*\{0.77[(\frac{v^*}{v_a})^{11/2} - (\frac{v^*}{v})^{11/2}] - 2.32[(\frac{v^*}{v_a})^{5/2} - (\frac{v^*}{v})^{5/2}]\} \tag{36}$$

2. Statistical Mechanical Model. Pace and Datyner[21,22] used the same assumption as DiBenedetto and Paul. See Figure (3). An average chain co-ordination number of 4 is assumed rather than 6 as for crystalline closest packing of rods. The diffusant molecules may move either (a) by sliding longitudinally down the x-axis parallel to the

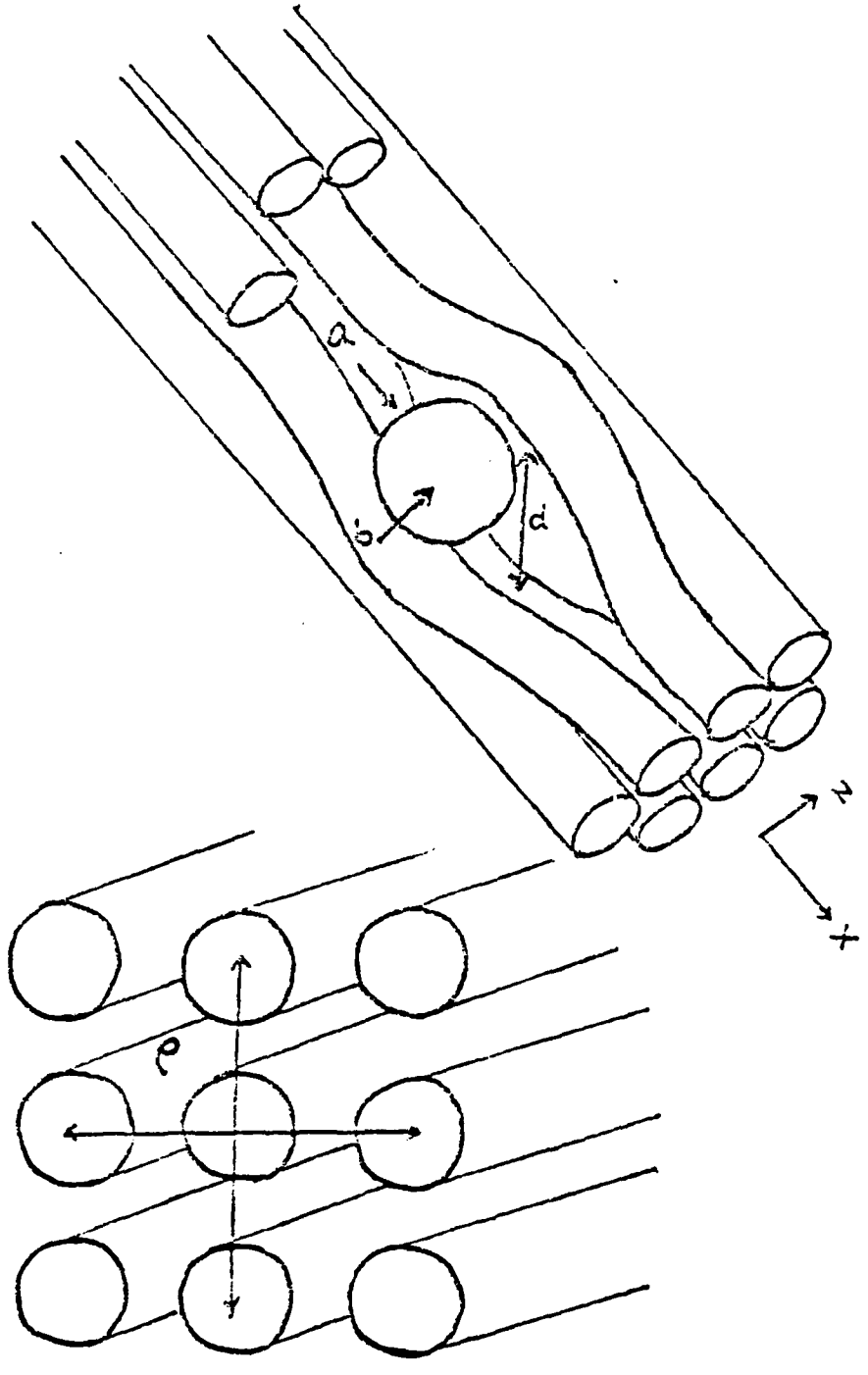

Fig. 3 (a) Proposed polymer microstructure with locally parallel chains and 4 coordination. (b) Possible motions of a spherical penetrant relative to this local structure.[21]

interstitial "channels" of a chain bundle or (b) by "jumping" at right angles to this direction when adjacent chains are sufficiently separated. One may readily show that process (a) is generally much faster than process (b) and so the penetrant proceeds until a barrier (entanglment, crystallite, etc.) is reached whose penetration requires more energy than chain separation. Process (b) is then rate determining and gives rise to the observed activation energy of diffusion and jump frequency. Process (a) establishes the root mean square displacement ($\bar{L}$) between jumps.

Pace and Datyner used a modified form of the equation from DiBenedetto

$$f(z) = (\epsilon^* \rho^* / \lambda^2)(0.77(\rho^*/z)^{11} - 2.32(\rho^*/z)^5) \qquad (37)$$

This equation is like equation (33) except for an extra division by λ, the spacing between attractive centers, so that $f(z)$ is the potential energy per unit length of a chain.

Neglecting the possibility of segmental "flips" and assuming that chain bending is distributed over a number of backbone bonds, one may show that the minimum energy, ΔE, necessary to produce a separation, d, between adjacent chains (neglecting any other elastic distortion of the environment) is given to good approximation by

$$\Delta E = \min \int_{-\infty}^{\infty} (f(z) + (B/2)(d^2z/dx^2)^2 - f(\rho)dx \qquad (38)$$

subject to

$$z = \rho^* + d \qquad \text{at } x = 0$$
$$z = \rho \qquad \text{at } x = \pm\infty \tag{39}$$

The second term in the integrand gives the intramolecular (chain-bending) energy and x measures distance along the chains. B is an effective chain-bending module and is estimated from the polymer backbone geometry and the shape of the bond rotation potential minima. By a suitable linearizing approximation, one may solve equation (38) to give

$$E = 5.23\left(\frac{B}{d'}\right)^{1/4}\left(\frac{\varepsilon^* \rho^*}{\lambda^2}\right)^{3/4}\{0.077[\left(\frac{\rho^*}{\rho}\right)^{11}(\rho - 10d') - \rho^*\left(\frac{\rho^*}{\rho^* + d}\right)^{10}] - 0.58[\left(\frac{\rho^*}{\rho}\right)^{5}(\rho - 4d') - \rho^*\left(\frac{\rho^*}{\rho^* + d}\right)^{4}]\}^{3/4} \tag{40}$$

$$d' = d + \rho^* - \rho \tag{41}$$

Pace and Datyner assume, both above and below T_g, that thermal expansion occurs by a uniform average increase in interchain spacing. Therefore, neglecting expansion along the chain one has (since $\rho^*/\rho \simeq 1.0$)

$$(d/dT)(\rho^*/\rho) \simeq -\tfrac{1}{2}\alpha_v$$

$$(d/dT)\rho \simeq \tfrac{1}{2}\rho^*\alpha_v$$

Where α_v is the thermal expansion of the polymer. Then the apparent activation energy, ΔE_{app}, as would be obtained from the Arrhenius plot, is constant.

ΔE_{app} is given by

$$\Delta E_{app} = [(\Delta E(T_1)/T_1) - (\Delta E(T_2)/T_2)]/(1/T_1 - 1/T_2) \qquad (43)$$

where T_1 and T_2 are the upper and lower temperature limits of the interval.

One may then write for the diffusion coefficient D_d, of a simple penetrant of diameter d

$$D_d = (1/6)\bar{L}^2 A \exp(-\Delta E/RT)\,cm^2 s^{-1} \qquad (44)$$

where A is given approximately by

$$A \simeq (1/\lambda^2)(\varepsilon^*/\rho^*)^{5/4}(\sqrt{B}/m^*)^{1/2} d'/$$

$$(d\Delta E/dd')X(5.46 \times 10^{-3})s^{-1} \qquad (45)$$

m^* is the mass per L-J center (daltons), length units are nm, and energy units J/mol, d equals d_v (taken from gas viscosity measurements).

For polymer chains, such as those indicated in Fig. 4, bulky side groups, d is given by $d = d_v - (\rho^* - \rho_c^*)$.

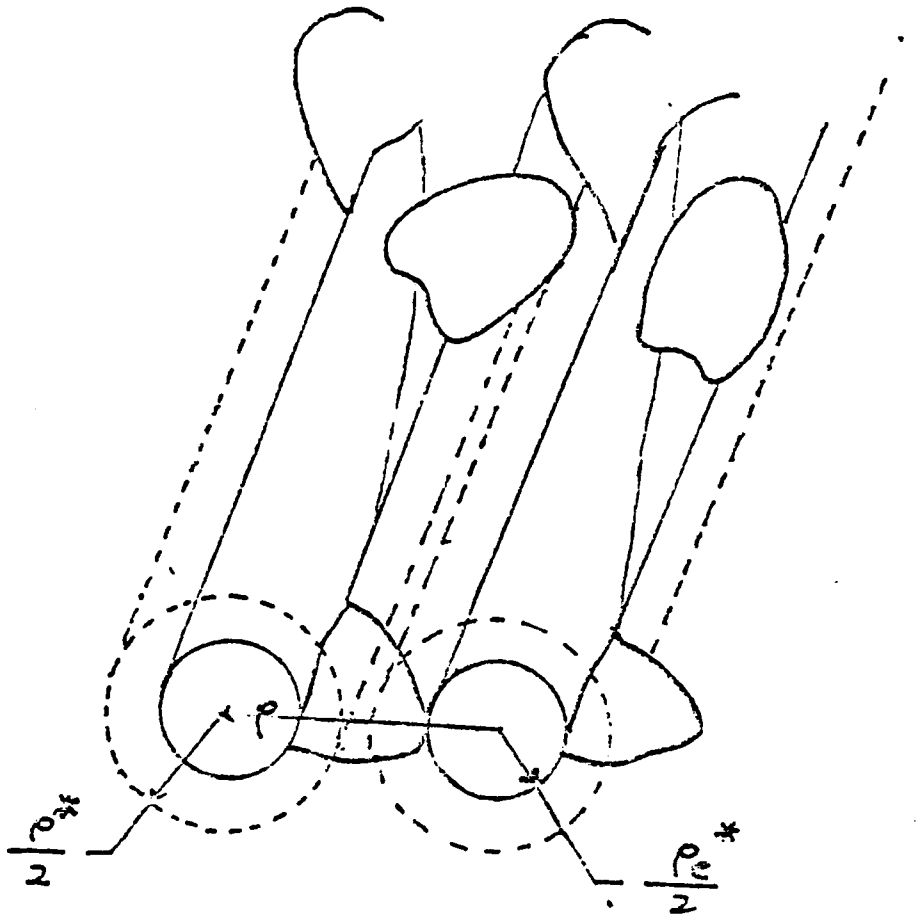

Fig. 4 Diagramatic view of two hypothetical closely packed helical polymer chains that possess closely spaced, bulky side groups. The solid cylinders define the effective outer surface of the chain "cores"; the dashed cylinders are defined by the average Leonard-Jones parameter ρ^*. There is considerable free space within the structure.[22]

Equation (40) is the minimum energy to separate two chains by an amount d, as determined by their stiffness and mutual attraction, and neglects any displacement of compression of the environment. It is therefore a lower bound for the true activation energy. The expression contains no adjustable parameters but $\bar{L}^2$ in equation (44) is not predictable within the limits of the present theory.

B. Free Volume Theory

Cohen and Turnbull[23] treated diffusion as translation of a molecule across the void within its cage. In other words, diffusion is a result of redistribution of the free volume within the polymer and to some extent the diffusant is carried along as the cage moves.

The free volume of a given diffusant molecule is defined as the volume within its cage less the volume of the molecule. Let the total free volume V_f be divided into i small regions or packets; each molecule in the ith region has an average free volume v_i. N_i is the number of diffusant molecules having free volume in the ith region.

In order to correct for overlap of free volume, a numerical factor m is introduced to give

$$m \sum_i N_i v_i = V_f \qquad (46)$$

The value of m should lie between ½ and 1. The average free volume v_f is given by $v_f = V_f/N$ and the distribution function P(v') is

$$P(v') = (m/v_f)\exp(-mv'/v_f). \tag{47}$$

The probability of finding a hole of volume v^* or larger is

$$P(v^*) = \int_{v^*}^{\infty} P(v')dv' = \exp(-mv^*/v_f) \tag{48}$$

Cohen and Turnbull assumed a molecule moved translationally across the void within its cage with gas kinetic velocity u. The distribution of this molecule to the diffusion coefficient is

$$D(v) = ga(v')u \qquad \text{for } v' > v^* \tag{49}$$

where a(v') is roughly the diameter of the cage and g is a geometrical factor. The average diffusion coefficient is

$$D = \int_{v^*}^{\infty} D(v')P(v')dv' = ga^*u\exp(-mv^*/v_f) \tag{50}$$

where a^* equals approximately the molecular diameter.

It is then further assumed that the free volume v_f may be expressed by an approximate expression

$$v_f = \alpha\bar{v}_m(T - T_0) \tag{51}$$

where T_o is the temperature at which the free volume disappears α and $\bar{v}_m$ are the mean values of the coefficient of thermal expansion and the molecular volume over the temperature range of interest, respectively, substitution of equation (51) into equation (50) gives

$$D = ga^*u\exp(-mv^*/\alpha\bar{v}_m(T - T_o)) \qquad (52)$$

C. Barrer's Zone Theory

Barrer[24] based his theory on the idea that a diffusing molecule moves to successive positions as segments of the surrounding polymer chains fluctuate in an activated zone within which the activation energy is distributed through many degrees of freedom. The expression for the diffusion coefficient is

$$D = (\nu/2)\lambda'^2 \sum_{f=1}^{f'max} P_f[(E/RT)^{f-1}(1/(f'-1)!)]\exp(-E/RT) \qquad (53)$$

where ν is the thermal vibration frequency of the penetrant molecule. λ' is the jump distance, f' is the number of degrees of freedom involved in a particular movement, f'max is the value of f' for which the expression in the square bracket has a maximum, E is the total energy of 1 mole of the activated zones under consideration, and P_f is the probability that the f' degrees of freedom will co-operate in a diffusion step. The complete expression in the square

brackets is the probability that the energy E is distributed over f' degrees of freedom.

D. Transition State Theory (Absolute Rate Theory)

Eyring[25] proposed a model that the molecule vibrating within an energy well had a tendency occasionally to jump over an energy barrier to the new energy well, causing diffusion to occur.

The expression for D is given by

$$D = g\lambda'^2 (kT/h) e^{\Delta S^*/R_e - \Delta H^*/RT} \qquad (54)$$

where ΔS^* and ΔH^* are activation entropy and activation enthalpy respectively, λ' is jump distance, k the Boltzmann constant, h Planck's constant, and g represents a geometrical parameter which reflects the dimensionality of the diffusion process. For isotropic diffusion in three dimensions, g = 1/6.

The rate of jumping $(kT/h)e^{\Delta S^*/R_e - \Delta H^*/RT}$ is given by the product of the attempt frequence kT/h and the probability per attempt of hopping over the potential barrier, $e^{-\Delta G^*/RT}$.

In more recent variants of the rate theory, the jumping probability is enhanced by quantum tunneling through the barriers.

E. Dual Sorption Theory

Wolf R. Vieth and Mary A. Amini[26] formulated the "dual sorption theory" to explain certain classes of negative and positive deviations from Henry's law which are frequently observed in sorption plots of penetrants in polymers. The dual modes are either that the penetrant molecule is normally dissolved and free to diffuse or that it is immobilized, as in a sink or well. It is the second process which gives rise to deviations from normal behavior.

1. Negative Deviation From Henry's Law. The negative deviations can be associated with site binding and low penetrant levels, where some of the penetrant molecules are immobilized on sites or in sinks in the matrix. This would be characteristic of a glassy polymer.

The over all concentration of sorbed vapor can be written as the sum of two terms:

$$C = C_d + S_h \tag{55}$$

where C_d represents ordinary dissolution and S represents sorption in the microcavities or holes (S_h), Vieth and Amini explained the sorption behavior by using a model based on Henry's law and the Langmuir isotherm,

$$C_d = K_d p \qquad \text{(Henry's Law)} \tag{56}$$

$$S_h = S_h' bp/(1 + bp) \qquad \text{(Langmuir Isotherm)} \qquad (57)$$

where S_h' = the hole saturation constant

b = the hole affinity constant

At low pressures, where $bp << 1$, the sorption isotherm tends to linearity

$$C = (K_d + bS_h')p \qquad (58)$$

In the limit of high pressures, where $bp >> 1$, the solubility in the holes reaches the saturation limit, S_h'. Therefore, the isotherm should once again become linear

$$C = K_d p + S_h' \qquad (59)$$

Thus, a plot of C versus p will have two linear regions with a connecting nonlinear region. Vieth and Amini applied these relations to diffusion. To analyze the diffusion process for dual mode sorption, a more complex model is necessary. A differential mass balance is performed for penetrant diffusing across a flat film. One term (left term in equation 60) allows for the rate of accumulation by simple dissolution; the other (right term in equation 60) for the fact that the film is also entrapping an amount of the penetrant and holding it. The result is a modification of Fick's law.

$$D\frac{\partial^2 C}{\partial x^2} = \frac{\partial}{\partial t}\,(S_h + C_d) \tag{60}$$

For sorption of a gas in a glassy polymer the equilibrium partial pressure of the gas at any position in the film is the same for both types of sorption. By equating the pressure from the two formulations, a relationship is found between the concentrations of the bound and the free species.

$$S_h = [(S_h'b/K_d)C_d]/[1 + (b/K_d)C_d] \tag{61}$$

Substituting this expression for S_h into equation (60) yields the diffusion equation for dual mode sorption.

$$D\frac{\partial^2 C_d}{\partial x^2} = \frac{\partial C_d}{\partial t}\left[1 + \frac{S_h'(b/K_d)}{(1 + (b/K_d)C_d)^2}\right] \tag{62}$$

At low pressures equation (61) reduces to a linear relationship between S_h and C_d.

$$S_h = RC_d \tag{63}$$

where

$$R = bS_h'/K_d \tag{64}$$

The diffusion equation can be expressed in a modified form of Fick's law, where an effective diffusivity is defined.

$$D_{eff}\frac{\partial^2 C}{\partial x^2} = \frac{\partial C}{\partial t} \tag{65}$$

where D_{eff} = the effective diffusivity

$$= D/(1 + R) \tag{66}$$

The measured diffusion coefficient is less than the true diffusion coefficient; that is, the attainment of sorption equilibrium is slowed down by the immobilization process.

At higher pressure, the partial differential equation for diffusion is nonlinear. Numerical solutions can be found for the equation by using finite difference techniques.

For normal sorption processes occurring in finite baths of penetrant, the dimensionless pressure decay, is a simple function of the square root of dimensionless time θ

$$\theta = Dt/L^2 \tag{67}$$

where 2L = the thickness of membrane

$$\phi = (p_i - p)/(p_i - p_f) \tag{68}$$

where p_i = the initial pressure

p_f = the final pressure

The pressure decay is plotted versus the square root of

$$\theta' = \theta(1 + (S_h'b/K_d)/(1 + bp)^2)^{-1}. \tag{69}$$

Vieth and Amini found three numerical solutions by varying the sorption parameters, b, S_h', and K_d over a wide range. Expressed graphically all of the data were correlated within a narrow band. Therefore, the mean of the band was taken as the correlation.

2. Positive Deviation From Henry's Law. In this case, the polymer network swells to expose more sites, increasing the sorption level synergistically. Now, the site density is not constant when swelling occurs; it changes with the extent of sorption. A clustering phenomenon displays a significant deviation from Henry's law, which predicts no cluster formulation at all. A more detailed discussion of this point is not appropriate in this thesis.

The result is

$$D_{eff} = [D_d'/(1 + R)](1 + (\partial \ln\gamma/\partial \ln C))^{-1} \qquad (70)$$

In this case, the true diffusion coefficient is modified by two factors; one for the second mode of sorption which reduces it, and another for network swelling, which increases it.

F. Barker's Entropy Correlation Theory[18]

The central point of the theory is that in a structurally complex system undergoing a thermally activated

rate process, any organizing influence which produces a reduction $-\Delta S_c$ in the configurational entropy will be accompanied by a correlated increase $\Delta(\Delta S^*)$ in the activation entropy associated with the rate process. Thus,

$$\Delta(\Delta S^*) = -\Delta S_c \tag{71}$$

$$\Delta S^*_{final} = \Delta S^*_{initial} - \Delta S_c. \tag{72}$$

The experimental support for this theory was obtained by studying permeation of various gases in a series of oriented polyalkyl methacrylates. The conclusions drawn were that in a noncrystalline polymer, when the configurational entropy S_c is reduced by an ordering process such as stretching, an additional amount of local disorder must occur in the neighborhood of a diffusing molecule before a unit diffusional step can occur, so that the decrease in the configurational entropy is equal to the increase in the activation entropy for diffusion. It may be seen that this theory is in at least qualitative agreement with many other facts. For example, crystallization reduces the configurational entropy so that one would expect a large increase in the activation entropy and also a large increase in the activation energy. The competition between these two effects appears to be such that without the entropy

correlation, the value of D would be much more strongly reduced than it actually is.

C. Ionic Conduction in Polymers*

In a given polymer system, it should be considered that electrical conduction may be due to the movement of any of the following types of charge carriers: electrons, holes, protons, bare elemental ions, molecular ions, and solvated or hydrated ions. From the viewpoint of diffusion experiments, ionic conduction should play the most important role in this sort of study. Barker's "Local Structure Hypothesis"[27] provides a useful concept to approach the problem. The idea is that the actual concentration of ions needed to provide a typical level of conductivity (σ) is quite small compared to the number of mers present in the same volume and furthermore, that the electric field near a given ion is very large, so that a measurement of σ proves a small volume fraction of the sample in regions that may be atypical due to the presence of the ions.

The ionic conductivity of polymers can originate either from ionically dissociable groups in the pure polymer or from the dissociation of an ionic impurity in the polymer. The latter case is much more common. Water plays an

---

*The close collaboration of D. Y. Chen in this section is gratefully acknowledged.

important role in conduction in polymers according to Barker and Sharbaugh's "Weak Electrolyte Model."[28] The existing ionic impurity will be only partially dissociated as a weak electrolyte into anions and cations due to the presence of water. The pure water itself will also provide H^+ and OH^- (or H_3O^+) ions. These dissociated ionic species will move toward the electrodes when an external electric field is applied. The process gives an electrical conduction current.

One approach used to deal with the problem of electrical current due to ionic diffusion is the concept of an activation barrier.[29] For a simple ionic solid composed of atomic ions, the diffusing ion would move either by exchange with adjacent vacancy or by being excited to an interstitial position from which activated diffusion becomes easier. For a general diffusion mechanism, the number per unit volume of ions (n) in sites from which motion is possible is $n = Ne^{-W/kT}$, where N is the total number per unit volume of ions, W is the formation energy of sites. If the activation barriers for jump itself is U and the frequency of vibration is ν, the number of jumps per second for each of n potential diffusive centers in the absence of an applied field is $\nu e^{-U/kT}$. Thus, the total jumps J_0 per second is $J_0 = N\nu e^{-(W+U)/kT}\lambda' g$. The effect of an applied

field E is to raise the activation barrier in the direction of the field by $eE\lambda'/2$, where λ' is the average diffusion jump distance, and to lower the barrier in the opposite direction by the same amount (Fig. 5). The factor g is a term involving geometrical and entropic features of the system. The net number of jumps per second in the direction opposed the field is

$$\begin{aligned} J &= J_- - J_+ \\ &= \lambda' g N \nu e^{-W/kT} \left(\exp(-(U-eE\lambda'/2)/kT) - \exp(-(U+eE\lambda'/2)/kT)\right) \\ &= 2\lambda' g N \nu e^{-(W+U)/kT} \sinh(eE\lambda'/2kT) \\ &= 2J_0 \sinh(eE\lambda'/2kT) \end{aligned} \tag{73}$$

The current density (j) due to this diffusion process is

$$j = Jq = 2N\nu q g \lambda' e^{-(W+U)/kT} \sinh(eE\lambda'/2kT) \tag{74}$$

where q is the charge per ion.

The implications from the above equation are:

(i) the conduction is non-ohmic at high values of the applied field

(ii) j increases with temperature T.

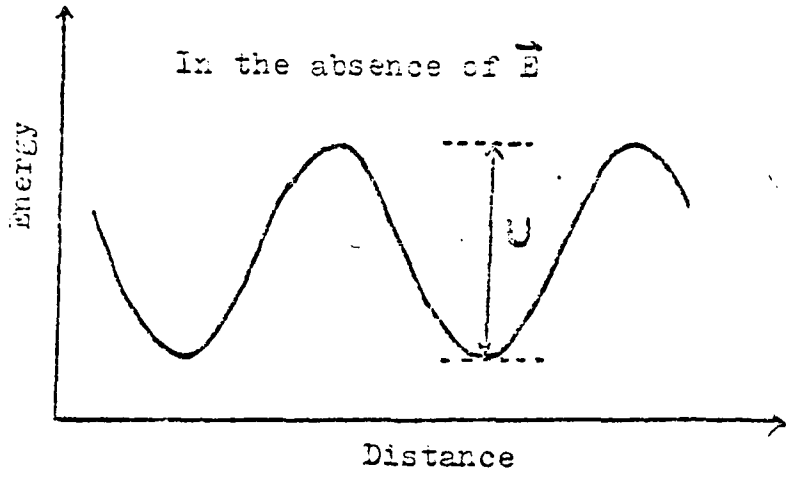

(a). In the absence of E.

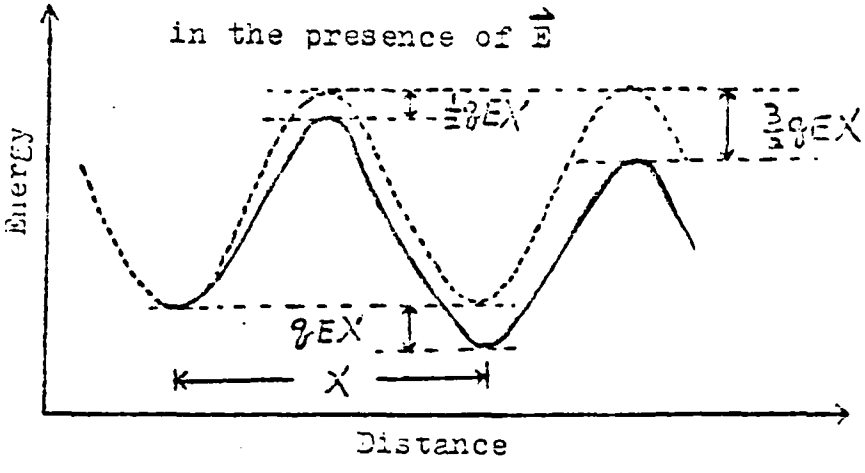

(b). In the presence of E.

Figure 5. Energy barrier of sites.

Chapter III INSTRUMENTATION AND EXPERIMENTAL PROCEDURE

A. X-Ray Energy Dispersive Analysis

1. Instrumentation. X-ray analysis has become widely accepted as a powerful tool for qualitative and quantitative analysis of the distribution of chemical elements because it is nondestructive, is direct in sample preparation techniques, can analyze nearly all of the elements of the periodic table, and is very accurate. It is unique among analytical instrumental methods in that it provides a considerable amount of information quickly. Within minutes, useful data concerning the atomic composition of the sample for the elements with atomic numbers from Na up can be generated.

a. General Principles. When an X-ray photon or electron beam from a source interacts with the inner shells of an atom, an electron moves from one shell to a higher, but unstable level. When this atom returns to its stable position, an X-ray is released that is characteristic of the particular element. These X-rays are sensed by a Si(Li) detector, amplified, digitized, and stored in memory for use by a microprocessor. Such data are then reduced to answers that are meaningful to the operator.

b. Spectrometer. There are two types of X-ray spectrometers. One is wavelength-dispersive, and the other one is energy-dispersive. The energy dispersive X-ray (EDX) systems are lower in cost, but may not provide sufficient resolution or may not have the ability to handle high concentrations.[30,31] The wavelength-dispersive X-ray (WDX) spectrometer has better resolution, but it needs time to scan the entire spectrum of interest with the diffraction crystal. The systems analysis time-typically between 50 s and 3 min for a single sample with as many as eight measured elements is somewhat longer than more complicated instruments. Also this kind of spectrometer will be affected by the geometry of the sample. So, the proper alignment between the collimating slits, the diffraction crystal, and the direction should be established. The spectrometer used in this experiment is of the EDX type. Figure (6) is a schematic diagram of the energy dispersive X-ray Spectrometer.[32] The detector is a semiconductor which can distinguish one chemical from another on an energy selection basis. The typical Si(Li) spectrometer is diagramed in Figure (7).[33,34] The Si(Li) detector is essentially a reverse-bias diode which acts as a transducer; converting the energy of the X-ray photons to electron-hole pairs. The electron-hole pairs are swept out of the detector by the

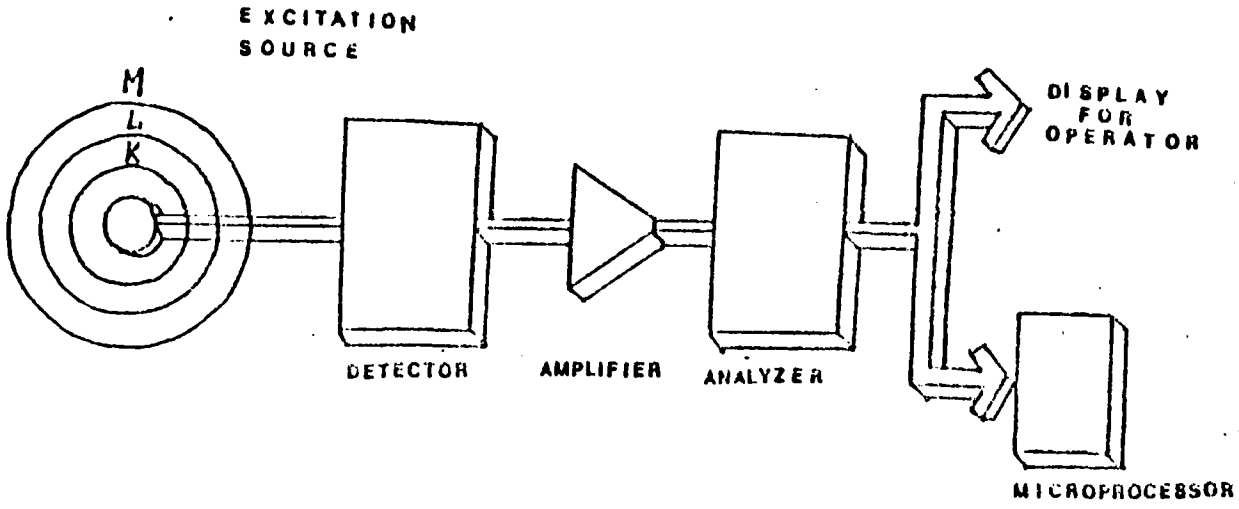

FIGURE 6 BLOCK DIAGRAM SHOWING PROCEDURAL STEPS IN AN EDX SYSTEM[32]

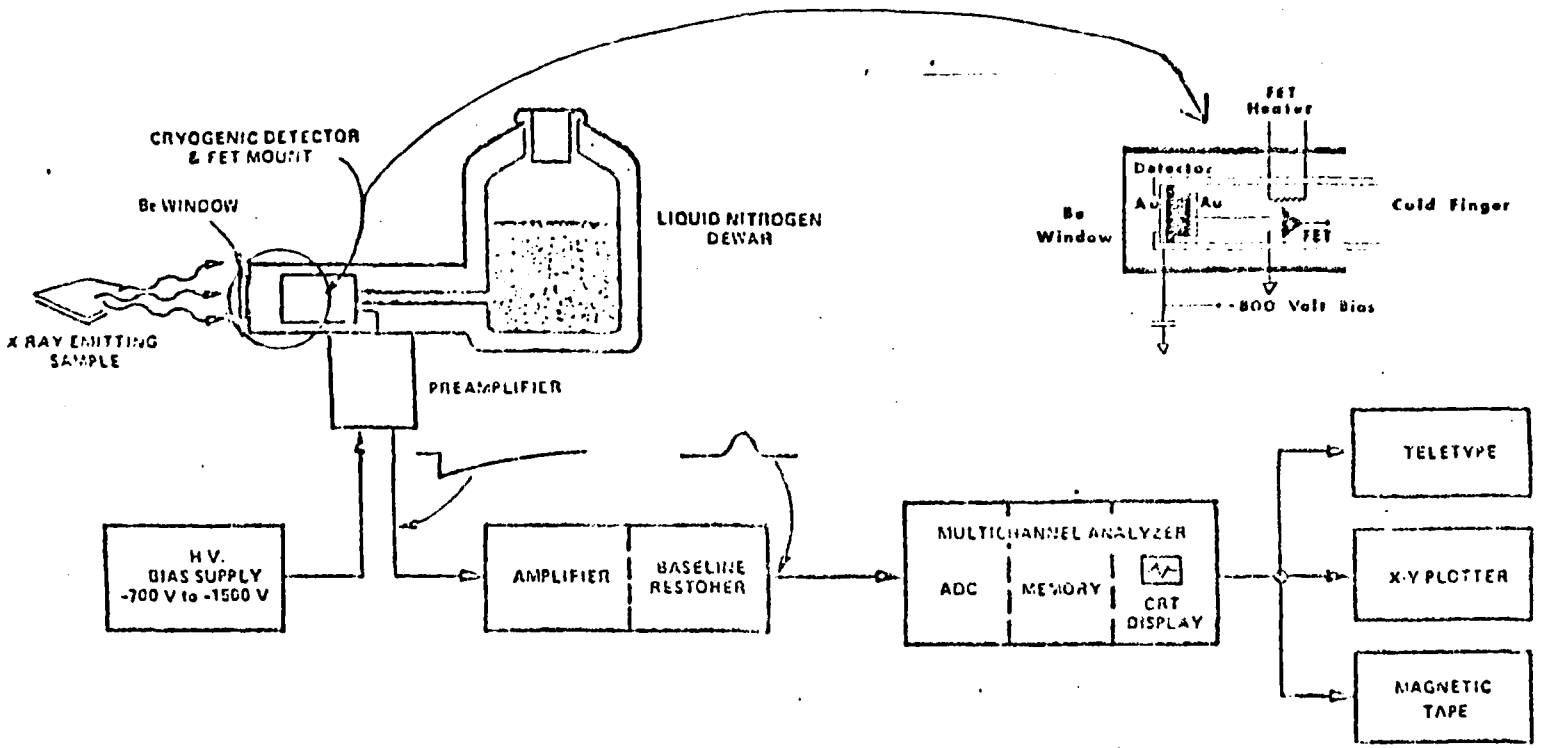

Fig. 7

Si(Li) X-Ray Energy Analyzer[33,34]

applied bias voltage and the total charge produced in the current pulse is directly proportional to the energy of the X-ray that was absorbed in the detector. The Si(Li) diode and the field effect transistor (FET), which is the first amplifier stage, are cryogenically mounted to reduce the electronic noise of the devices. The detector has good operational performance at the boiling point of nitrogen, -190°C, but the FET must be warmed 70°C above this for optimal performance, necessitating the heater resistor.

The amplifier increases the signal level from the FET and also reduces noise. Before the signal goes to the multichannel analyzer, it enters the base line restorer which maintains a base line between pulses. The base line restorer output is passed to an analog-to-digital converter (ADC). Each time an X-ray pulse is processed by the ADC a number is generated that represents the channel to be incremented by one, thereby resulting in an intensity versus energy distribution. A magnetic core memory accumulates the number of times each energy interval is detected and the information is displayed on a cathode ray tube (CRT).

c. Applications. The applications include scanning electron microscopes, electron microprobes, transmission electron microscopes and X-ray fluorescence analysis. The one used in this experiment is the scanning electron

microscope.[35] Figure (8) shows the interface between the scanning electron microscope and energy dispersive spectrometers. The SEM has a very small electron beam. For this reason the regions of the sample examined can be as small as 1-2 μm in diameter.

d. System Performance. Because the width of the band pass filter and the fact that only one X-ray can be processed at a time, the output count rate is less than the input count rate. To correct for this difference, the system uses a special livetime clock that runs only during the time the amplifier is able to accept another pulse for processing. When an X-ray is detected, the amplifier becomes busy, and the livetime clock is turned off. The system is dead during this period, and so this processing time is called deadtime. Realtime, the normal time measurement, is the sum of the livetime plus the deadtime, if the deadtime loss is over 20%, the livetime correction is no longer able to work accurately.

The specified resolution for the system was 153 eV full width at half maximum (FWHM) at 5.89 eV. The reason for using this is that the theoretical shape of the curve can be predicted. Usually the faster the amplifier can process counts, the poorer its resolution.

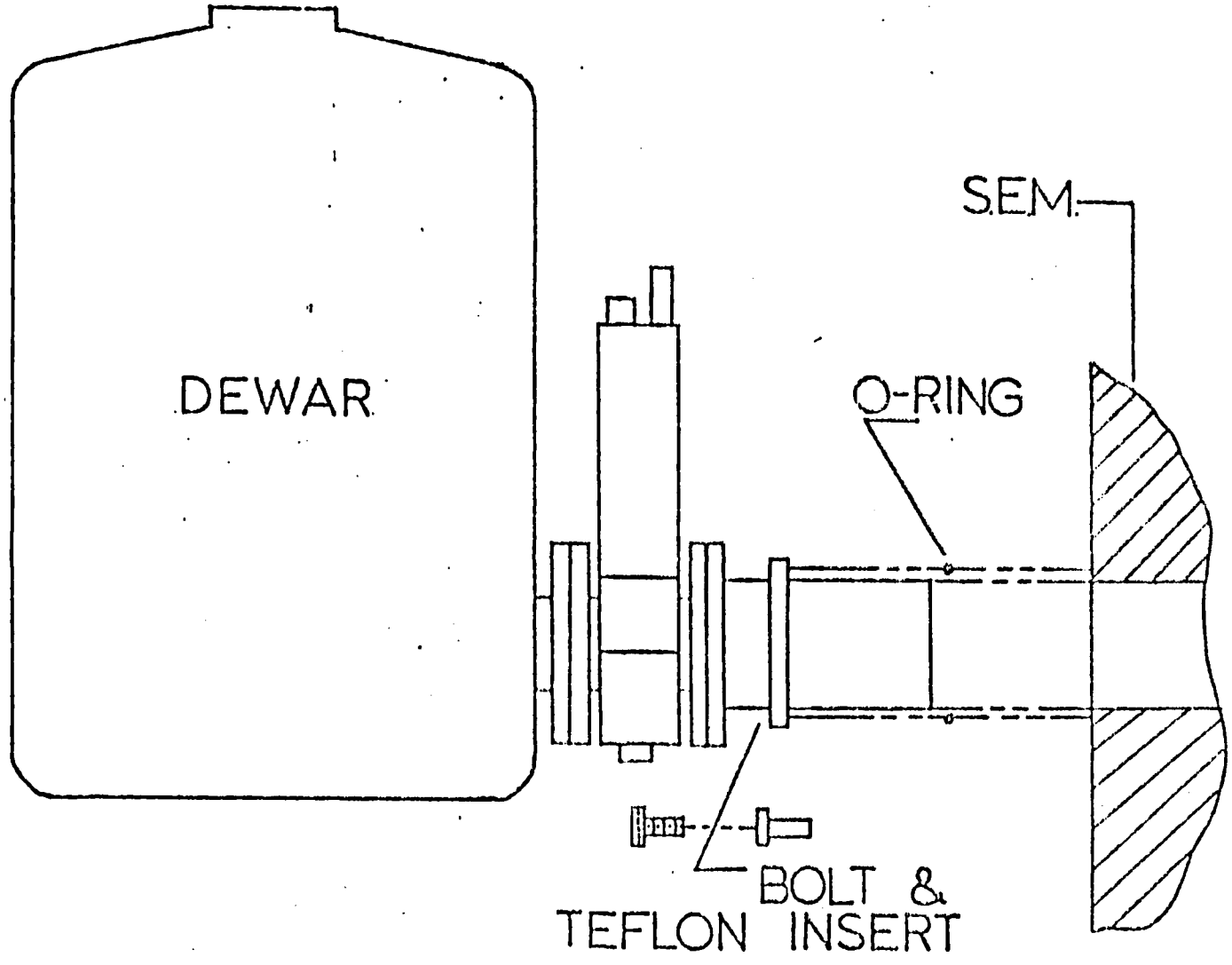

Figure 8

Schematic Showing the Interface Between an Energy Dispersive Spectrometer and a Scanning Electron Microscope[33-35] (after ORTEC)

2. Experimental Procedure. Many methods were considered as a possible means of introducing diffusant into the sample. Most of these failed because of the severe difficulty in dealing with such small thin films (10 μm-40 μm in thickness) and fine fibers (10 μm-40 μm in diameter). One of the methods tried is shown (Fig. 9.a.).

Salts such as NaCl, $Fe(NO_3)_3$,. . .etc. were dissolved in water to act as diffusants. The advantage of this arrangement is that the surface tension of the solution and the balance pressures (inside tube and outside tube) create a perpendicular surface to introduce diffusant into the fiber. Furthermore, the evaporation of water is insignificant. The disadvantage is that the experiment is still complicated by surface diffusion. After a certain time of diffusing, the sample was glued on the carbon mount using carbon paste (colloidal graphite). The reason for using carbon was to avoid peak overlaps between the specimen and specimen holder. The electron microscope only allows conductive specimens to be detected. Therefore, the specimen was coated with carbon about 100 Å thick. In this procedure, the sample was exposed in a vacuum. We assume that the water vaporized in this step and that diffusion was quenched. The first essential problem here is that during the coating procedure the sample was heated up to about 100°C for 10

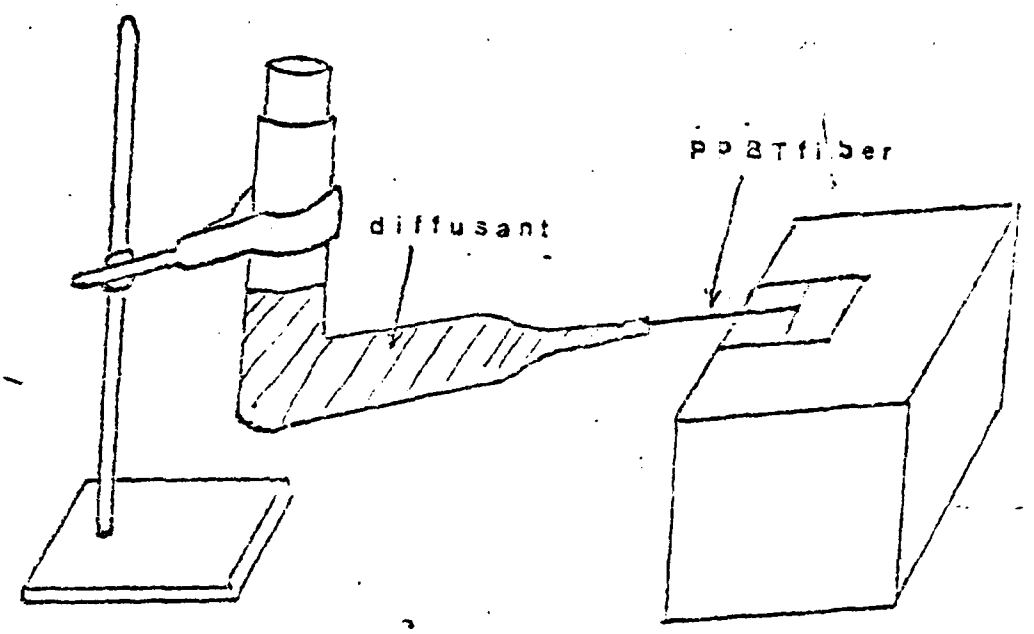

Fig. (9.a) Method of introducing diffusant into PPBT fiber.

QUALITATIVE ELEMENT IDENTIFICATION

SAMPLE ID:EXEC(2-P) DATA LABEL

ELEMENTS IDENTIFIED
S KA
CU KA
P KA
ZN KA

PEAK LISTING

	ENERGY	AREA	EL. AND LINE
1	1.996	1197	P KA
2	2.308	48001	S KA
3	8.030	1358	CU KA
4	8.609	839	ZN KA

Fig. (9.b) Computer output of qualitative analysis method.

minutes for the process to finish. Another problem is that the specimen is exposed to a large electric field. Consequently, this step will cause a severe error in determining the diffusion rate of mobile diffusant.

The coated fiber was scanned by the electron beam from an edge along the axis at each distance. If diffusion did occur, the excited X-ray could be analyzed to determine the diffusion rate.

PPBT fiber 29022-48-4 was examined by EDAX using the qualitative identification program. The computer output is shown (Fig. 9.b.).

This fiber was made from polyphosphericacid (PPA) solution. The residual acid corresponds to the peak of the element P. The peaks of Cu and Zn are due to the chamber materials.

One $Fe(NO_3)_3$ doped PPBT Fiber was examined at the same place six times. The results show a 25% deviation. Figure (10) gives the computer output of the semiquantitative analysis method.

The proposed explanations are: 1. the rough surfaces cause errors in the take off angle (35° here). 2. The inhomogeneous structure inside PPBT. 3. The sensitivity of EDAX is not high enough for the available samples.

```
DO:INIT

NO. OF ELEMENTS=?3
CSC OF TAKEOFF ANGLE=?1.24345
EXCIT. VOLT.=?25
BE WINDOW THICKNESS=?2.5

ELMNT( 1)=S  LINE(K,L,M)=?K
ELMNT( 2)=FE LINE(K,L,M)=?K

DO:SSQ

SEMI-QUANTITATIVE ANALYSIS: EXEC(2-P) DATA LABEL
EL    NORM. K-RATIO

S -K 0.90743 +- 0.01272
FE-K 0.09256 +- 0.00666

ZAF CORRECTION

ITER  5
----    K      [Z]    [A]    [F]   [ZAF]  CONC
S -K  0.907  0.987  1.072  0.999  1.057  0.895
FE-K  0.092  1.141  1.045  1.000  1.216  0.105

S -K 0.91320 +- 0.01283
FE-K 0.08679 +- 0.00648

ZAF CORRECTION

ITER  5
----    K      [Z]    [A]    [F]   [ZAF]  CONC
S -K  0.913  0.988  1.067  0.999  1.054  0.901
FE-K  0.086  1.142  1.046  1.000  1.218  0.099

S -K 0.91169 +- 0.01327
FE-K 0.08830 +- 0.00677

ZAF CORRECTION

ITER  5
----    K      [Z]    [A]    [F]   [ZAF]  CONC
S -K  0.911  0.987  1.069  0.999  1.055  0.900
FE-K  0.088  1.142  1.046  1.000  1.217  0.101

S -K 0.90114 +- 0.01315
FE-K 0.09885 +- 0.00713

ZAF CORRECTION

ITER  5
----    K      [Z]    [A]    [F]   [ZAF]  CONC
S -K  0.901  0.986  1.076  0.999  1.061  0.889
FE-K  0.098  1.140  1.045  1.000  1.215  0.112

S -K 0.90084 +- 0.01308
FE-K 0.09915 +- 0.00711

ZAF CORRECTION

ITER  5
----    K      [Z]    [A]    [F]   [ZAF]  CONC
S -K  0.900  0.986  1.076  0.999  1.061  0.889
FE-K  0.099  1.140  1.045  1.000  1.215  0.112

S -K 0.92627 +- 0.01337
FE-K 0.07372 +- 0.00618

ZAF CORRECTION

ITER  5
----    K      [Z]    [A]    [F]   [ZAF]  CONC
S -K  0.926  0.989  1.058  0.999  1.046  0.915
FE-K  0.073  1.144  1.037  1.000  1.221  0.085
```

Fig. 10 Computer output of semiquantitative analysis

Accordingly, we should require better samples and higher concentrations of diffusants before the EDAX method can be fully successful.

Fig. (11) demonstrates the inhomogeneous surface and residual PPA solution for PPBT fibers.

Figure (12) shows the typically rough surface of a PPBT film under low magnification in the electron microscope.

B. Weighing Method with the Cahn Electrobalance

1. Instrumentation. The Cahn Electrobalance (Model-RG) is based on the nullbalance principle,[36] which is generally accepted as being the most accurate and reliable method of measurement. When the lowest dial range (1 mg) is chosen, the resolution can be as small as 0.2 μg.

a. Theory of Operation. Figure (13) is the schematic diagram for the operating system. When the sample weight changes, the beam tends to deflect momentarily. The flag moves with it, changing the light to the phototube and the phototube current. This is amplified in a two-stage servo amplifier and the amplified current is applied to a coil attached to the beam, which is in a magnetic field. The current in the coils acts like a d.c. motor, exerting a force on the beam to restore it to the original balance position. Thus the change in electromagnetic force is equal

(a)

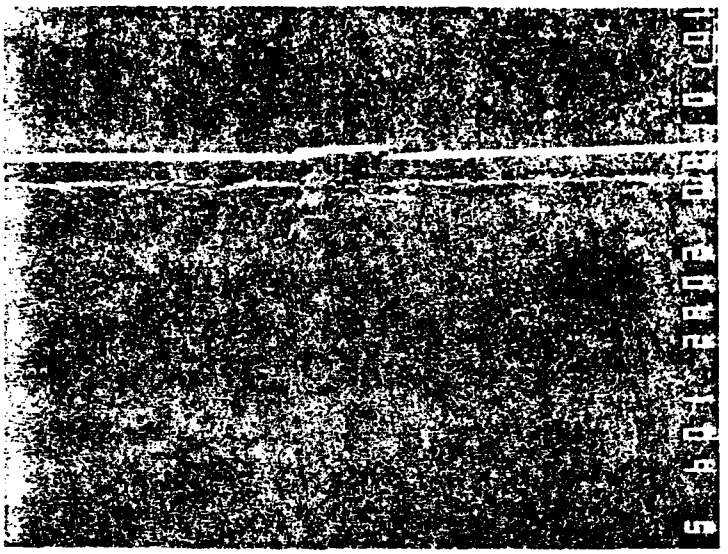

(b)

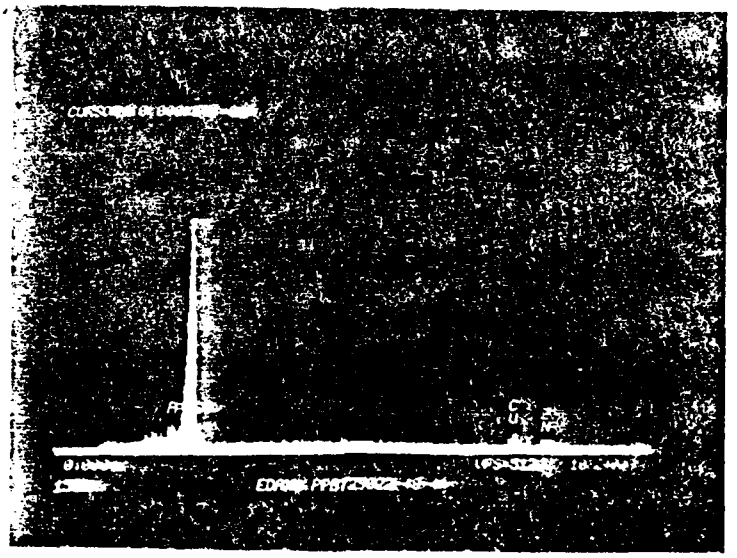

Fig.11 (a) Scanning electron micrograph of PPBT fiber(29022-48-4) under 600 magnification. (b) Spectra of EDAX on this PPBT fiber.

(a)

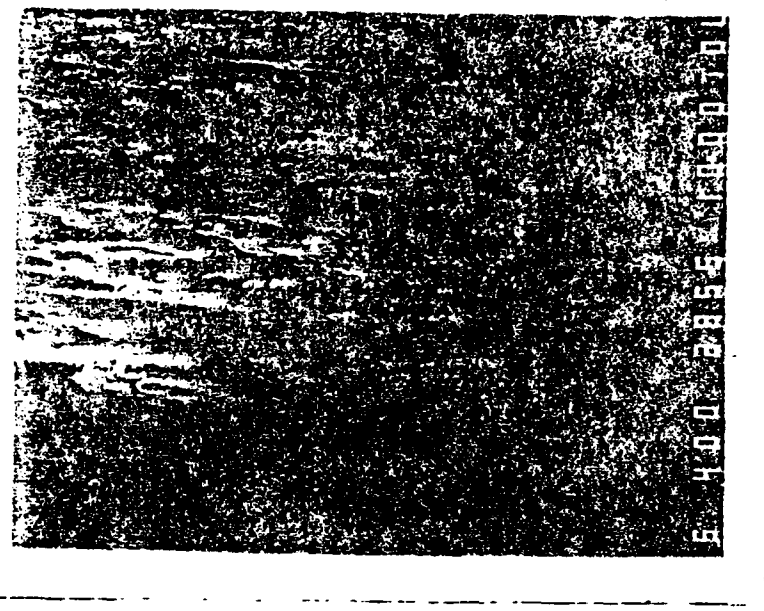

(b)

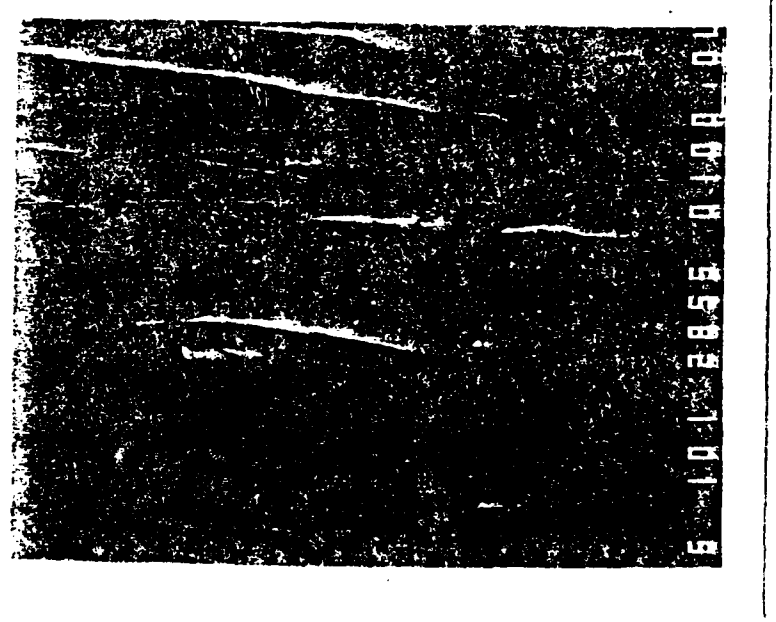

Fig.12 Two scanning electron micrographs of PPBT film (28555-25-6). (a) Under 40 magnification. (b) Under 100 magnification.

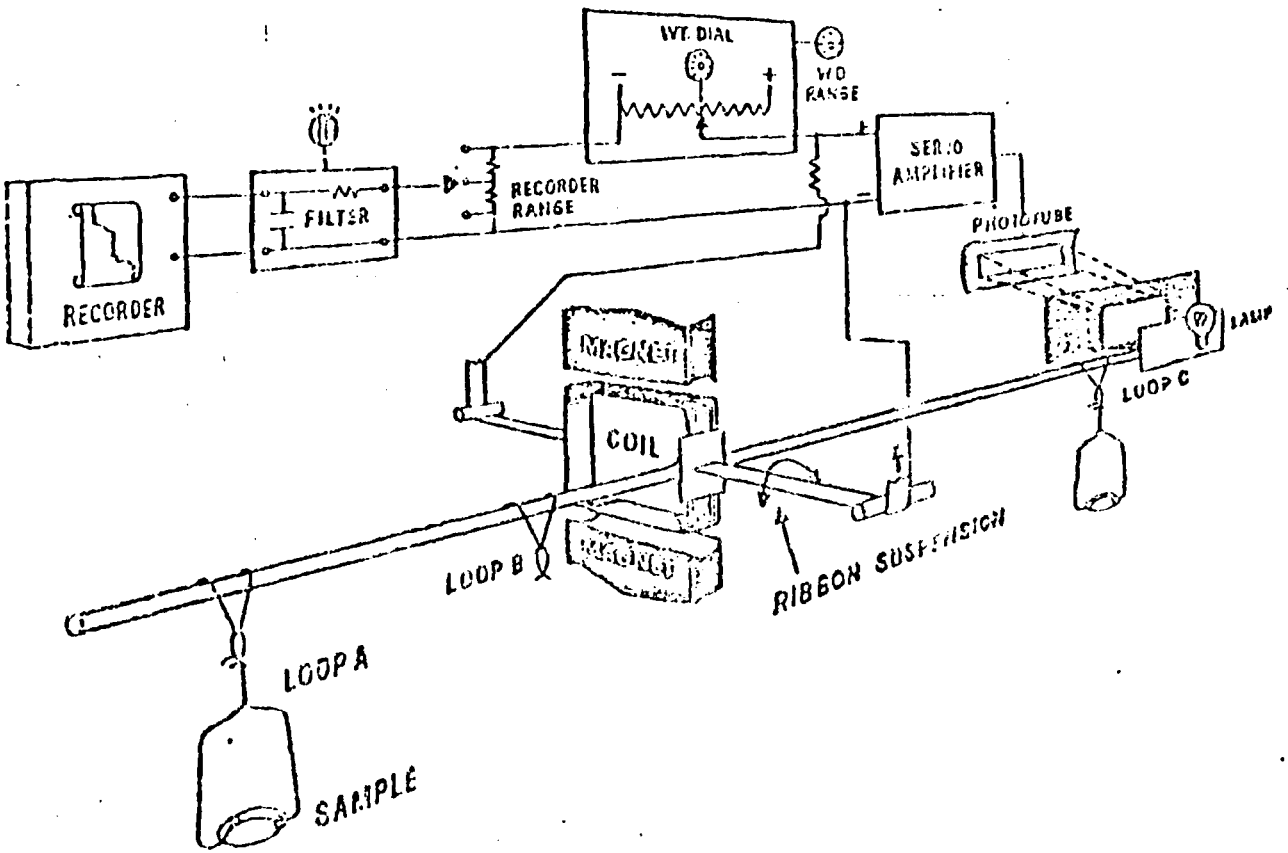

Fig.13 Schematic diagram of operating system of RG electrobalance.[36]

to the change in sample weight. The beam is always in dynamic equilibrium, with the sum of the moments on it equal to zero. The restoring force is powerful and fast so that the beam appears visually to be locked in place. By means of accurate potentiometers, an accurately calibrated voltage is subtracted from the voltage across the coil. A dial on the potentiometer reads directly in milligrams, corresponding to the amount of voltage being subtracted in the circuit. The excess of coil voltage over reference voltage is then available for the recorder.

In order to return the beam to exactly the original position after a weight change, a slight offset of the beam is required to cause the added current in the coil. The ratio of the offset which would occur without feedback to that which occurs with the servo operating is called the servo loop gain, G. It is a dimensionless quantity in excess of 1000. This factor reduces the power supply changes and speed up response time.

Figure (14) and (15) show the circuits of the servo amplifier and control units respectively. The force induced by the phototube current is limited by the slit opening. Optimum adjustment of the SLIT potentiometers R7 occurs when the maximum up and down forces are equal. Due to this feedback system, drastic changes in tube characteristics

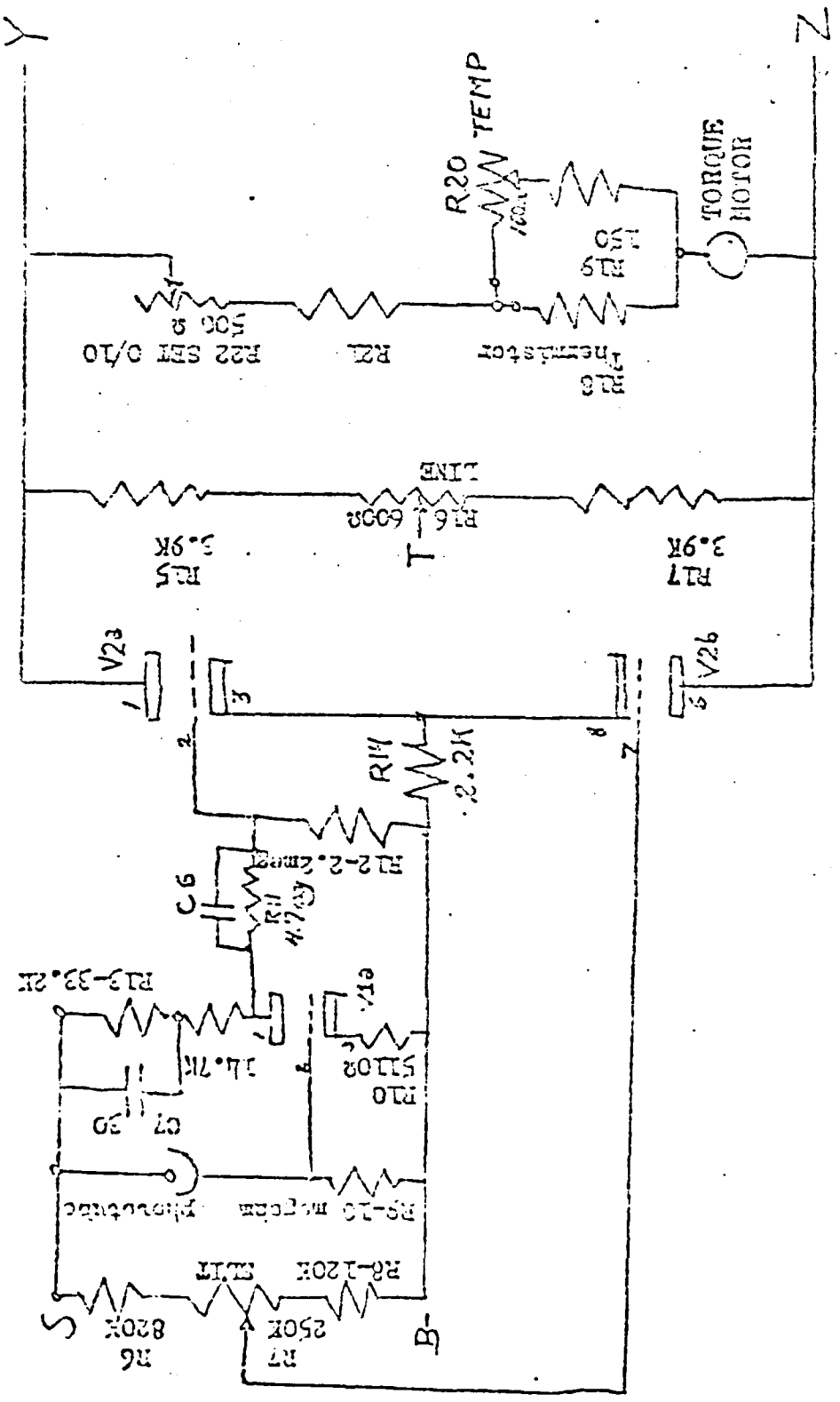

Fig.14 Servo Amplifier of RG Electrobalance.[36]

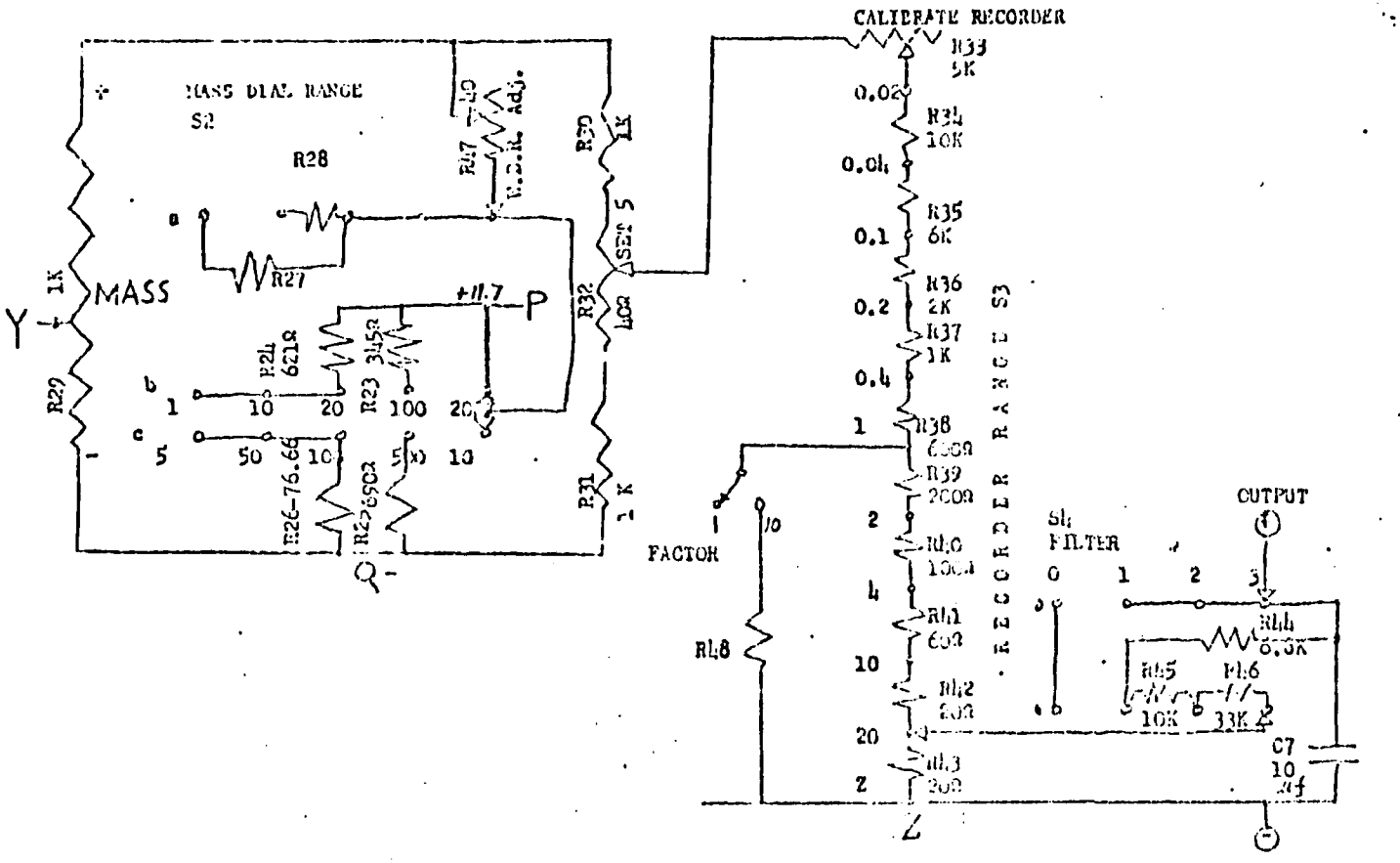

Fig. 15 Control circuits of Cahn RG electrobalance.[36]

with time will have no effect on balance performance within its range. When the beam is in balance, the current is zero. Weight added to the sample pan will cause a positive current. On the other hand, removing weight from the sample pan will cause a negative current. The maximum current is ±3mA, maximum voltage about ±9 volts, correspondingly, the reference voltage supplies across the mass potentiometers R29 is made + and - by means of resistors R30 and R31, so that the mass-reference-voltage can equal coil-voltage over the useful range. Zero net weight corresponds to 0.5 on the dial, - maximum output corresponds to 0, and + maximum to 1.0. The voltage output at a dial setting of 0.5 is changed by means of R32 to compensate for variations in pan and stirrup weights, etc; it is basically a zero control, and is called "set 5," because that is what you do with it. The voltage at a given weight is adjusted by means of R22, in series with the torque motor coil. The more resistance, for the same current, the more voltage. This is similar to the Calibrate controls on other Electrobalances, but is called SET 0/10 here.

The excess of coil voltage over reference voltage is applied through R33 to a step voltage divider, used to establish the recorded range. The actual voltage per

milligram is determined by adjusting R33 (Calibrate Recorder) on any recorder range.

To reduce the stray forces, from vibrations, etc., the output voltage can be applied to a low-pass filter, depending on recorder characteristics. If more filtering is necessary, add more capacitance in parallel with the one in the balance. Additional capacitors should be of Mylar, and should be added in increments of 5 or 10 μF to be significant.

Some other signal can be introduced to the recorder, by connecting its + lead to x positive of the recorder range switch, and its - lead to z, and turning switch to x.

b. System Performance. There is a residual mechanical zero shift as a function of temperature, even at 0.5000. At no load it is about -0.5 μg/°C; that is, the balance reading will go down that much as the temperature increases. The effect of load is in the opposite direction, so that somewhere between the half-and full-rated-load the effective temperature coefficient will be zero. The electromagnetic system is temperature compensated, so that the MASS dial and recorder calibrations are independent of temperature. This compensation is fully effective for a range of about 10°C around ambient.

Minimum recommended recorder ranges are indicated by the small pointers on the back of the mass dial range knob. They are chosen so that the minimum increase of mass dial setting will be 1% on the finest recorder range. If the mass dial is not moved, the stability of the reference power supply for the mass dial will permit readings to 1% on the recorder for 2 ranges below the minimum recommended, at full scale on the mass dial (0 or 10). If the mass dial happens to be close to 5, even finer ranges can be employed.

The instruction manual #3124-1 for #200-1 Cahn electrobalance model RG has the details of fine points of operation, general applications, and operating procedures etc.

The information, such as operation in a vacuum, thermomolecular flow and aerodynamic effects, is very useful for the person working in this kind of area.

In the experiments of absorption carried out here, high precision was needed so that the long-term zero drift and cumulative zero drift became serious problems. The balance needs 18 hours to warm up and longer may even be better. In many installations the blank will show a daily 24-hour cycle, superimposed on a steady drift, even after all temperature effects are eliminated. The daily cycle may be as large as 10 micrograms peak-to-peak at no load, and 15 micrograms at full load. The steady drift rate may

be as large as +0.1 microgram/hour. The explanation for this is that it may be due to level shifts in the building. Other factors will cause drift, too. Periodic blasts of cold air from an air conditioner may cause periodic errors. Turning room lights on and off may produce a shift of as much as 1-2 micrograms in balance indication, and people walking in front of it may shift it one or two tenths of a microgram. The supply voltage change of ± 15% will cause a few tenths of a microgram shift.

2. Experimental Procedure. PPBT films 28555-25-6 were cut to 3.5 cm long. The weight was ~7 mg. Each sample was put in one small specimen container. Then, they were transferred to the desiccator for 48 hours drying. The desiccator was set up as in Figure (16).

After the samples had been dried, the vacuum was released. During this releasing process, the air passed through a long column containing desiccant before entering the desiccator. So, the moisture of the air was absorbed. Then, those dried samples were placed in the electrobalance for measurement.

During measurements, the mass dial was adjusted to the value where the recorder went to the zero position, and it was locked at that moment. The recorder was in the highest sensitivity range. (2 ranges below the minimum recommended.)

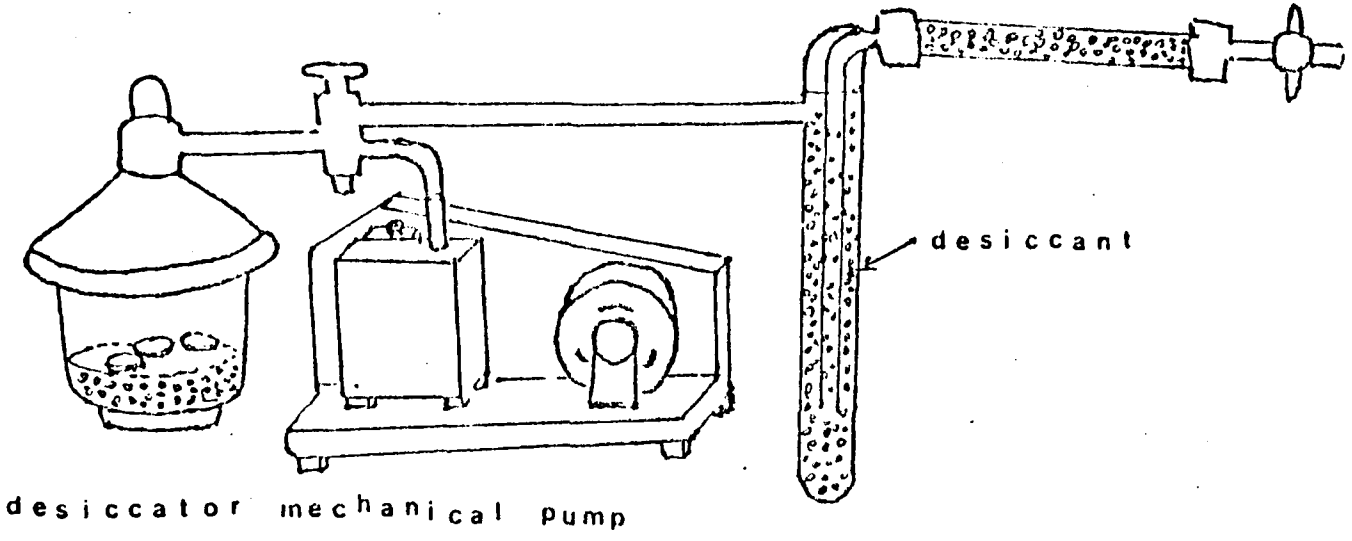

Fig.16 Diagram of sample drying system.

The full scale (100%) position of recorder was down to 0.11 mg at the 5 mV-set. Drifting and noise became a big problem but we had no choice. The reasons for drifting have been discussed in the section on System Performance. Noise was caused from the electrical circuits. Obviously we were dealing with the instrument near its margin of capability. There was one other important factor which had to be considered: the recorder did not record the mass change from instant that the diffusion began. Figure (17) is based on a curve traced from the recorder. Points were chosen on the curve and plotted as relative mass increase vs $t^{\frac{1}{2}}$ in Figure (18). The curve is clearly non-linear in the initial region. If we assume the recorder has a time lag t_0, then the curve is naturally based on $(M_t - M_{t_0})/(M_\infty - M_{t_0})$ vs $(t - t_0)^{\frac{1}{2}}$. Hence consider

$$(M_t - M_{t_0})/(M_\infty - M_{t_0}) = [(M_t/M_\infty) - (M_{t_0}/M_\infty)]/[1 - (M_{t_0}/M_\infty)]$$

$$M_t/M_\infty = 1 - (8/\pi^2) \sum_{m=0}^{\infty} (2m + 1)^{-2} \exp[-D(2m+1)^2\pi^2 t/b^2]$$

(See equation (14))

According to above equations, we can fit the experimental curve by changing t_0 and D. The best fit is shown on

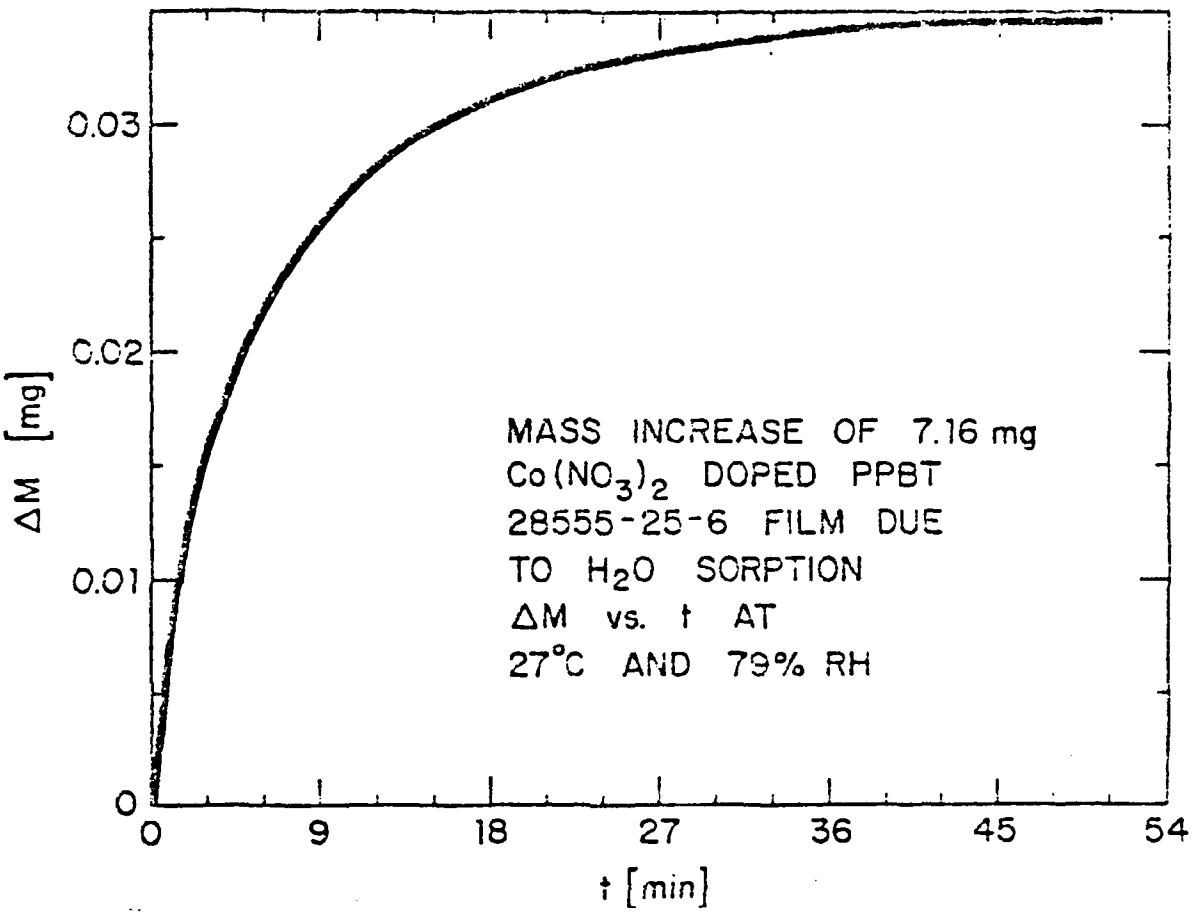

Fig. 17 Redrawn plot of a curve from strip chart recorder. The noise from circuits made the curve become a band. The smooth curve here was drawn through the center of the band

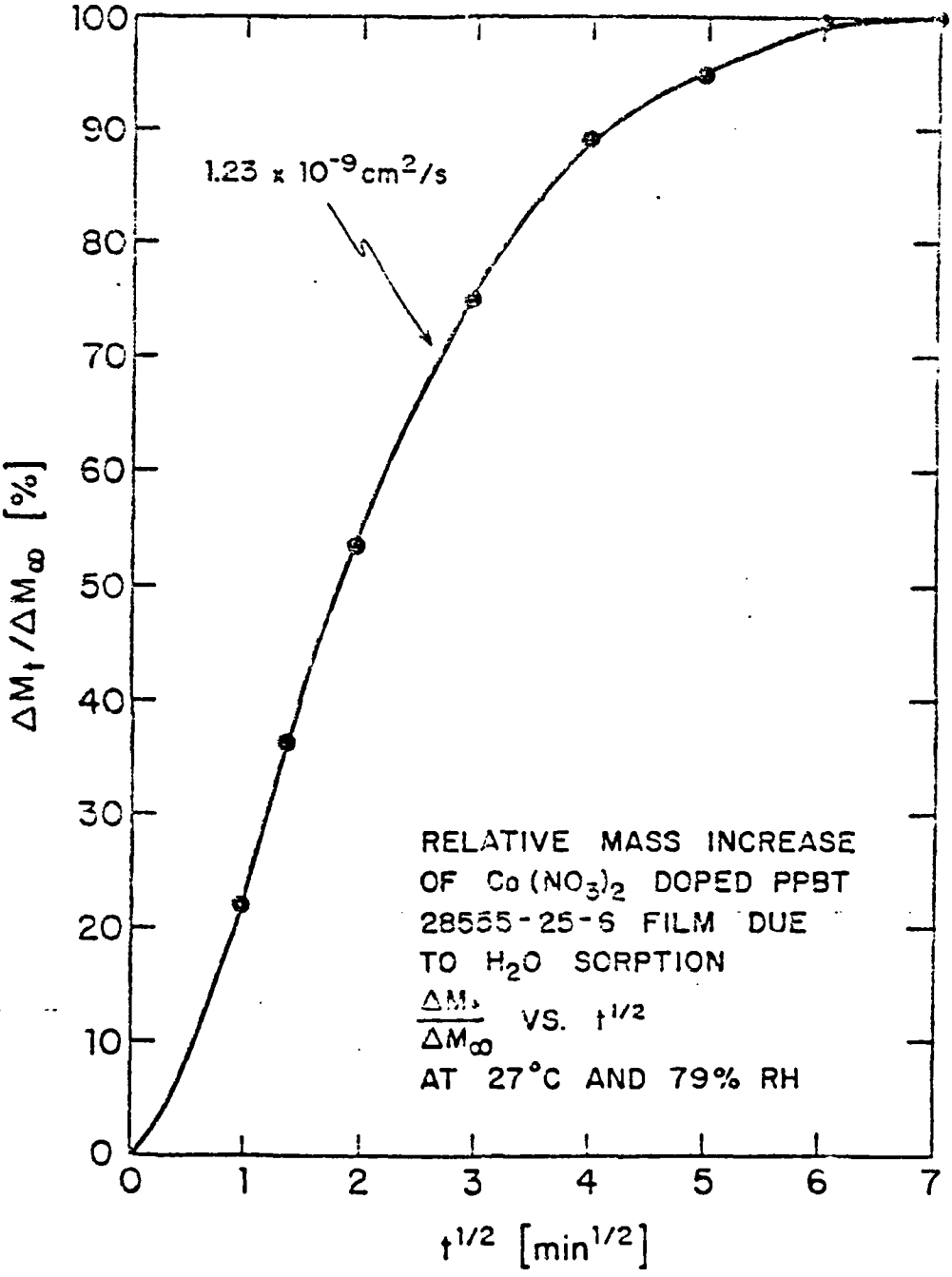

Fig.18 Reduced absorption curve which is based on figure 17

Figure (19), where t_0 = 0.1 min, D = 1.05 x 10^{-9} cm^2/s and M_{t_0}/M_∞ = 0.08954895483.

Curves such as the one in Figure (19) were drawn using the 21 step curve-drawing program of a Hewlett-Packard Desk Top Microcomputer with a 7225A plotter.

C. Sorption Method with a Sample Suspending on a Quartz Spring in an Evacuable Chamber

This method is a traditional technique for sorption measurements. Figure (20) illustrates the essential components for this system. The chamber is evacuable and under thermal control. It connects with a vapor source to cause a mass change of sample which can be measured through a telescope. Figure (21) shows the main parts in more graphic detail. Figure (22) depicts the vacuum system. The thermal source contains a 50 Ω heater, a temperature controller model 49 (or 50), a 10 switch OMEGA's digital temperature indicator (model 175), a centrifugal fan, and a variator. Six thermocouples attached to the system allow us to calibrate the temperature of different parts of the system. The curves shown on Figure (23) and (24) show these temperatures and will be discussed below. From Figure (24), it is easy to see the time needed to reach steady-state is at least 50 min. The vapor source is a removable tube

AN EXAMPLE OF
CALIBRATION CURVE

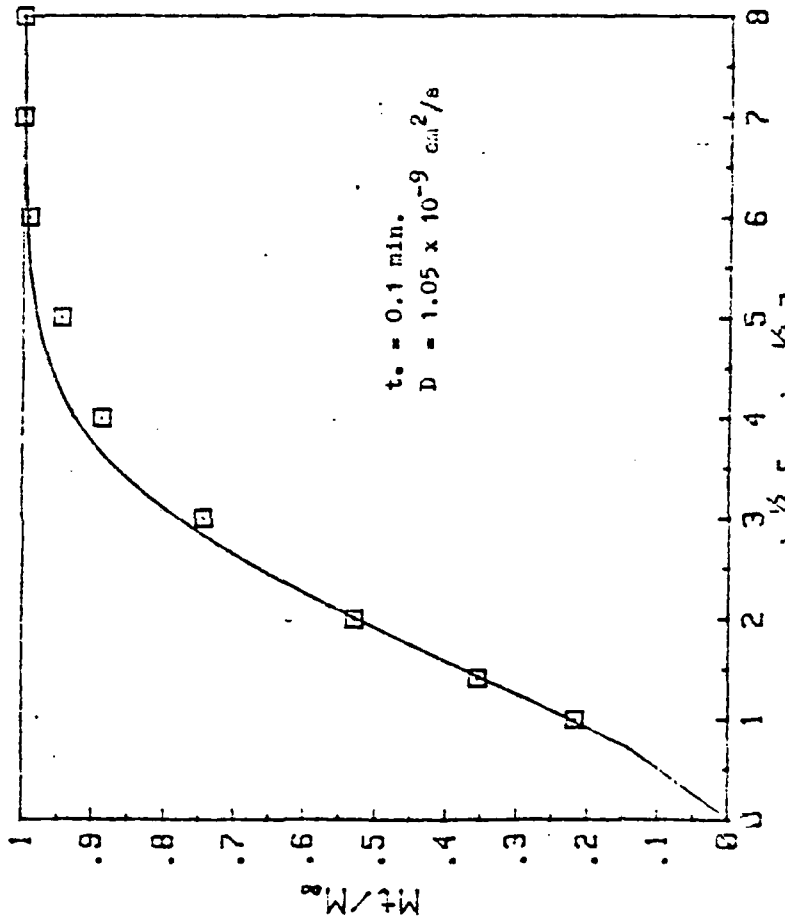

Fig. 19

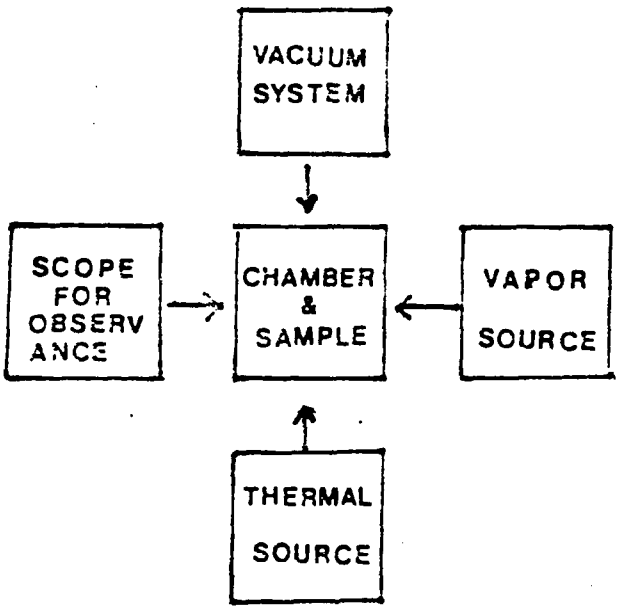

Fig. 20

COMPONENTS IN THE APPARATUS FOR SORPTION & DIFFUSION MEASUREMENTS

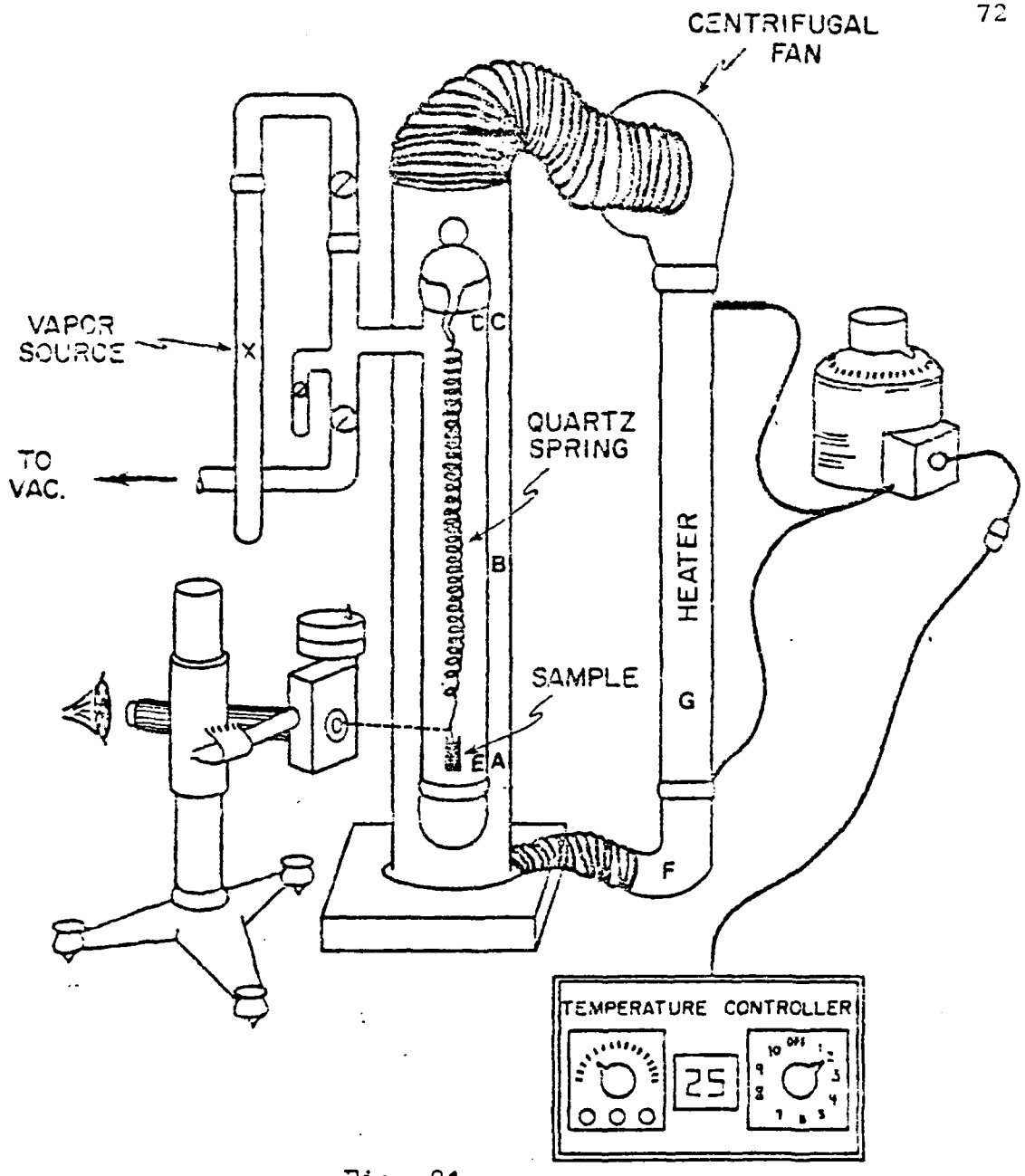

Fig. 21

THERMOSTATIC AND OPTICAL SYSTEMS FOR CONTROLLED ENVIRONMENT DIFFUSION CELL

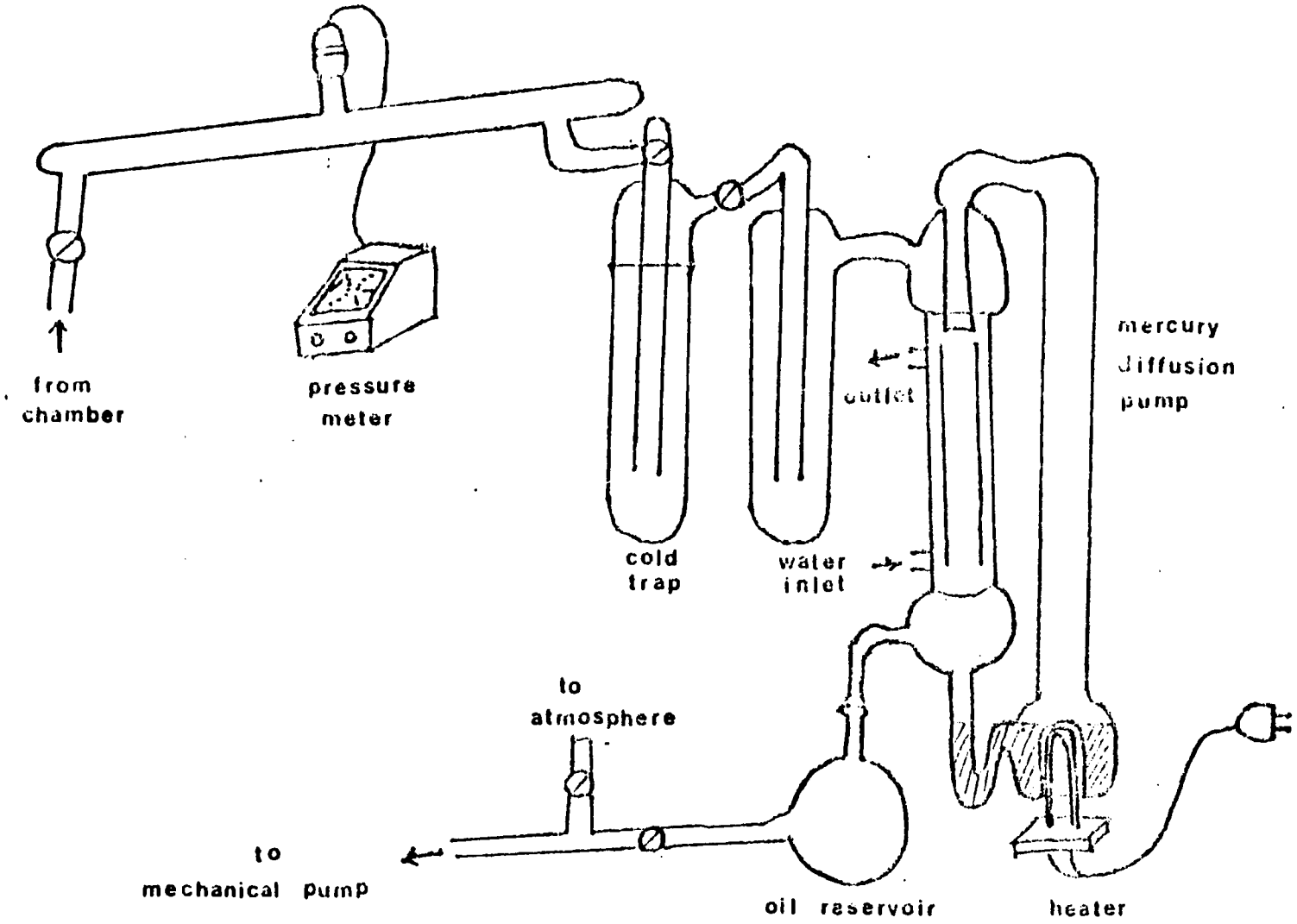

Fig.22 Vacuum system.

TEMPERATURE CALIBRATION
CURVES OF VACCUM CHAMBER

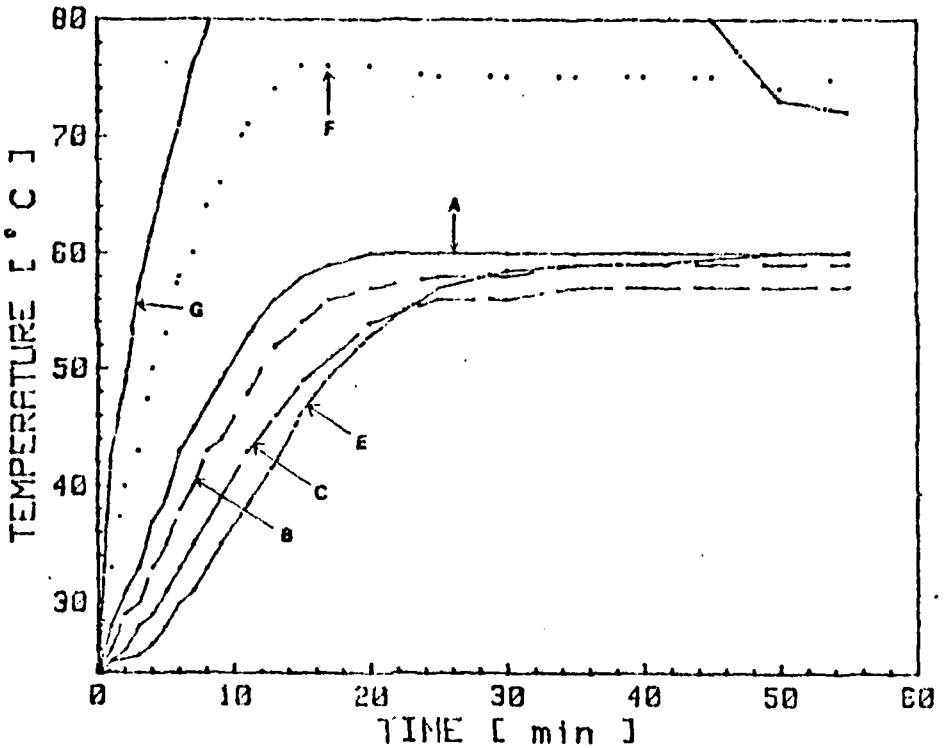

Fig. 23

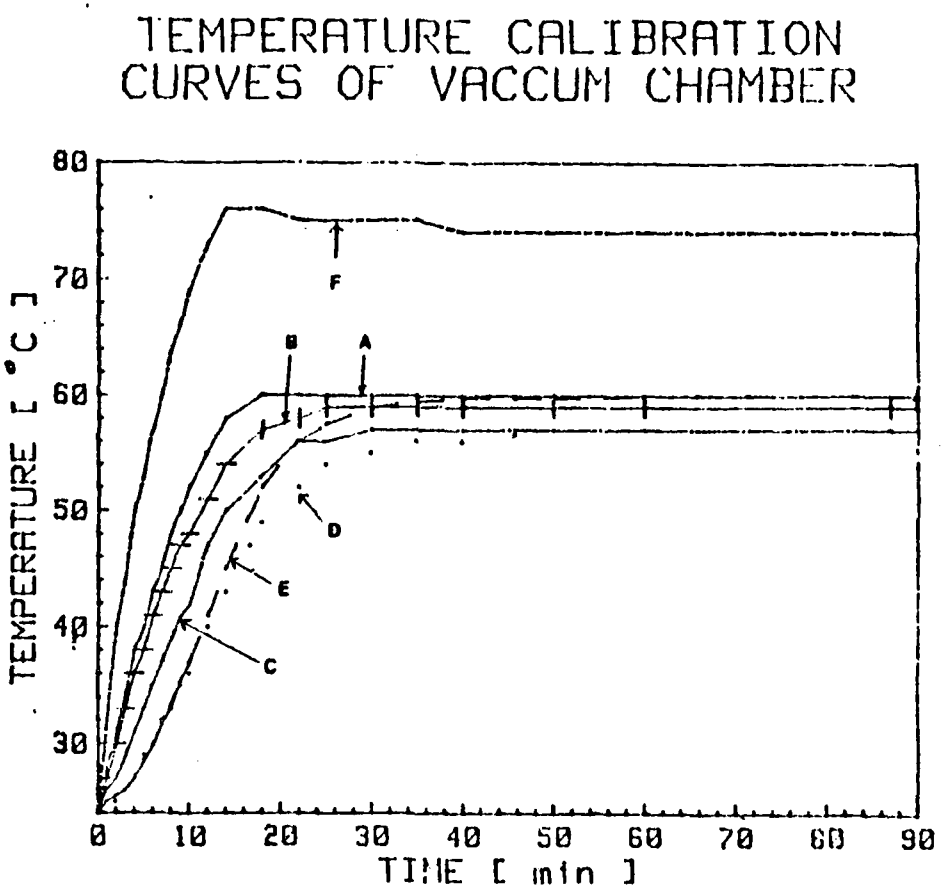
TEMPERATURE CALIBRATION
CURVES OF VACCUM CHAMBER
TEMPERATURE [°C]
80
70
60
50
40
30
0
10
20
30
40
50
60
70
80
90
TIME [min]
F
B
A
D
E
C

Fig. 24

connected to the chamber through a three-way stopcock. The vacuum system is composed of a combination of a mercury diffusion pump and a mechanical pump.

In order to demonstrate the reliability of this set up PET (Poly-ethylene Terephthalate) film was chosen because extensive reliable data for H_2O diffusion in this polymer were available. The sample was 10.15 cm long, 1.97 cm wide and 80 μm thick. Obviously the edge effect is insignificant. (See Appendix D). Figure (25) gives sorption and desorption curves of PET at 36°C. Figure (26) gives the curves for sorption at three different temperatures. Diffusion coefficients were calculated based on the initial gradients of the curves. The slopes were quite linear up to $M_t/M_\infty \sim 60\%$. This is called Fickian behavior. Figure (27) is an Arrhenius plot of H_2O diffusion in PET. The result shows good agreement with literature values.

The activation energy 10.4 kcal/mol (43.5 kJ/mol) is the same as is given in the literature. The deviation of diffusion coefficients are within 10%. These results demonstrate that the system is reliable. That is not to say that problems were not still there. For example the tiny weight of the PPBT samples was beyond the sensity of our original quartz spring, then a new quartz spring with 10 mg maximum load and 47.5 ug/mm sensitivity came to replace the old one,

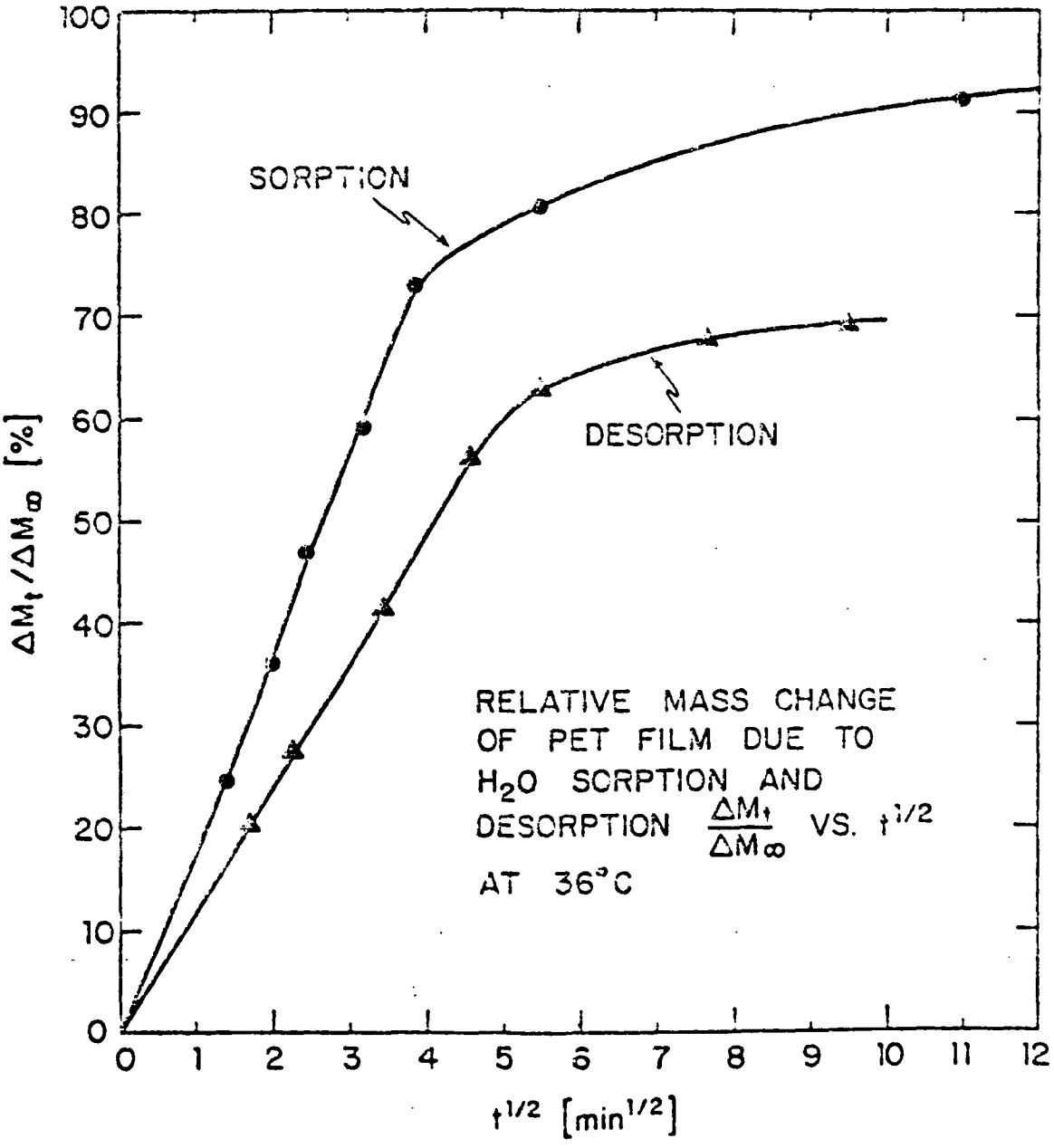
100
90
80
70
60
50
40
30
20
10
0
0 1 2 3 4 5 6 7 8 9 10 11 12
$\Delta M_t / \Delta M_\infty$ [%]
$t^{1/2}$ [$min^{1/2}$]
SORPTION
DESORPTION
RELATIVE MASS CHANGE
OF PET FILM DUE TO
H_2O SORPTION AND
DESORPTION $\frac{\Delta M_t}{\Delta M_\infty}$ VS. $t^{1/2}$
AT 36°C

Fig. 25

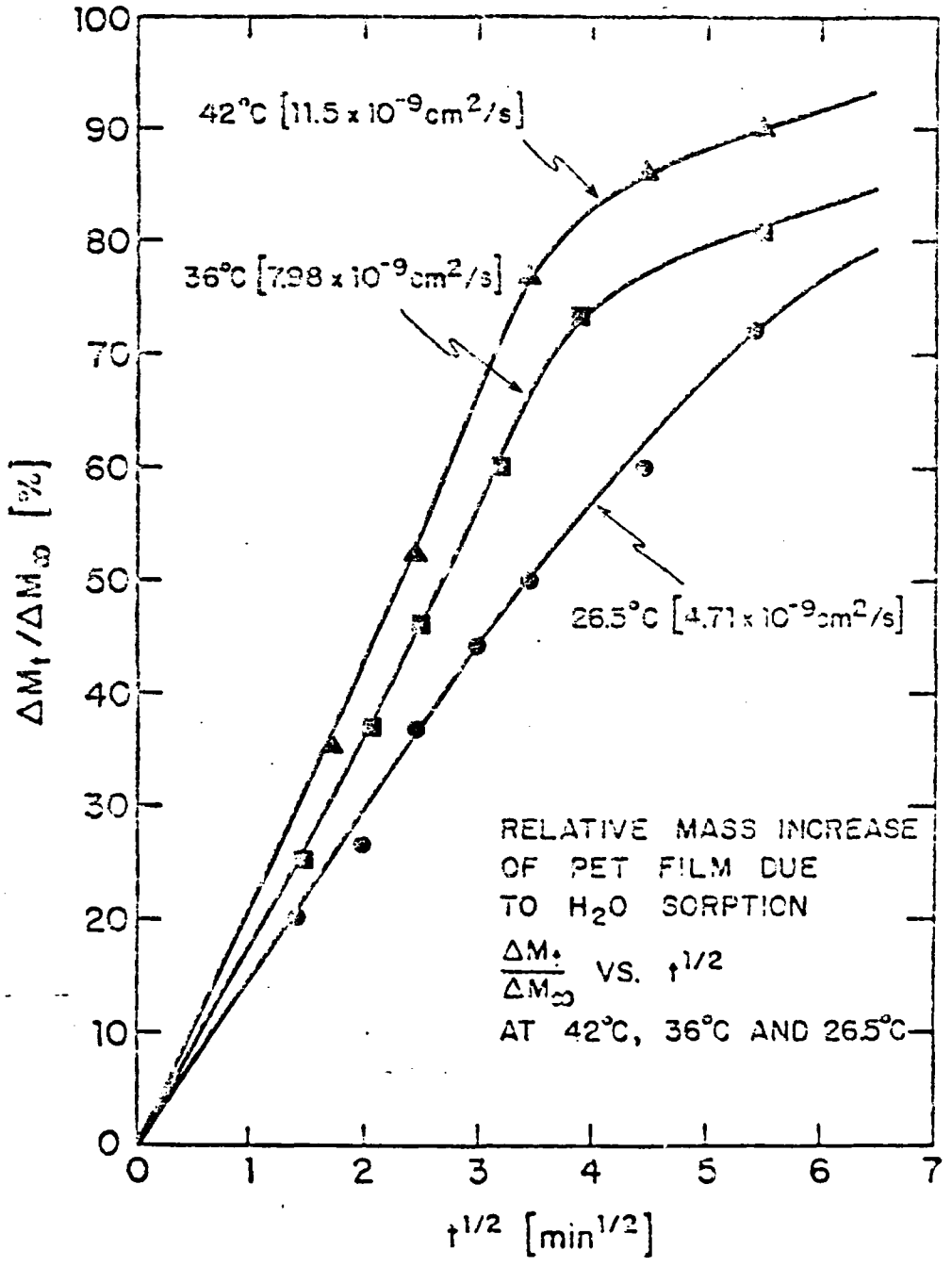
100
90
80
70
60
50
40
30
20
10
0
0
1
2
3
4
5
6
7
$\Delta M_t / \Delta M_\infty$ [%]
$t^{1/2}$ [$min^{1/2}$]
42°C [$11.5 \times 10^{-9} cm^2/s$]
36°C [$7.98 \times 10^{-9} cm^2/s$]
26.5°C [$4.71 \times 10^{-9} cm^2/s$]
RELATIVE MASS INCREASE
OF PET FILM DUE
TO H_2O SORPTION
$\frac{\Delta M_t}{\Delta M_\infty}$ VS. $t^{1/2}$
AT 42°C, 36°C AND 26.5°C

Fig. 26

AD-A162 766 STUDY OF TRANSPORT PROPERTIES AND STRUCTURE OF EXTENDED-CHAIN POLYMERS D (U) VIRGINIA UNIV CHARLOTTESVILLE DEPT OF MATERIALS SCIENCE 2/2

UNCLASSIFIED R E BARKER ET AL SEP 85 F/G 11/9 NL

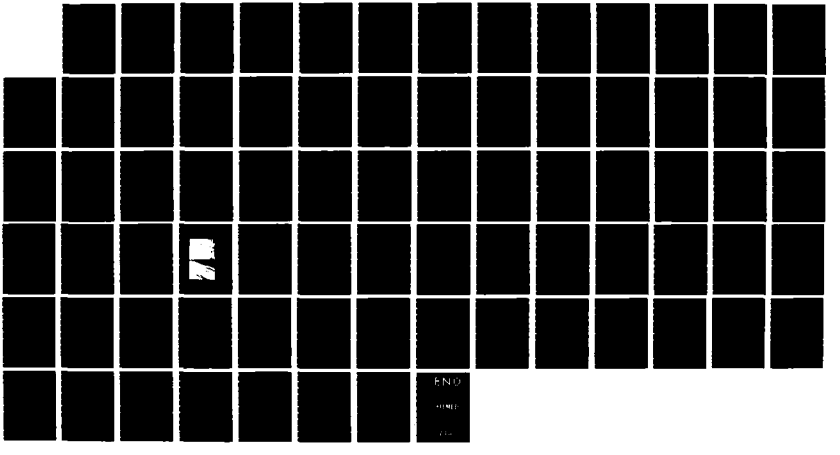

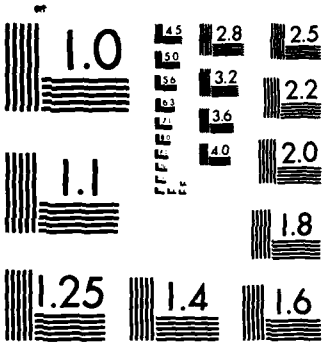

MICROCOPY RESOLUTION TEST CHART
NATIONAL BUREAU OF STANDARDS-1963-A

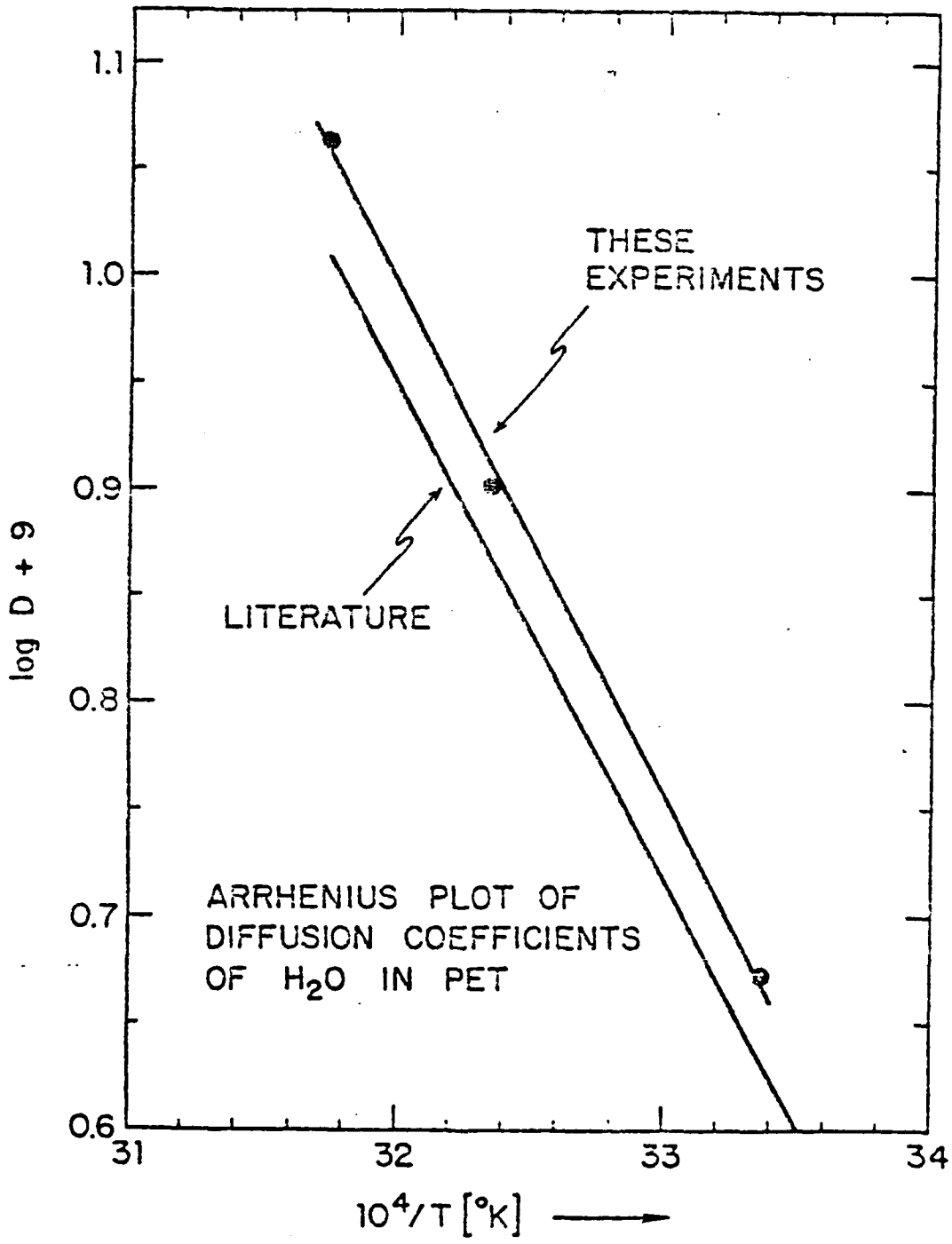
1.1
1.0
0.9
0.8
0.7
0.6
log D + 9
THESE
EXPERIMENTS
LITERATURE
ARRHENIUS PLOT OF
DIFFUSION COEFFICIENTS
OF H_2O IN PET
31
32
33
34
$10^4/T$ [°K]

Fig. 27

which was 200 mg maximum load and 9.75 mg/cm sensitivity. The new spring is so fine that it is almost impossible to handle. To my knowledge, the manufacturing company can not make any finer quartz springs than this.

One protecting column was added to the system to protect the spring from being hit by air or vapor flow, or being sucked into the vacuum system. The solubility of diffusant in PPBT came out to be so low that the thermal expansion of the chamber had to be considered in some experiments. The sample used in this method is 28555-25-6 PPBT film with weight 9.658 mg, length ~5.2 cm, width ~6 mm, and thickness 20 μm.

Chapter IV RESULTS AND DISCUSSION

A. The Effect of Microcavities on Diffusion

I have previously mentioned that the PPBT film available for these experiments is still very rough. The surface contained erupted voids which can be seen at high magnification in the electron microscope. According to a report from the University of Massachusetts,[37] they referred to the microvoids inside PPBT fibers and films as needle-like in shape. Perhaps football-like would be an alternative description. The Average Void Sizes obtained by Debye analysis of small angle X-ray scattering is 163 ± 10 Å along the extrusion direction and 135 ± 11 Å perpendicular to the extrusion direction. This correlates to ~13 monomers (12.35 Å each) along the extrusion direction and ~11 monomers (still based on length 12.35 Å) perpendicular to the extrusion direction. These microvoids will act as deep trapping sites in diffusion. When penetrants are sorbed into voids, they become virtually immobilized. Naturally, the observed diffusion rate will decrease.

Figure (28) shows three curves for sorption rates measured by the electrobalance. The changing of room conditions and the different time delays for transferring samples from the desiccator to the electrobalance correspond

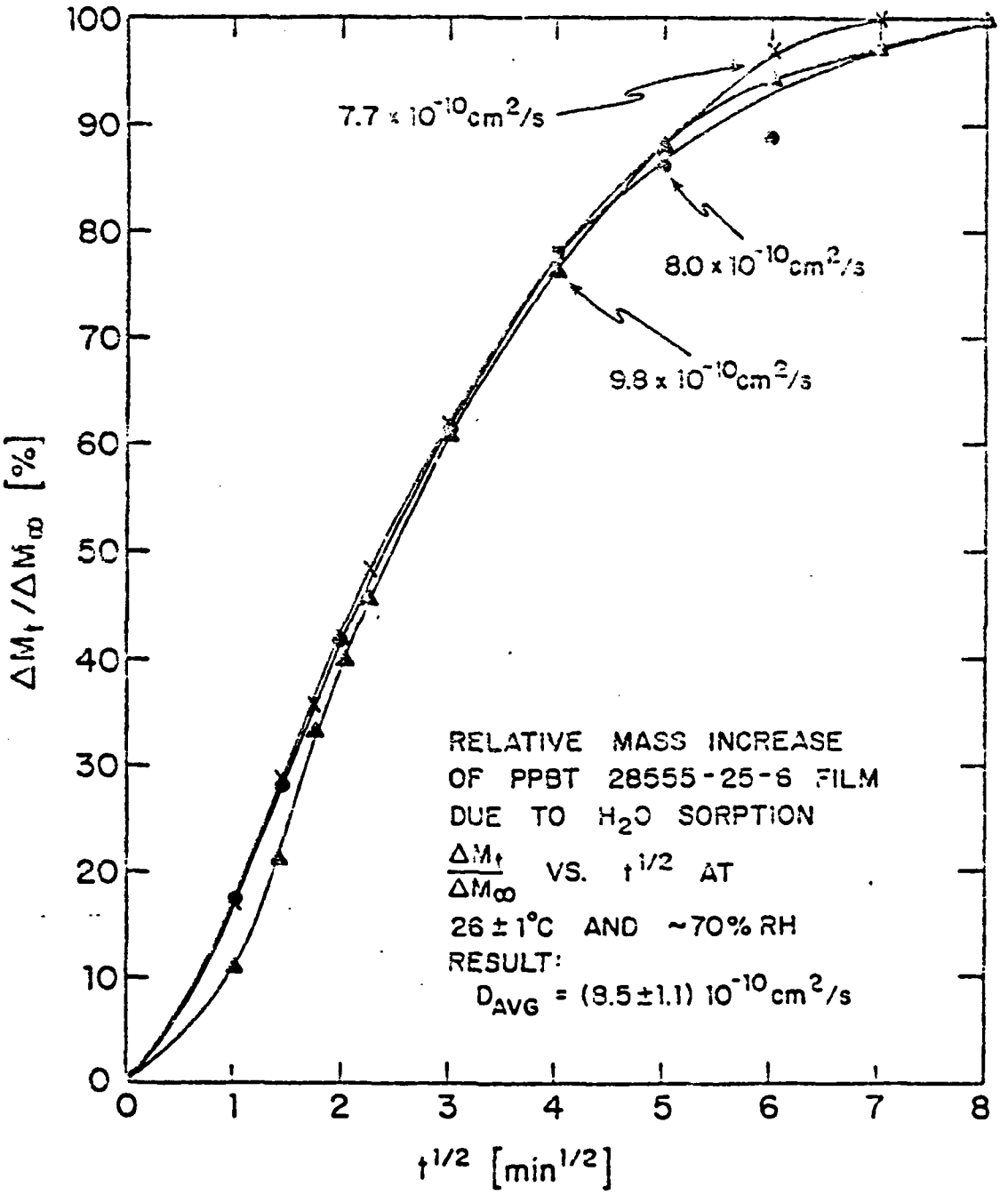

Fig. 28 Uncorrected curves of H_2O sorption in PPBT film

to the main reason for the curve shift. Another factor is the drifting of the electrobalance, which has been mentioned before. After calibration, the D value is 6.0×10^{-10} cm^2/sec (see Figure (29)) and solubility is 1.28×10^{-3}. Compare these values to the data from the quartz spring method which has $D = 1.79 \times 10^{-10}$ cm^2/sec and $s = 5.23 \times 10^{-3}$. (See Figure (30), (31)) The results are dramatically different. One is forced to inquire "What causes this difference?" There are some important differences in the way the experiments were done. The experiment with the electrobalance occurred in air with 70% humidity. On the other hand, the experiment in which the quartz spring was used is in vacuum initially and then has almost 100% humidity. But these factors would not be expected to make any big difference in the measured diffusion rates for normal rubbery polymers or other homogeneous polymer systems. Due to the fact that PPBT has lots of microcavities, a "dual sorption theory"[26] was introduced which enabled us to resolve the conflict. First, we assume, when the sample is measured in air, that the microvoids have been filled with air. Water will not be trapped in these voids. Then, we apply equation (66) from chapter II,

$$D_{eff} = D/1 + R$$

CALIBRATION CURVE OF H2O IN PPBT

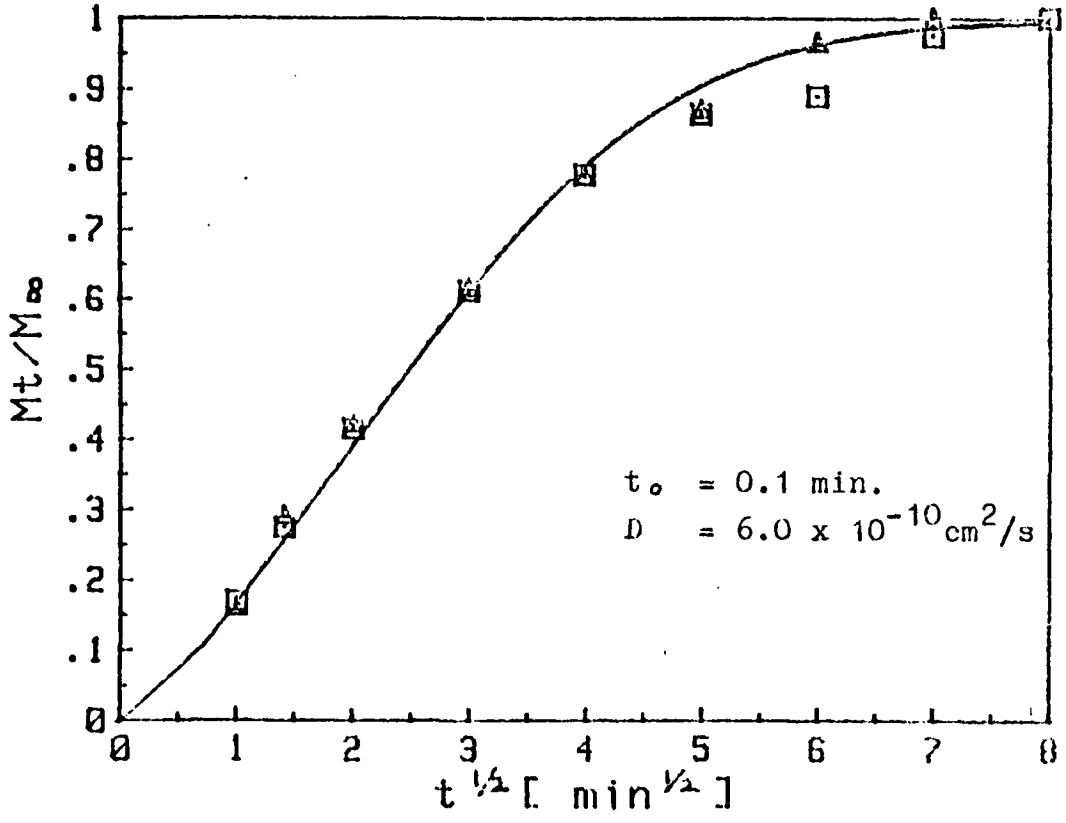

Fig. 29

SOLUBILITY COEFFICIENTS OF WATER IN PPBT

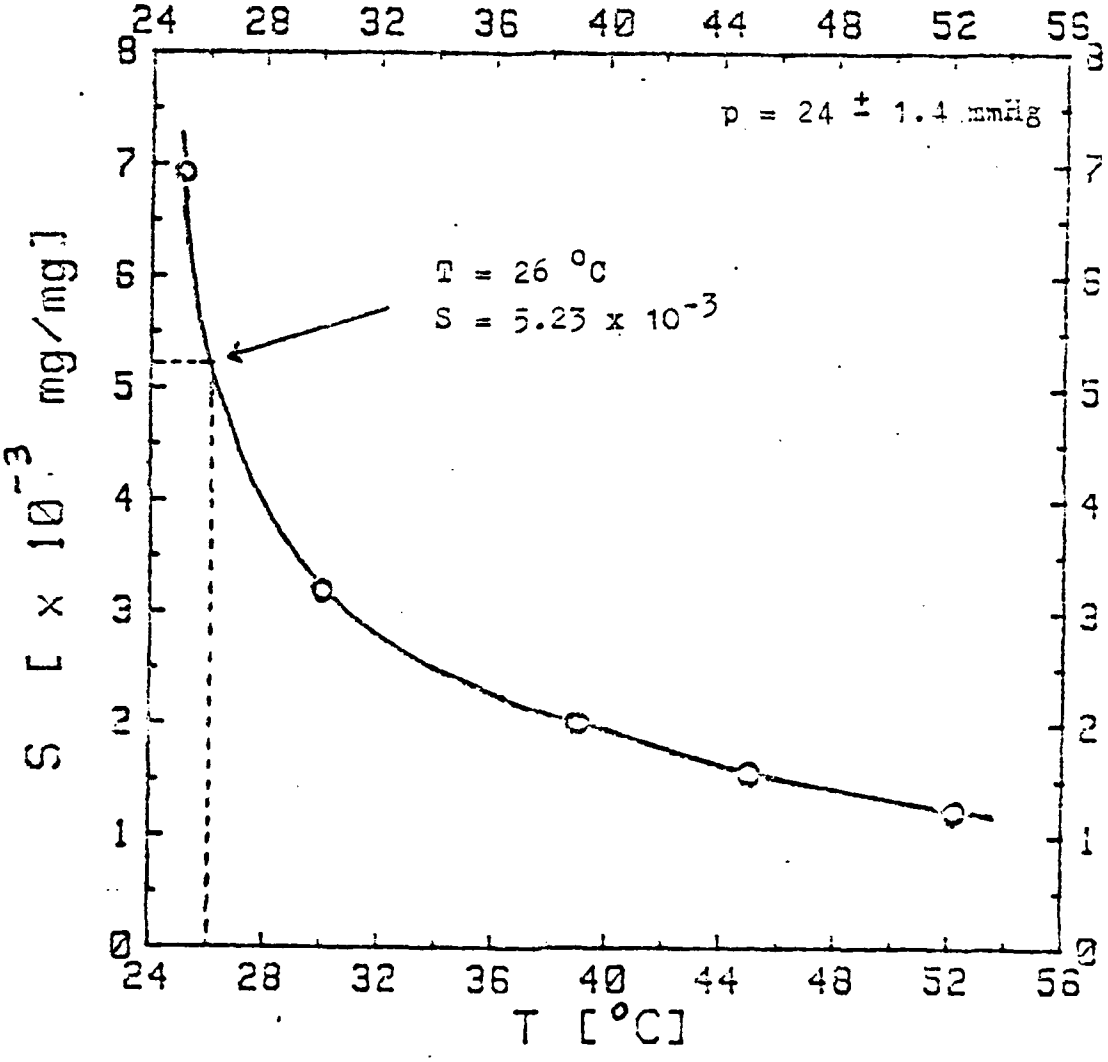

Fig. 30

TEMPERATURE DEPENDENCE OF D WATER IN PPBT

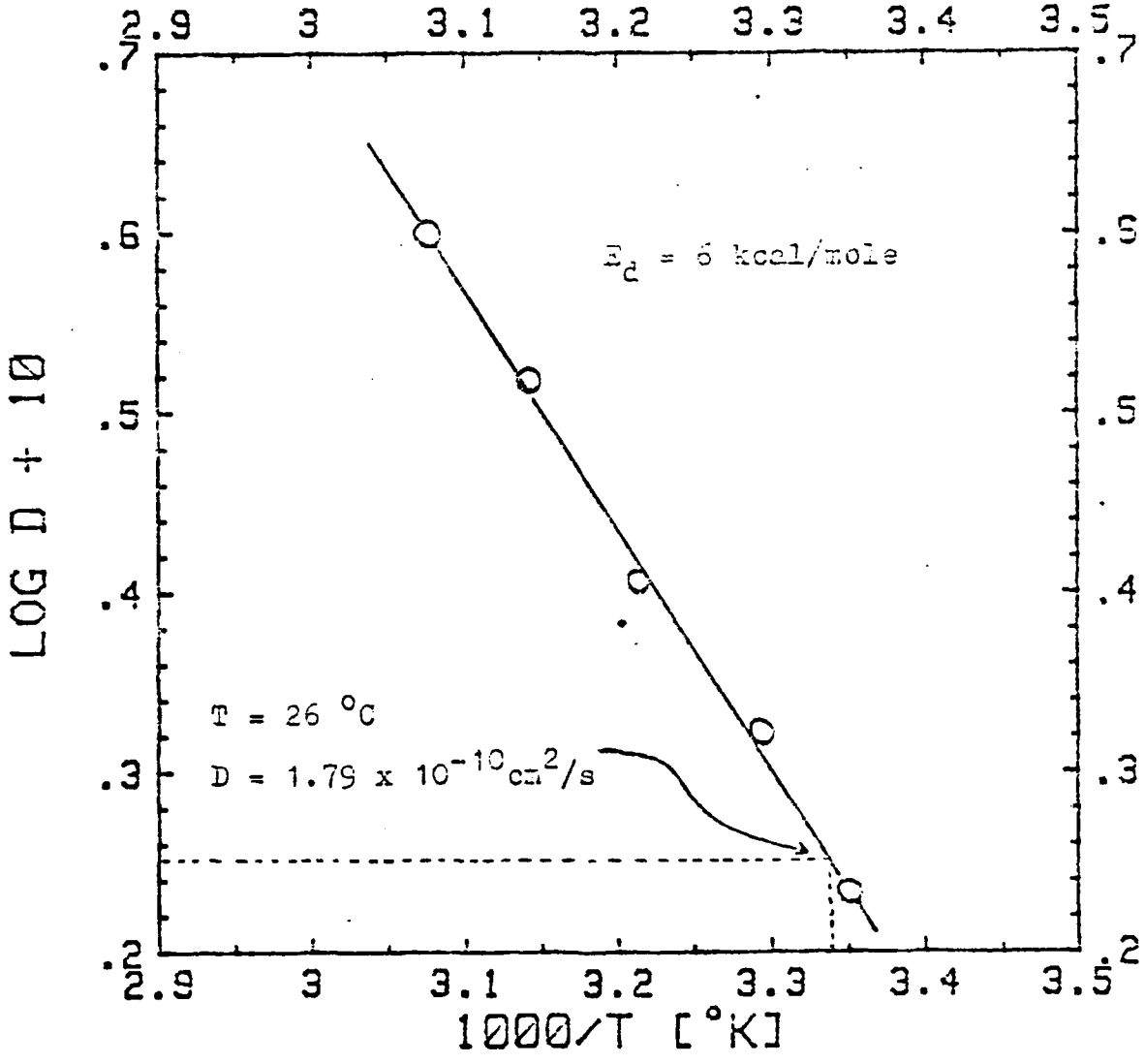

Fig. 31

Now $D_{eff} = 1.79 \times 10^{-10}$ cm^2/sec that is the value from the quartz spring and $D = 6.0 \times 10^{-10}$ cm^2/sec which is the value from electrobalance.

We can get

$$R = 2.35, \quad \text{where } R = bS_h'/K_d$$

then

$$bS_h' = 2.35K_d$$

In this case, the pressure is low so equation (58) is used.

$$C = (K_d + bS_h')p$$

$$= (K_d + 2.35)p$$

$$= 3.35K_dp$$

where $C = 5.23 \times 10^{-3}$ which is the solubility of H_2O in PPBT using the method of quartz spring. Therefore,

$$K_dp = 1.56 \times 10^{-3}$$

According to our assumption that water won't be trapped inside the microvoids by using the electrobalance. The solubility will follow Henry's law. So, the value can be calculated by putting 0.7p (because of 70% R.H. in room) into above equation.

$$K_d x(0.7p) = 1.09 \times 10^{-3}$$

Now, comparing this value to the experimental result, 1.28×10^{-3} from the electrobalance, the results are in reasonable agreement with each other. A little bit higher value from electrobalance implies that the microcavities still trapped some small quantity of water.

From the above demonstration, the water sorbed by microvoids at 25°C is approximately 3.67×10^{-3}. That corresponds to 3.54×10^{-2} mg. If the water were in the liquid phase, the volume should be 3.54×10^{-5} cm^3. Dividing by the sample volume (6.24×10^{-3} cm^3) yields the volume ratio 5.67×10^{-3}. Obviously, the water is not saturated in the voids unless the vapor pressure is very high. Consequently, the voids volume should be much bigger than this amount. That is voids volume > 5.67×10^{-3} (0.567 v/o).

B. Activation Energy Relates to Rotation Energy of Chain Segment

PPBT film is anisotropic in structure. Thomas, Farris, Hsu et al. of the University of Massachusetts[2] analyzed the wide angle electron diffraction pattern and proposed two probable monoclinic unit cells

Cell I Monoclinic	Cell II Monoclinic
$a' = 5.83$ Å	$a = 7.10$ Å
$b' = 3.54$ Å	$b = 6.65$ Å
$c' = 12.35$ Å	$c = 12.35$ Å
$\gamma = 96°$	$\gamma = 63°$
$z = 1$	$z = 2$

The proposed arrangement of PPBT in its crystal structure is shown as Figure (32). How does this relate to diffusion? According to the molecular model proposed by DiBenedetto and Paul[20] the activation energy for diffusion is related to the variation in the average potential energy of molecular interaction which accompanies a volume change of $\lambda n(\pi/4)r_g^2$.

Pace and Datyner,[22] following this idea, proposed a statistical mechanical model in which the activation energy is related to the bending energy and Van der Waals energy for producing a separation d between the surfaces of adjacent chains where d is the diameter of the diffusant. Both theories point out that the activation energy for diffusion is the energy necessary to produce and effective volume large enough to accommodate the diffusant. Now, we are dealing with a polymer which has flat rigid chain segments. (See Figure (33)). It displays the possibility of rotation on the two single bonds. According to the

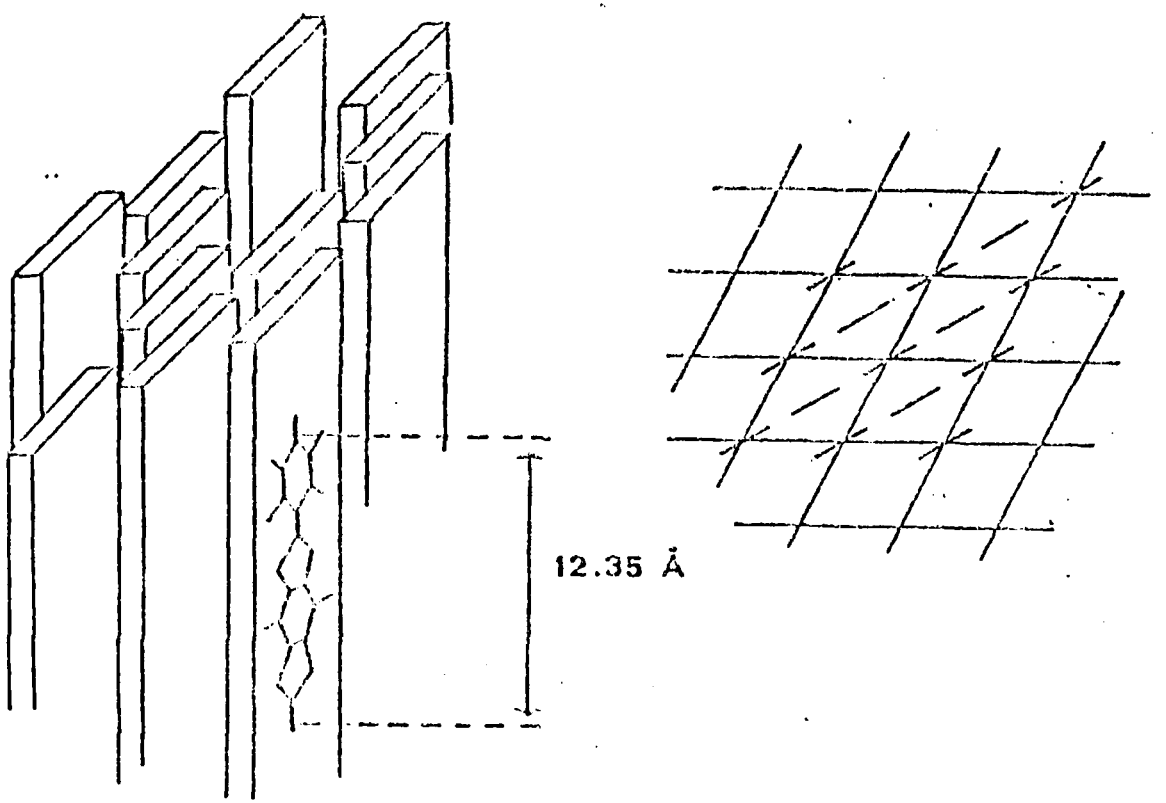

Fig. 32 Schematic of the proposed arrangement of PBT molecules in a crystallite.[2]

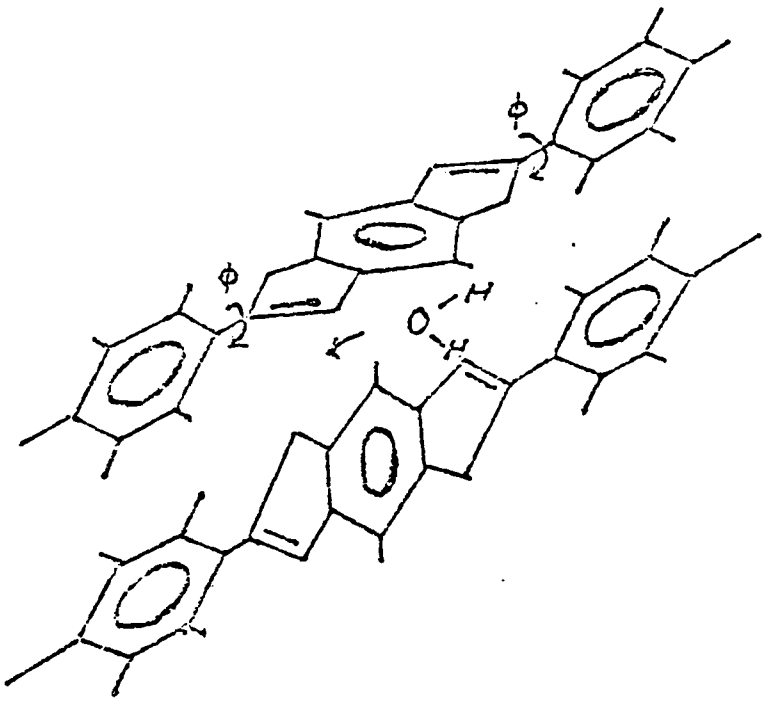

(a) Mechanism of rotating one chain segment to accomodate water molecule.

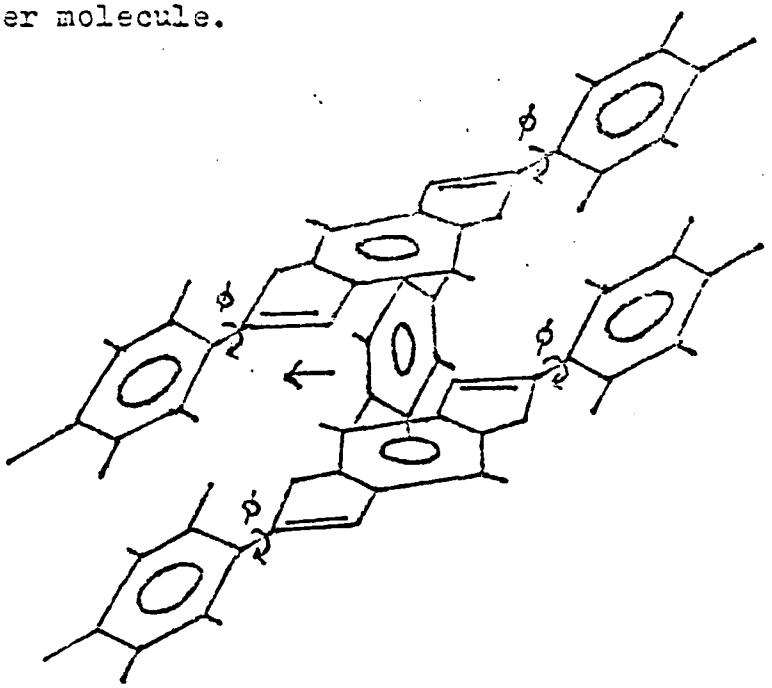

(b) Mechanism of rotating two chain segments to accomodate benzene molecule.

Fig. 33

report of J. E. Mark, et al. of the University of Cincinnatti, that the ring groups freely rotate to 20° from the origin. The activation energy is 2 kcal/mol. If it rotates to 90°, the rotation energy is 6 kcal/mol. The activation energy for H_2O diffusion in PPBT is 6 kcal/mol and that for benzene diffusion is 12 kcal/mol. (See Figure (31), (34)). This implies a diffusion mechanism as suggested in Figure (33). H_2O needs only one chain segment to rotate 90° for it to pass through; however, benzene needs both chain segments to rotate 90° for it to get through. If one remembers the discussion in the previous section of how microcavities affect diffusion, it can be seen that the activation energies measured are not the true values. The effective diffusivity $D_{eff} = D/1 + R$ will change with R. If R decreases when temperature increases, the measured effective activation energy will be higher than it supposed to be. Generally, this is the tendency that $d\ln b/d(1/T)$ higher than $d\ln K_d/d(1/T)$. Consequently, this will cause an abnormal high negative enthalpy of solution. Figure (35) and (36) show the evidence for this.

C. Interpretation of Coefficients

The sample of PPBT has a very rough surface, uneven thickness, voids, and impurities. Rough surface and uneven

ARRHENIUS PLOT OF BENZENE IN PPBT

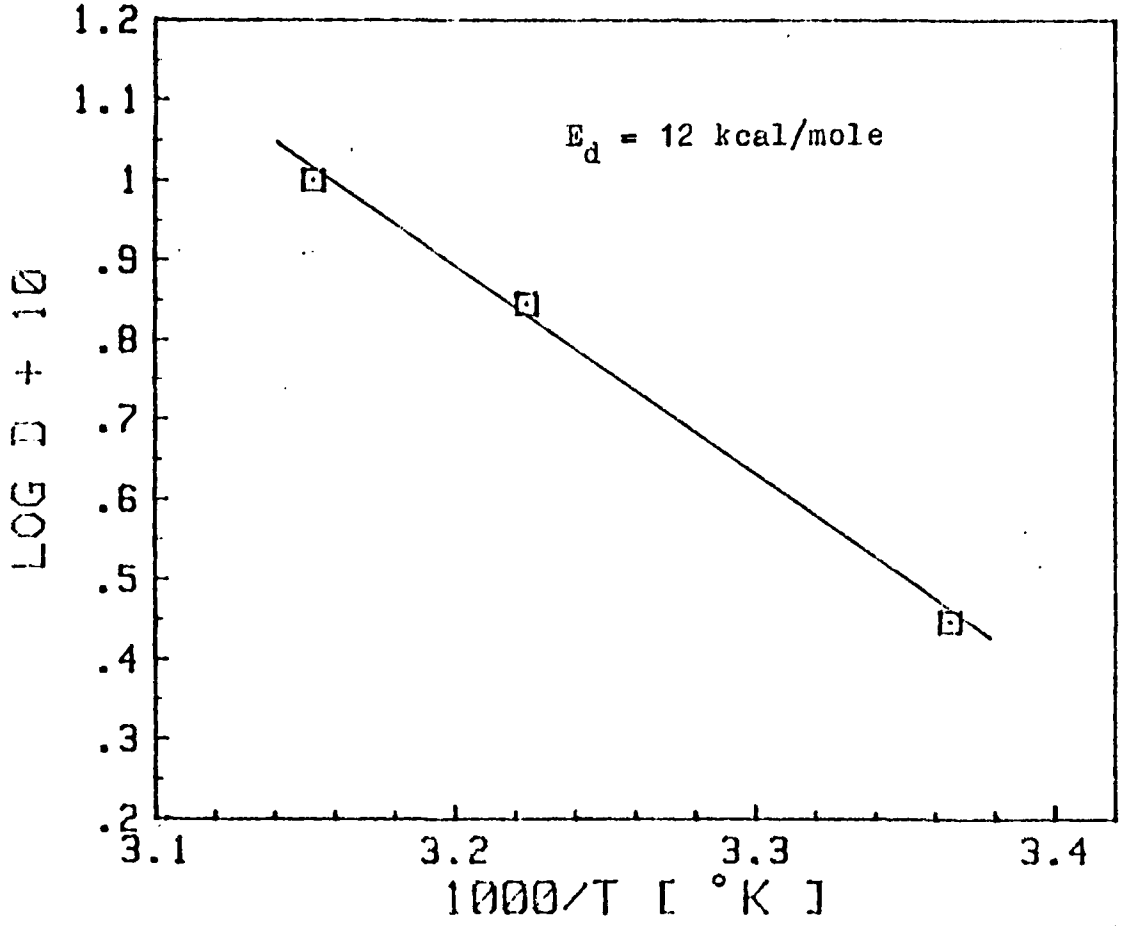

Fig. 34

SOLUBILITY OF BENZENE IN PPBT

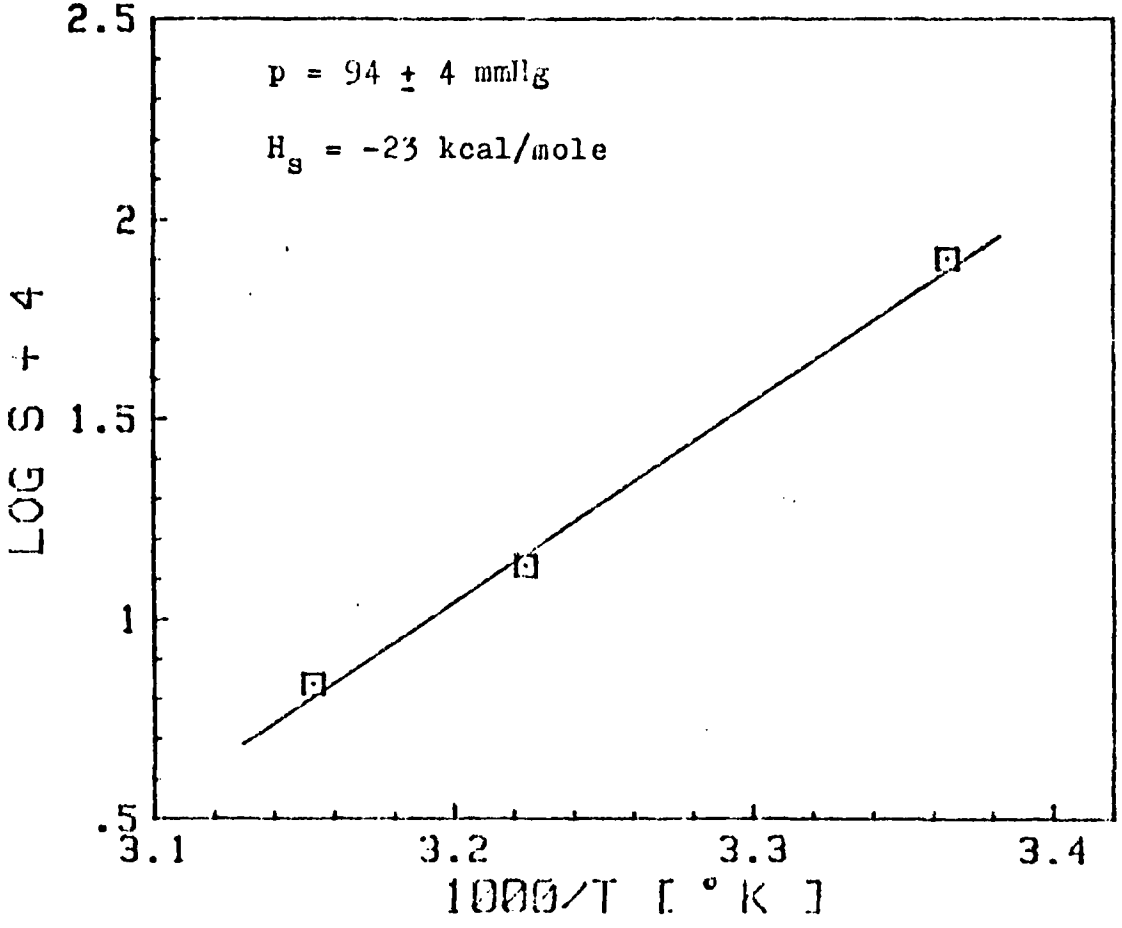

FIG. 35

SOLUBILITY COEFFICIENTS OF WATER IN PPBT

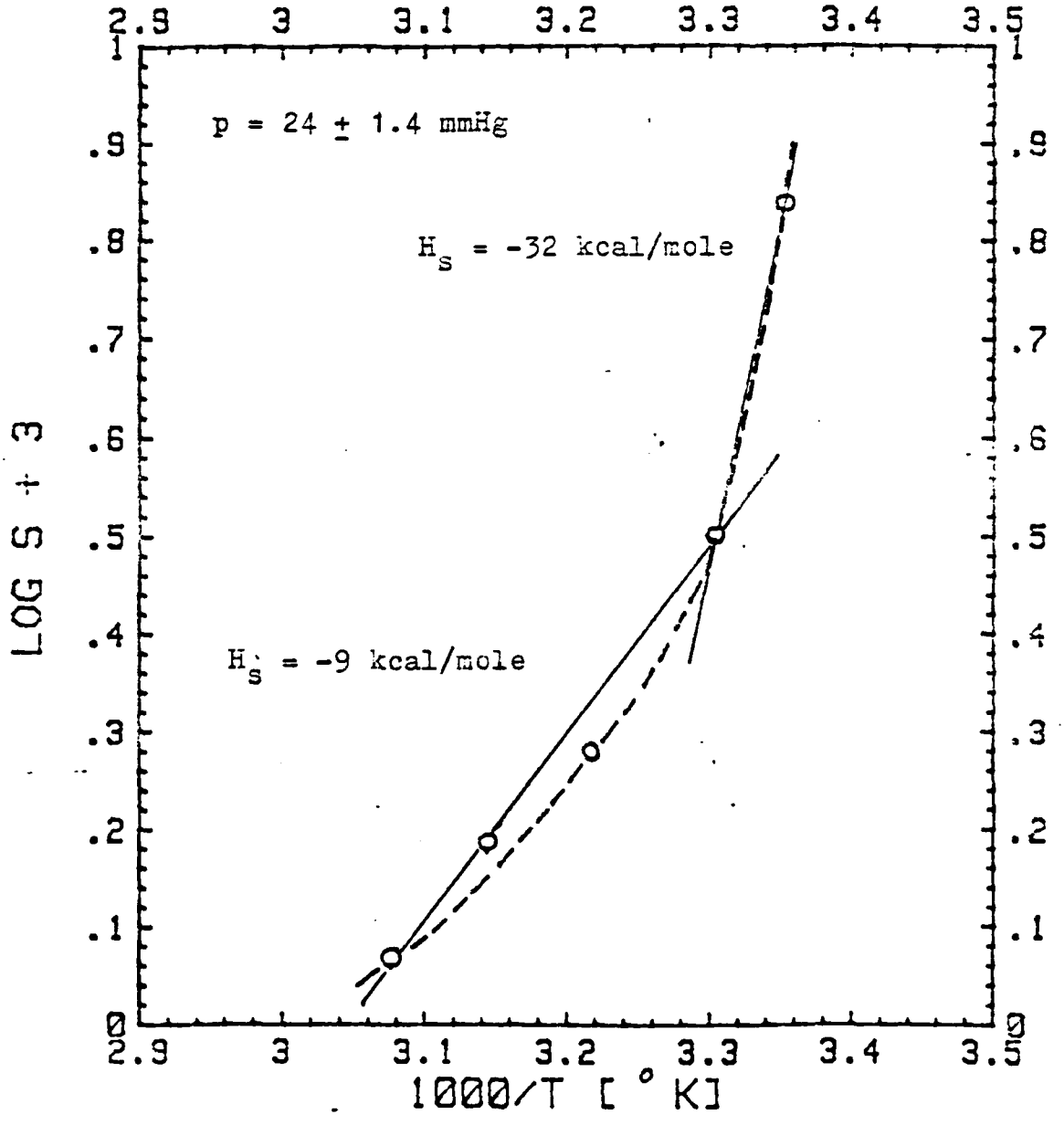

Fig. 36

thickness can even be seen by the naked eyes. Voids have been studied by using small angle X-ray scattering patterns. That voids exist in substantial amounts also has been supported by previous discussion in this thesis. The probable impurities in PPBT are residual methane sulfonic acid (or PPA which has been found in EDAX in this thesis) and other impurities which could be introduced in the synthesis procedure. All these effects will shift the diffusion character significantly from the theoretical predictions of well dimensioned pure samples. Table I gives the coefficients of water, benzene, and ethanol. The lack of enough experimental data on ethanol is because the solubility of ethanol is too low to be detected at high temperature. The temperature-dependence of the solubility coefficient includes the heat of condensation and the heat of mixing. In our case, the Langmuir isotherm of solution in pre-existing cavities also exists. The abnormal enthalpy of solvation is mainly attributed to the $S_h'b$ quantity which is the hole filling term in $S = (K_d + bS_h')p$ as discussed in chapter II. The order of solubility coefficients in terms of mole numbers is water > benzene > ethanol. In contrast, the diffusion coefficients at room temperature have the order as ethanol > benzene > water. If we recall that $D_{eff} = D/(1 + (bS_h'/K_d))$ and $S = (K_d + bS_h')p$, it is obvious

	Water	Benzene	Ethanol
E_d(kCal/mole)	6	12	∿
D(cm^2/sec)	$1.71x10^{-10}$ (25°C)	$2.8x10^{-10}$ (24°C)	$1.1x10^{-9}$ (24°C)
H_s(kCal/mole)	-9 (high T) -32 (low T)	-23	∿
D_o(cm^2/sec)	$4.28x10^{-6}$	0.188	∿
S(mg/mg)	$6.93x10^{-3}$ (25°C) (24±1.4mmHg)	$7.99x10^{-3}$ (24°C) (94±4mmHg)	$1.48x10^{-3}$ (24°C) (55±1mmHg)

Table I

Diffusion Data of PPBT (28555-25-6) Film.

that the higher the bS_h' value the higher the S value, but the lower D_{eff} value. If we further assume that S_h' is the same for these three species, it will imply that the forces between polymer surface and diffusants are in the order water > benzene > ethanol. Figures (37)-(43) are diffusion curves for the three vapor species studied. The solid curves represent theoretical values. All data display a negative deviation in the long time region. This is the behavior of a concentration dependent diffusion rate. Again, microcavities are responsible as will be demonstrated below.[5] The flux of penetrant is only due to mobile molecules, not trapped ones, therefore

$$J = -D(C)\partial C/\partial x$$

$$= -D_1(C)\partial C_1/\partial x \qquad (75)$$

where C is the overall concentration, the suffix 1 refers to mobile molecules. We find $D(C) = D_1(C)\partial C_1/\partial C$. If the immobilized molecules are sorbed according to a Langmuir model and the mobile molecules according to Henry's law, then

$$C_2 = C_1/(\alpha + \beta C_1) \qquad (76)$$

where C_2 denotes the concentration of immobile molecules.

DIFFUSION CURVE OF ETHANOL IN PPBT AT 24° C

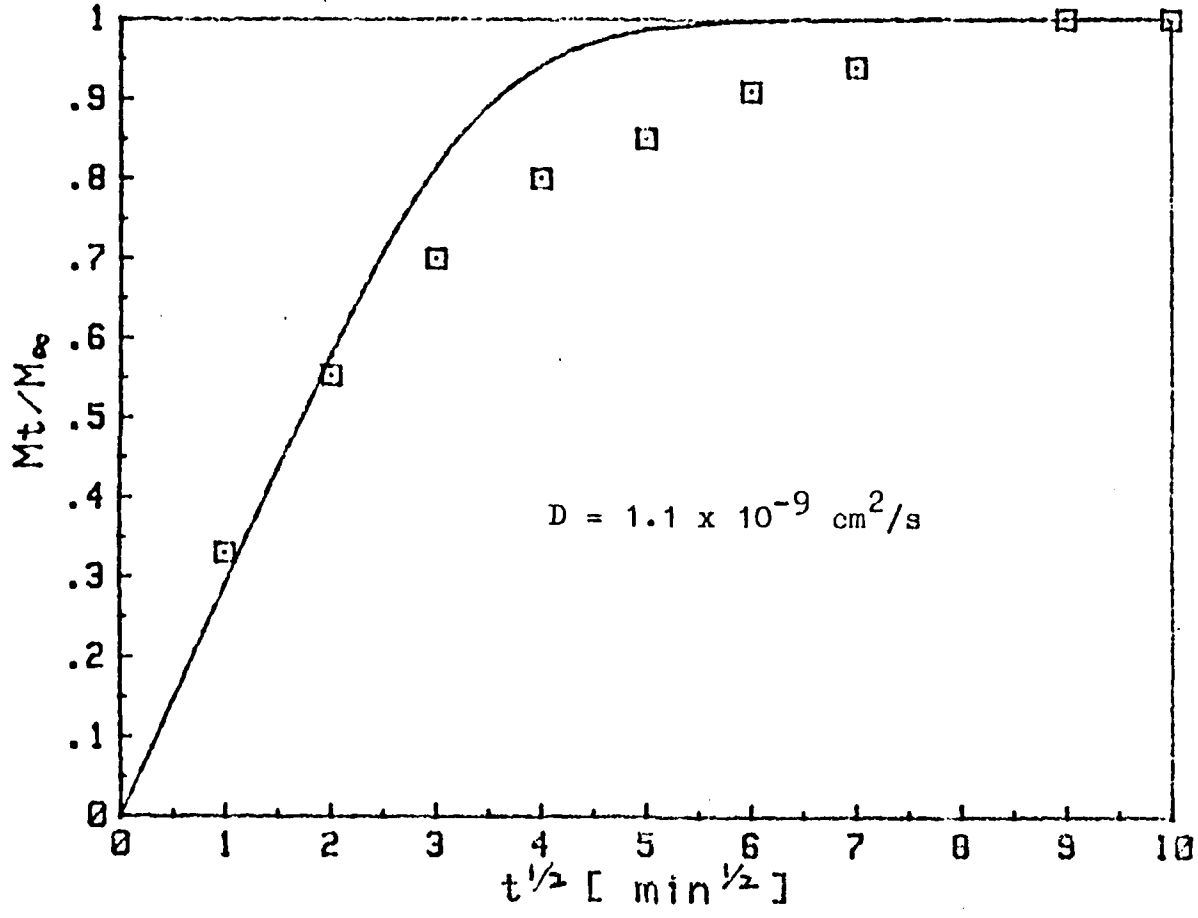

Fig. 37

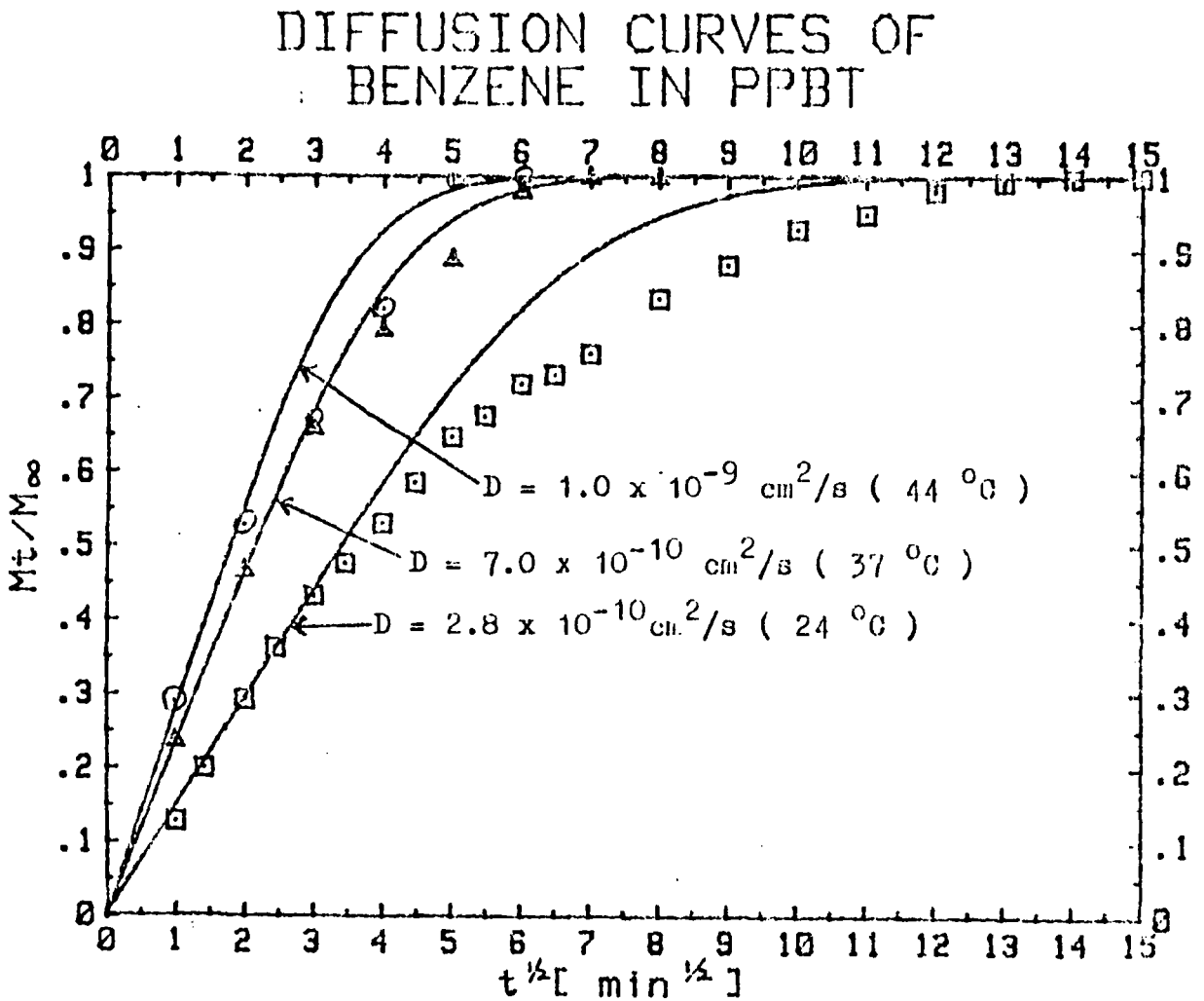
DIFFUSION CURVES OF
BENZENE IN PPBT
Mt/M∞
t½[min½]
D = 1.0 x 10-9 cm2/s (44 °C)
D = 7.0 x 10-10 cm2/s (37 °C)
D = 2.8 x 10-10 cm2/s (24 °C)

Fig. 38

EXPERIMENTAL CURVES COMPARED TO THEORETICAL CURVES

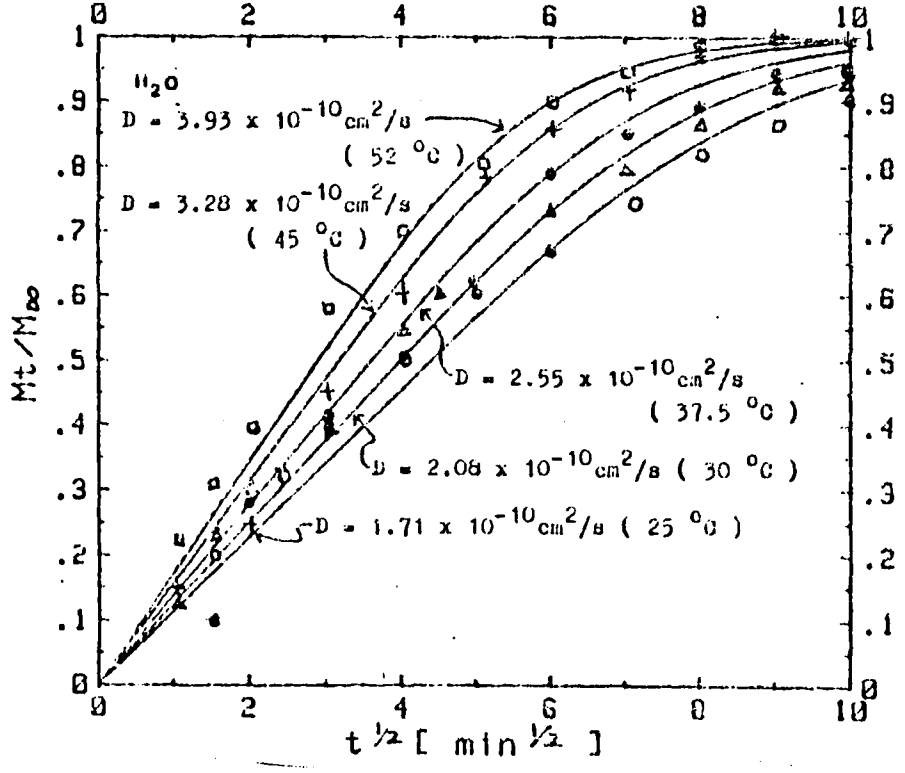

Fig. 39

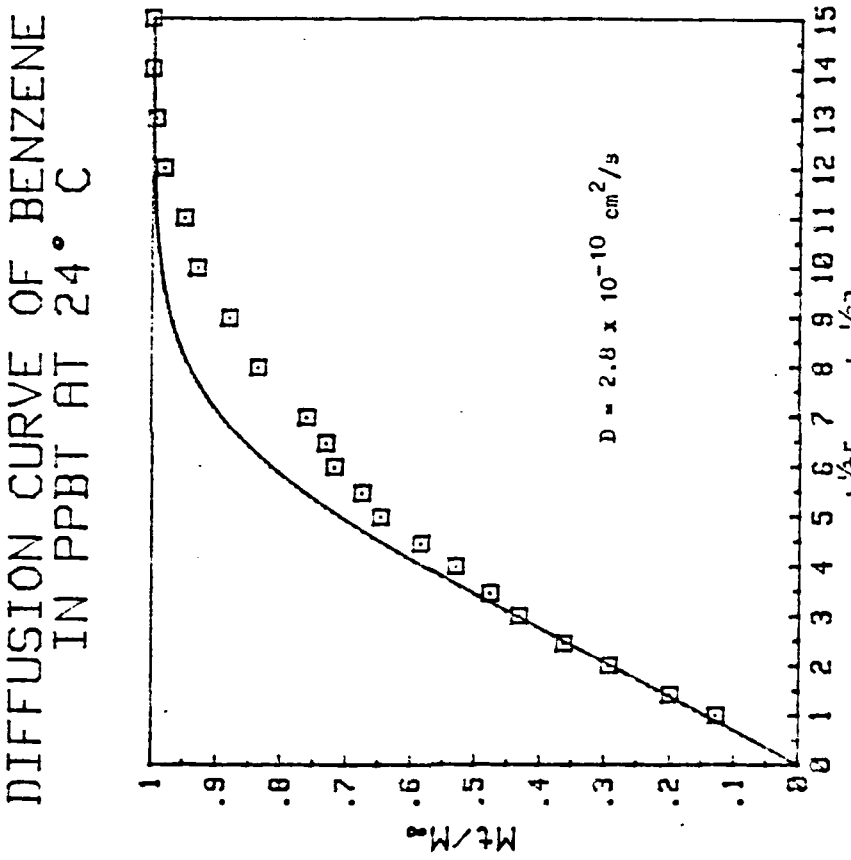
DIFFUSION CURVE OF BENZENE
IN PPBT AT 24° C
Mt/M∞
1
.9
.8
.7
.6
.5
.4
.3
.2
.1
0
0 1 2 3 4 5 6 7 8 9 10 11 12 13 14 15
t½[min½]
D = 2.8 x 10⁻¹⁰ cm²/s

Fig. 40

DIFFUSION CURVE OF BENZENE IN PPBT

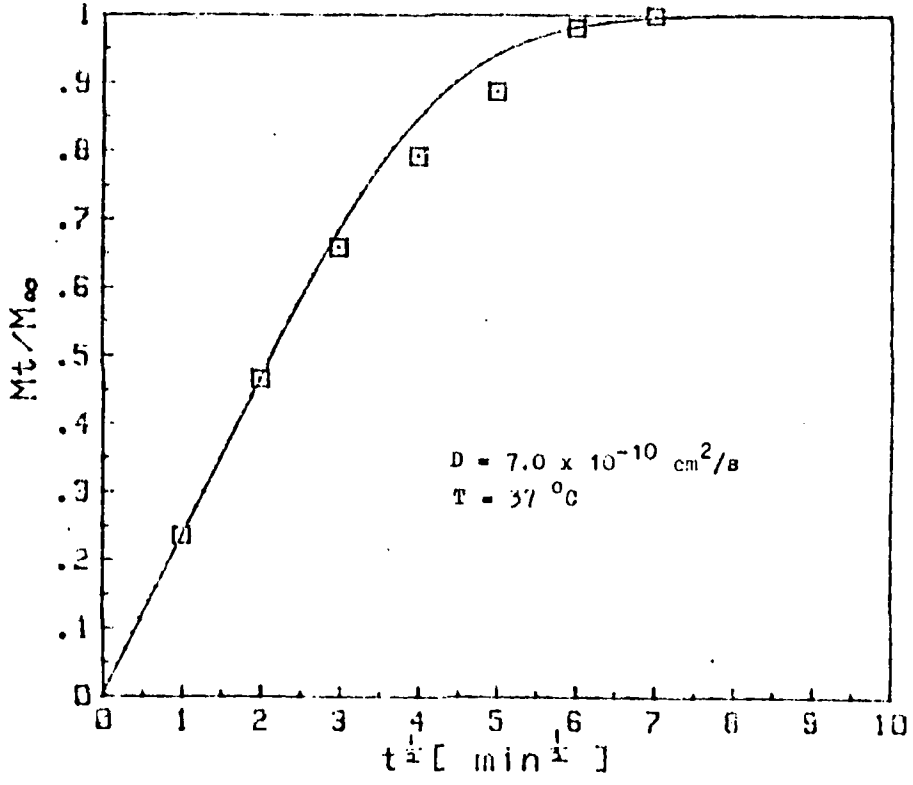

Fig. 41

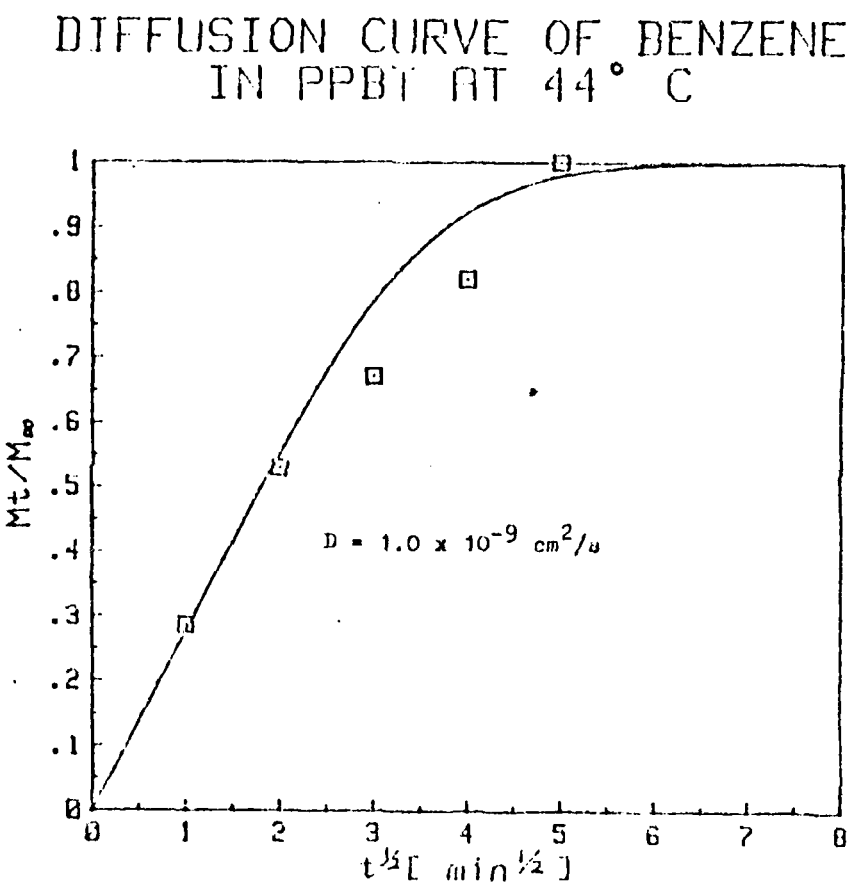
DIFFUSION CURVE OF BENZENE
IN PPBT AT 44° C
Mt/M∞
D = 1.0 x 10⁻⁹ cm²/s
t½[min½]
0
.1
.2
.3
.4
.5
.6
.7
.8
.9
1
0
1
2
3
4
5
6
7
8

Fig. 12

EXPERIMENTAL CURVE COMPARED TO THEORETICAL CURVE

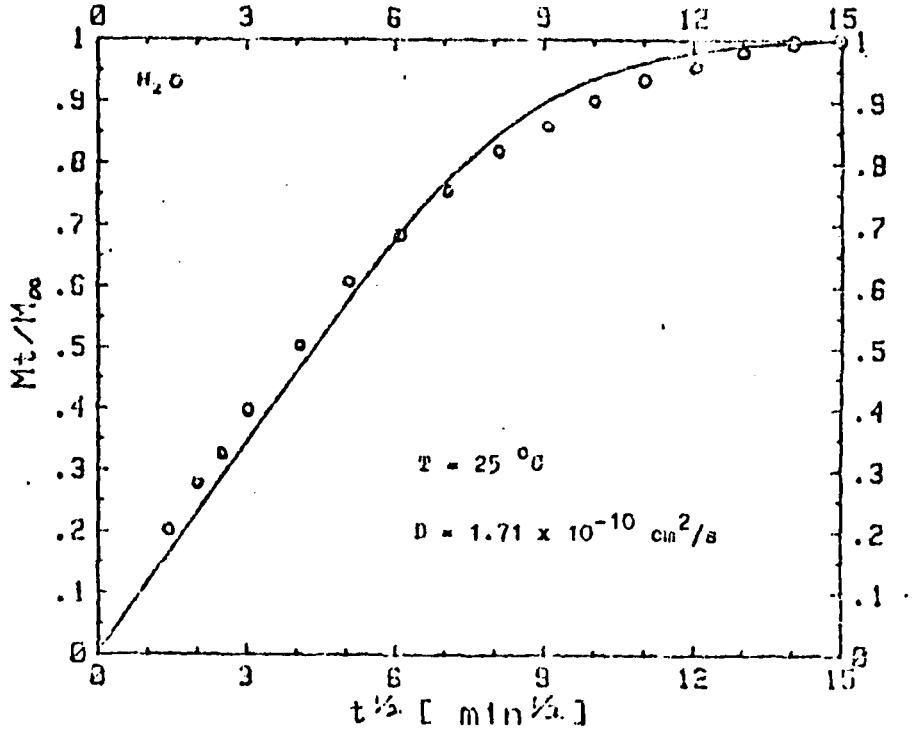

Fig. 43

If $C_2 >> C_1$ then

$$\partial C/\partial C_1 = \alpha/(\alpha + \beta C_1)^2 \qquad (77)$$

and so

$$D(C) = D_1(C)\alpha/(1 - \beta C)^2$$

This simple model leads to a diffusion coefficient which increases with concentration.[38] Thus, the doped materials acting as traps inside PPBT give the same effect. This phenomenon also was observed in this experiment.

Figure (44) displays the sorption and desorption curves of H_2O in PPBT. The curves are sigmoid in shape while the desorption curve crosses the sorption curve twice before equilibrium is reached. This sort of behavior which is described as anomalous or "non-Fickian" has been reported, for instance, in the sorption of water by cellulose (Newns, 1956),[39] Keratin (King, 1945)[40] and vinyl alcohol (Long and Thompson, 1955).[41]

The water remaining inside PPBT in the desorption procedure is 1.02×10^{-3} mg/mg.

D. Effect on D of Doping Salt

As mentioned in chapter II (part G) relative to ionic conductivity, water will enhance the dissociation of ionic

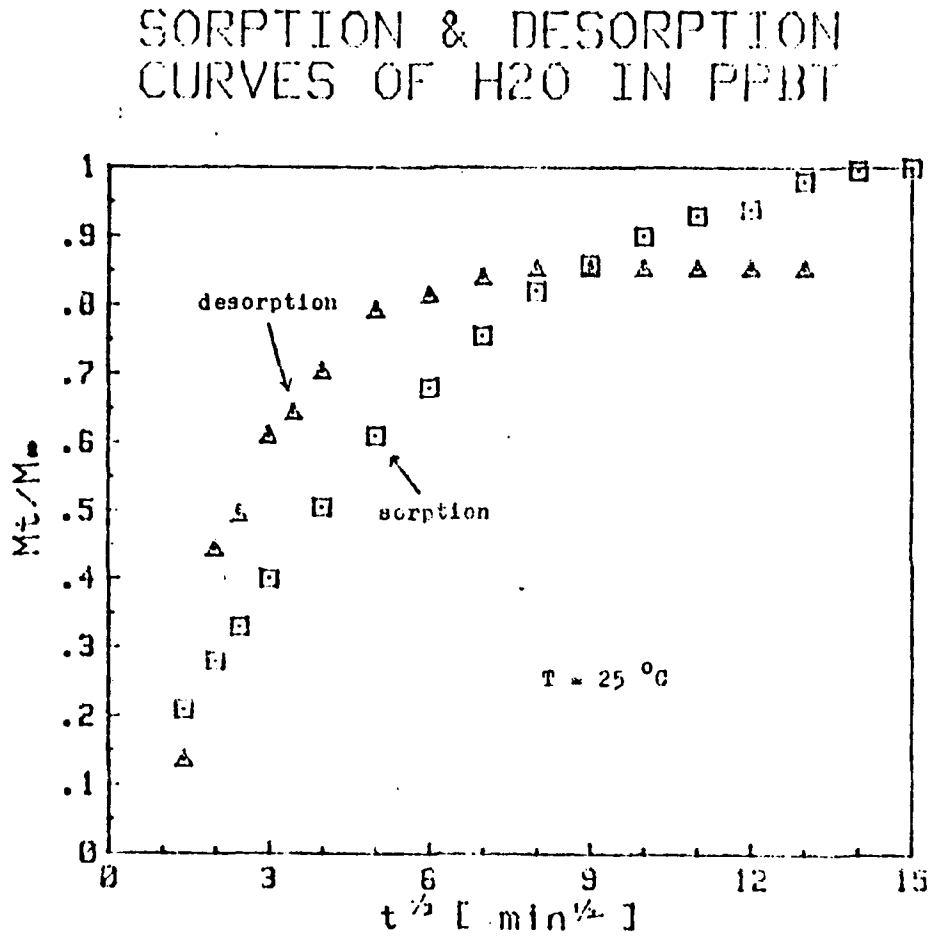
SORPTION & DESORPTION
CURVES OF H2O IN PPBT
desorption
sorption
T = 25 °C
Mt/M∞
t ½ [min½]
0
.1
.2
.3
.4
.5
.6
.7
.8
.9
1
0
3
6
9
12
15

Fig. 44

impurities into anions and cations, and consequently increase the conductivity. Will any impurities in polymers affect diffusion? Yes, this is demonstrated by measurements on the sorption characteristic of PPBT films soaked for 2 days in 1 molar salt solutions of three nitrates ($Fe(NO_3)_3$, $Co(NO_3)_2$, $Ni(NO_3)_2$) and two chlorides ($CaCl_2$, LiCl). PPBT samples were immersed in 1 molar salt solutions for two days and rinsed in distilled water before being dried. The dried samples were measured by the electrobalance. From the rates at which the weight increased, diffusion coefficients were determined (Figure (45), (46)). A plot of logD vs the charge to radius ration q/r came out to be a straight line (Figure (47)). This may be described by the following equation

$$\log D = 0.214q/r - 9.592 \qquad (78)$$

where q = the electric charge of cation

r = crystal ionic radius

The constant -9.592 corresponds to $D = 2.56 \times 10^{-10}$ cm^2/sec. This value is very close to the diffusion coefficient of water in pure PPBT using the quartz spring. It suggests that the ions are mainly in microcavities.

Let us consider any rate constant K can be expressed as an Arrhenius equation $K = Ae^{-E/RT}$, then $\ln K = \ln A - E/RT$

DIFFUSION CURVES OF H2O IN NITRATE DOPED PPBT

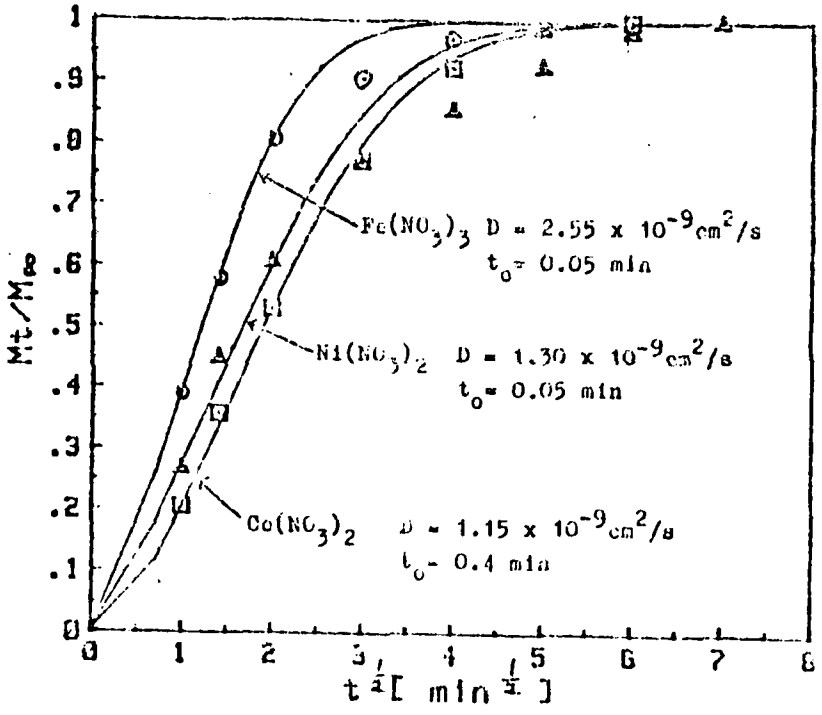

Fig. 15

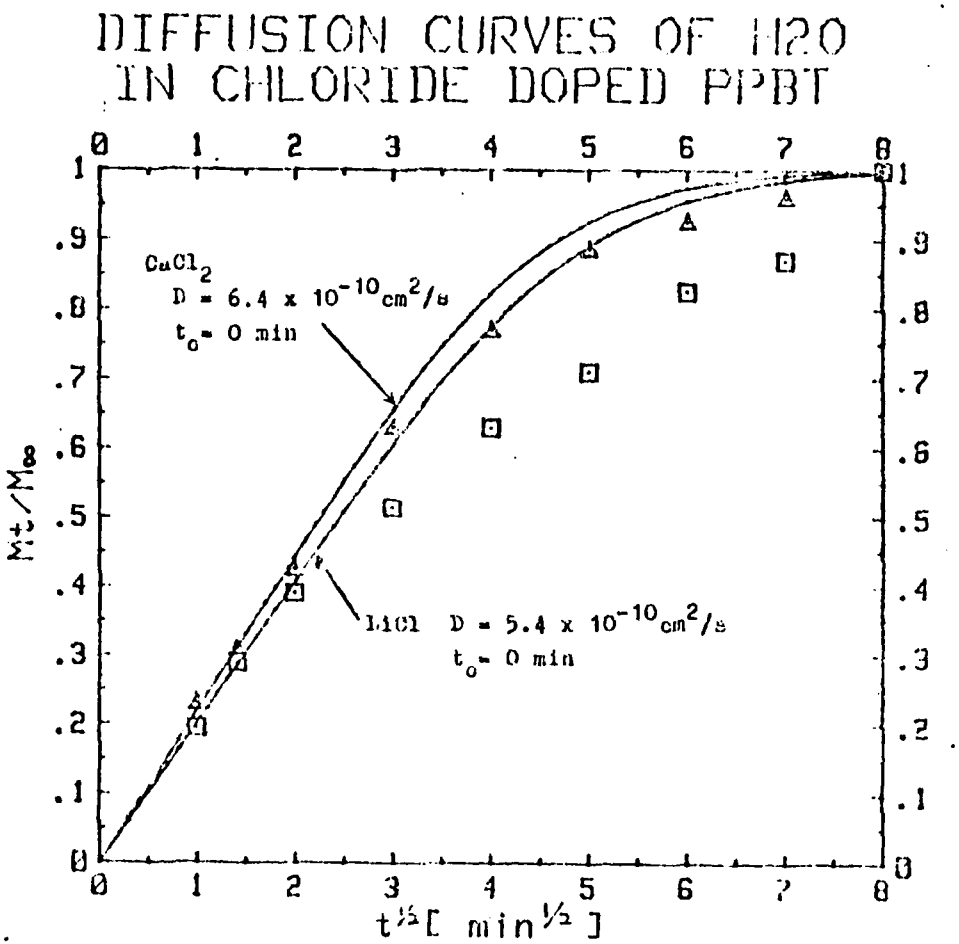
DIFFUSION CURVES OF H2O
IN CHLORIDE DOPED PPBT
CuCl2
D = 6.4 x 10-10cm2/s
to= 0 min
LiCl D = 5.4 x 10-10cm2/s
to= 0 min
Mt/M∞
t½[min½]
0 1 2 3 4 5 6 7 8
0 .1 .2 .3 .4 .5 .6 .7 .8 .9 1

Fig. 46

CATIONS EFFECT ON DIFFUSION RATE

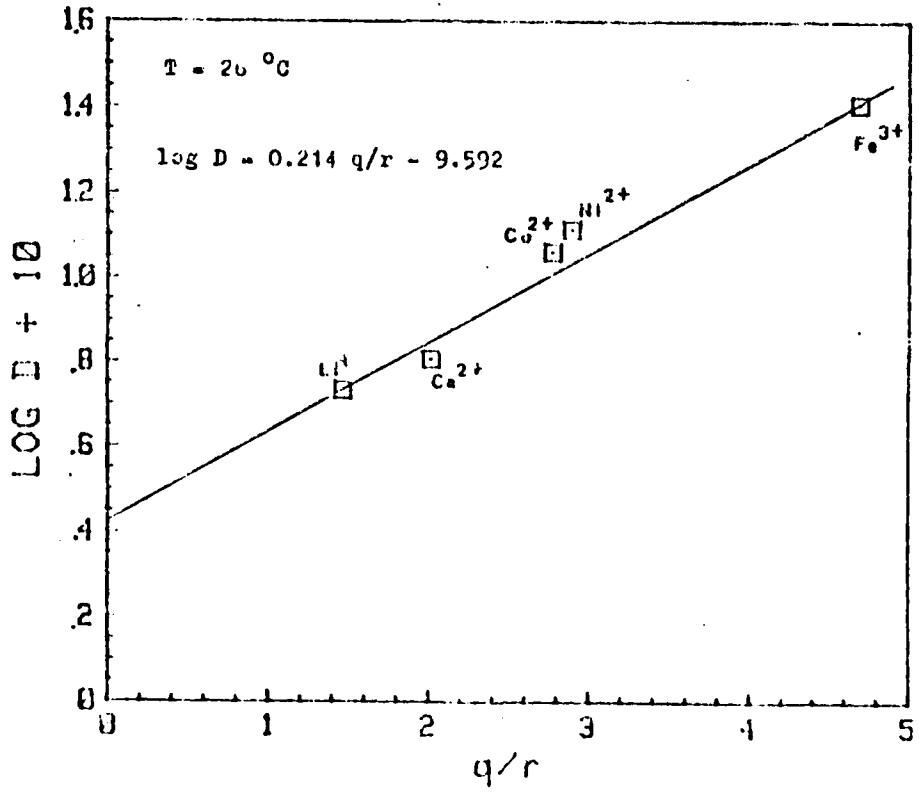

Fig. 47

compare this to equation (78), we find that if water acts on another negative charge $-q_w$ then $-qq_w/r$ correlates to the energy term E. Thus, the Diffusion rate is attributed to the reaction between water and cations. Also, the diffusion rate is directly proportioned to the electrical potential fields of cations. One experiment done by Takamatsu[42] about sorption phenomena in Nafion Membranes is described: during the neutralization process which cations replaced H^+ in $SO_3^-H^+$ site, the coefficients D of several cations were determined and logD was related linearly to q/a, where a is the separation distance between centers of charge of the cation and anion. This observation might have the same reason as ours.

E. Possible Interaction of Doped Salt with Polymer

There is a very important matter for organometallic chemistry, called the "sixteen and eighteen electron-rule."[43] According to this rule, stable organometallic compounds of the transition metals will have a total 18 valence electrons about the metal; in other words, they will have the "effective atomic number" (EAN) of the next higher inert gas. Molecules having only 16 valence electrons can often be just as stable as 18". In general, organic complexes of the transition metals are formed with those metals in low

oxidation states, since it is only in that condition that the metal will have populated orbitals of π symmetry and a low z^* to allow metal to ligand π electronic flow. Thus, the preferred oxidation states are Fe^{2+}, Co^{+}, Ni^{O}. Unfortunately, these are not the ones in our case. But, possible reactions will happen, if reduction of metal ions occurs.

Diffusion rates were measured repeatedly. (Figure (43)-(50), Tables II-V). Since the room conditions changed and due to the limited sensitivity of instrument, it is still not possible to make final conclusions. However, it is obvious that the diffusion rates decreased to some extent. The sample weight decreased somewhat and in some cases, even appeared to become lower than that of the original dry sample.

F. Discussion on Morphology and Anisotropic Character.

If diffusion in PPBT is a process of mass transport along the interchain channels, then the diffusion rate should be sensitive to the morphology of the polymer. It is then necessary to analyze the relation between morphology and diffusion.

According to Edwin L. Thomas et al.,[2] the PPBT fiber can be peeled and mildly sonicated into thinner and thinner ribbonlike fibrils. Each of these fibrils appears to

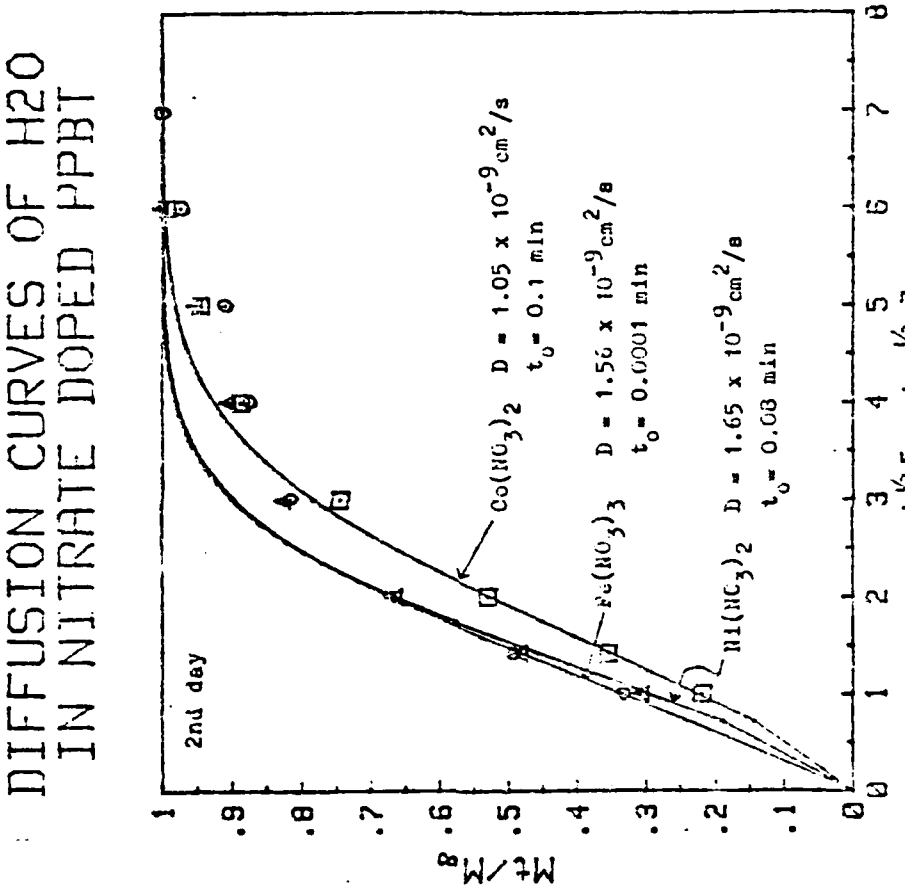
DIFFUSION CURVES OF H2O
IN NITRATE DOPED PPBT
2nd day
$Co(NO_3)_2$ D = 1.05 x 10^{-9} cm^2/s
t_o = 0.1 min
$Fe(NO_3)_3$ D = 1.56 x 10^{-9} cm^2/s
t_o = 0.0001 min
$Ni(NO_3)_2$ D = 1.65 x 10^{-9} cm^2/s
t_o = 0.08 min
M_t/M_∞
$t^{1/2}$[min$^{1/2}$]

Fig. 48

DIFFUSION CURVES OF H2O IN NITRATE DOPED PPBT

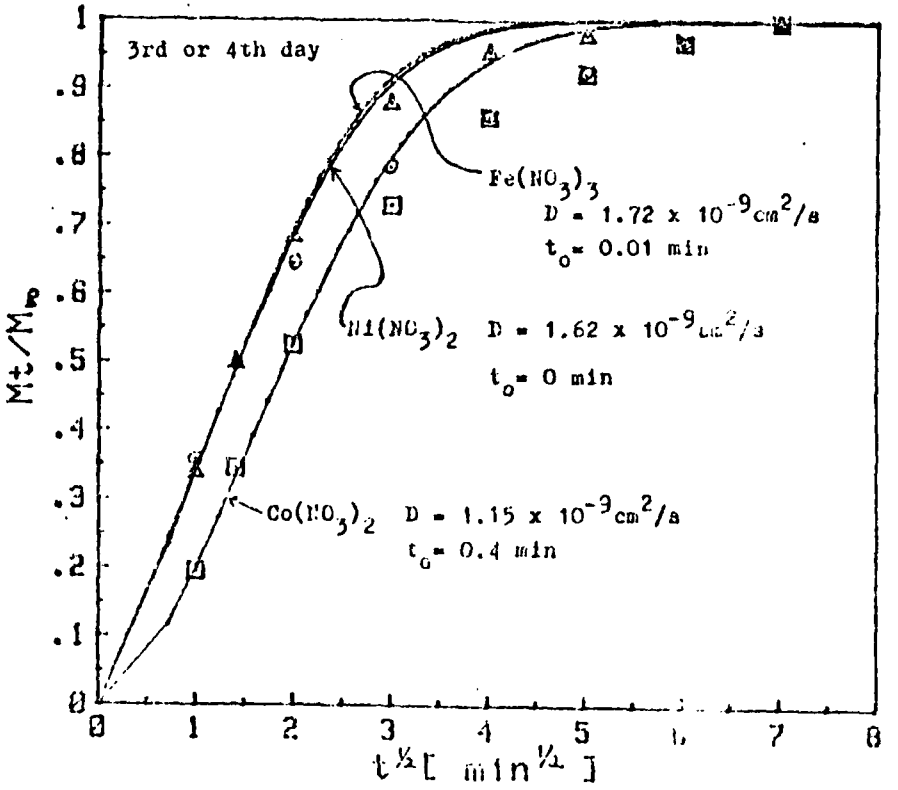

Fig. 49

DIFFUSION CURVES OF H2O IN NITRATE DOPED PPBT

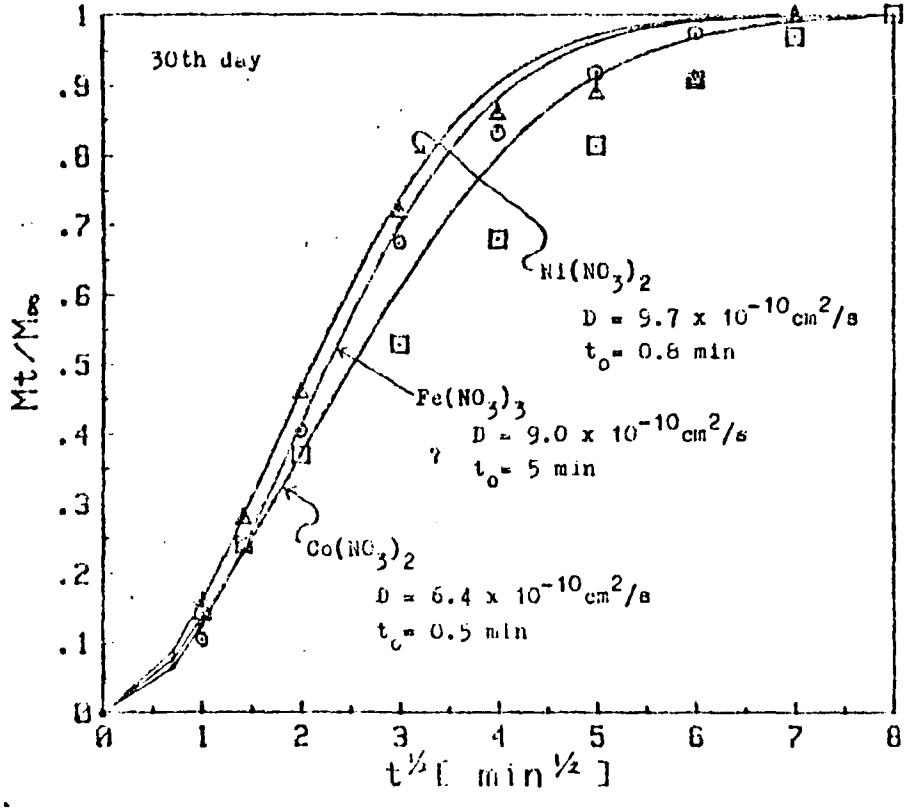

Fig. 50

	$Fe(NO_3)_3 \cdot 9H_2O$	$Co(NO_3)_2 \cdot 6H_2O$	$Ni(NO_3)_2 \cdot 6H_2O$
1st day (79% R.H.)	2.23×10^{-3} (26°C)	3.67×10^{-3} (26°C)	4.82×10^{-3} (26°C)
2nd day (79% R.H.)	2.36×10^{-3} (26°C)	4.84×10^{-3} (27°C)	4.45×10^{-3} (26°C)
3rd day (70% R.H.)	~	4.64×10^{-3} (23°C)	3.69×10^{-3} (23°C)
4th day (71% R.H.)	2.16×10^{-3} (26°C)	~	~
30th day (75% R.H.)	1.19×10^{-3} (26°C)	4.33×10^{-3} (26°C)	3.21×10^{-3} (26°C)

Table II

Sorption Coefficients of H_2O in Nitrate Doped PPBT Film After Several Days (before correction).

	$Fe(NO_3)_3 \cdot 9H_2O$	$Ni(NO_3)_2 \cdot 6H_2O$			$CaCl_2$
		$Co(NO_3)_2 \cdot 6H_2O$		LiCl	
1st day (79% R.H.)	2.48×10^{-3} (26°C)	4.51×10^{-3} (26°C)	5.31×10^{-3} (26°C)	2.425×10^{-3} (26°C)	2.25×10^{-3} (26°C)
2nd day (79% R.H.)	2.39×10^{-3} (26°C)	5.32×10^{-3} (27°C)	4.95×10^{-3} (26°C)	∿	∿
3rd day (70% R.H.)	∿	5.71×10^{-3} (28°C)	3.69×10^{-3} (23°C)	∿	∿
4th day (71% R.H.)	2.24×10^{-3} (26°C)	∿	∿	∿	∿
30th day (75% R.H.)	2.84×10^{-3} (26°C)	5.13×10^{-3} (26°C)	4.23×10^{-3} (26°C)	∿	∿

Table III

Sorption Coefficients of H_2O Diffusion for Salt Doped PBLG Film after Several Days (after Correction).

	Fe	Co	Ni
1st day	2.55×10^{-9}	1.15×10^{-9}	1.30×10^{-9}
2nd day	1.56×10^{-9}	1.03×10^{-9}	1.65×10^{-9}
3rd day	∿	1.15×10^{-9}	1.62×10^{-9}
4th day	1.72×10^{-9}	∿	∿
30th day	9×10^{-10}	6.4×10^{-10}	9.7×10^{-10}

Table IV

Diffusion Coefficients (cm^2/s) of Water in Nitrate Doped PPBT Film After Several Days.

	Fe	Co	Ni
Pure dry Sample before doped (mg)	6.86	7.11	6.85
1st day doped (mg)	6.901	7.16	6.90
2nd day doped (mg)	6.88	7.16	6.90
3rd day doped (mg)	∿	7.16	6.88
4th day doped (mg)	6.86	∿	∿
30th day doped (mg)	6.82	7.11	6.84

Table V

Weight (mg) of PPBT Film Measured Before and After Doping for Several Days of Drying.

consist of smaller "microfibrils" of lateral dimensions varying from 50 to 80 Å. (Figure (51)). A schematic of the texture of these kinked ribbons is proposed in Figure (52). Each microfibril consists of a succession of narrow crystallites (50 x 500 Å or smaller) embedded in somewhat less ordered matrix. The periodicity of the banding varies from 1000 to 2000 Å. At present, they still do not know whether the bands that appear are due to the fragmentation of the fibers during the sample preparation, or on the contrary, are characteristic of the as-spun fibers.

Based on above, Barker proposed that microvoids might exist between microfibrils as suggested by Figure (53.a.). Then the parallel diffusion will be much larger than transverse diffusion. If the voids are only a few Å width, the longitudinal diffusion, parallel to the axis of microfibrils, and the activation energy for a jump x is approximately proportional to a quantum χ of the order,

$$\chi \approx \sigma^* \rho^* / \lambda^2$$

From equation $D_{//} = g\bar{L}^2 \nu_0$, we have, as a first approximation

$$D = \nu_0 \lambda^2 = \nu_0 \left(\int_0^\infty \lambda^2 e^{-x/RT_{dx}} \right) / \left(\int_0^\infty e^{-x/RT_{dx}} \right)$$

$$= \nu_0 (RT)^2 / \chi^2$$

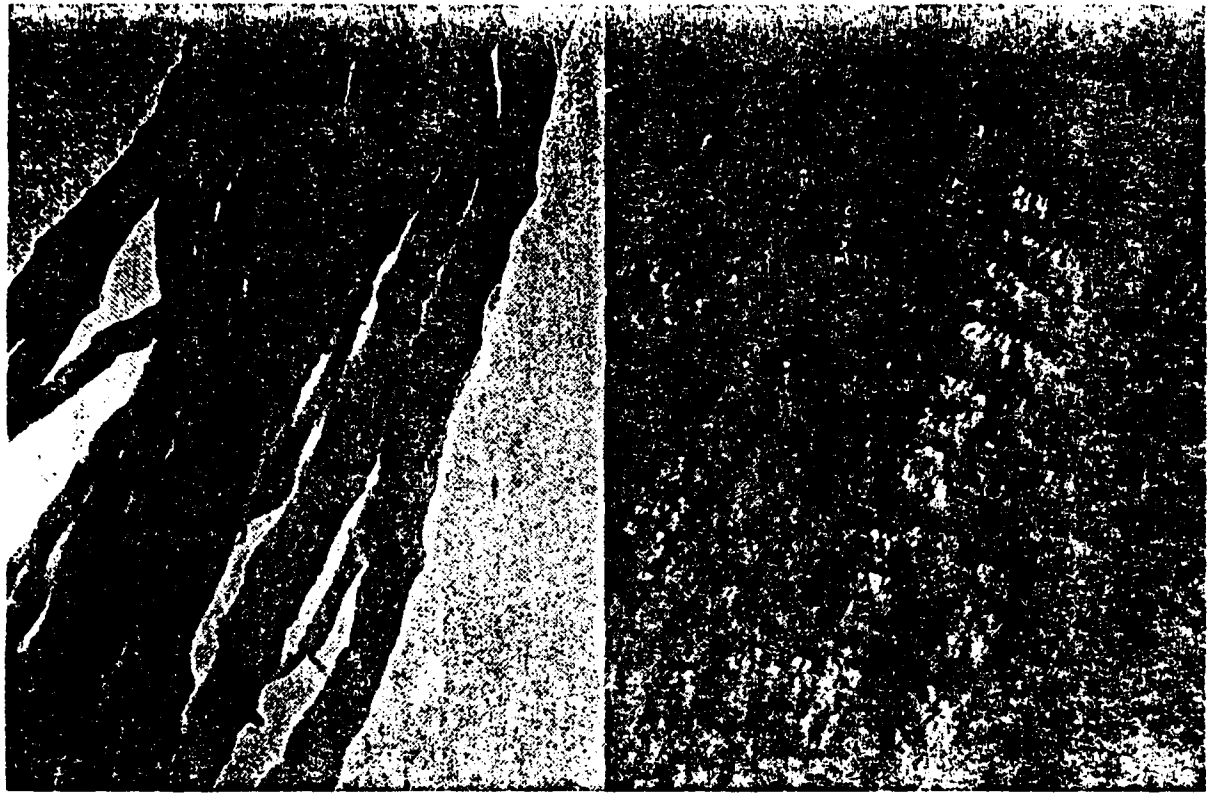

·5 μm

Figure 5.1 BF (left) and DF (right) images of ribbon-like fragments of a PbT fiber showing the fibrillar texture of the ribbons.[2]

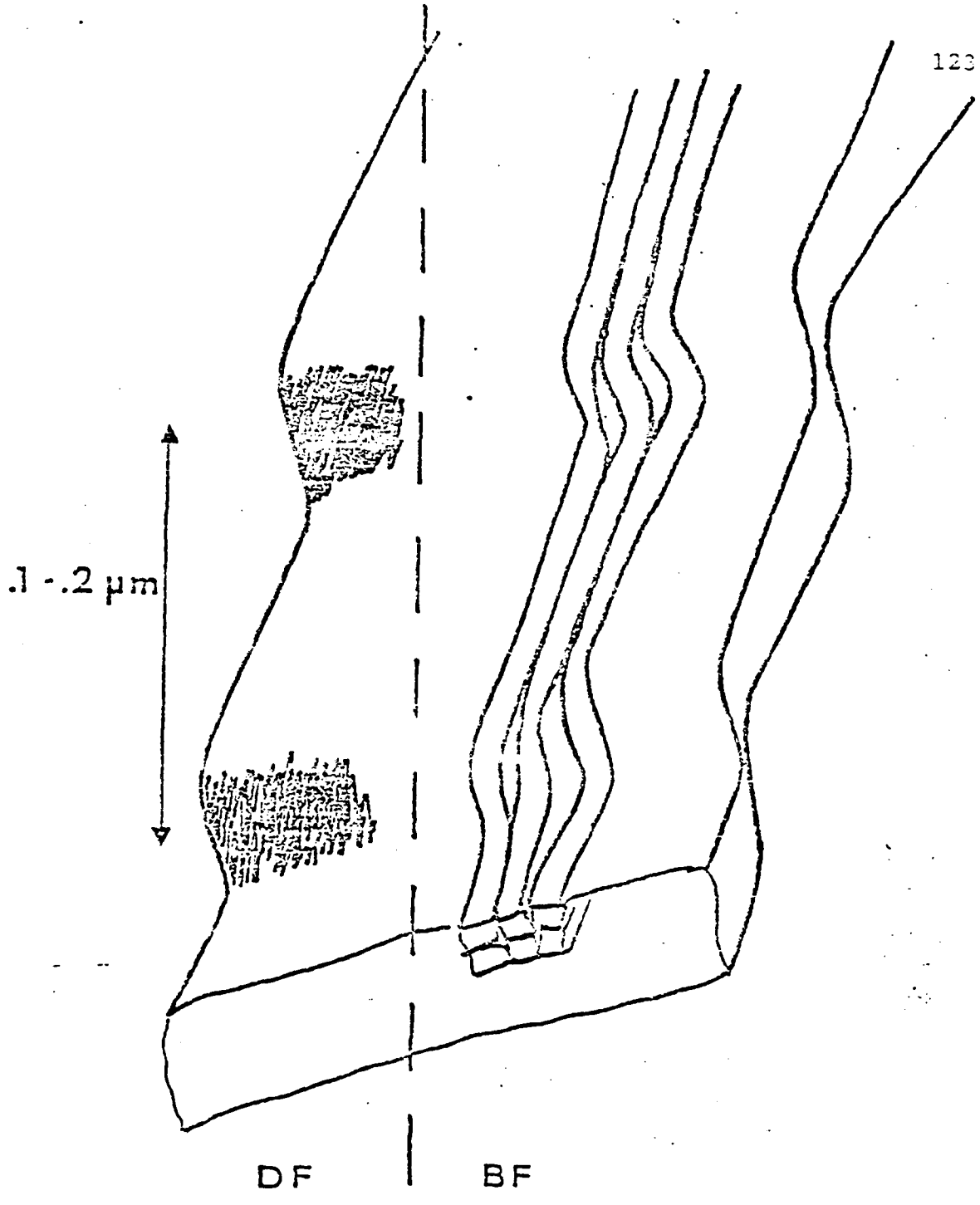

Figure 52 Schematic of the fibrillar structure of the ribbon-like fragments obtained after peeling and mild sonication of PBT fibers.[2]

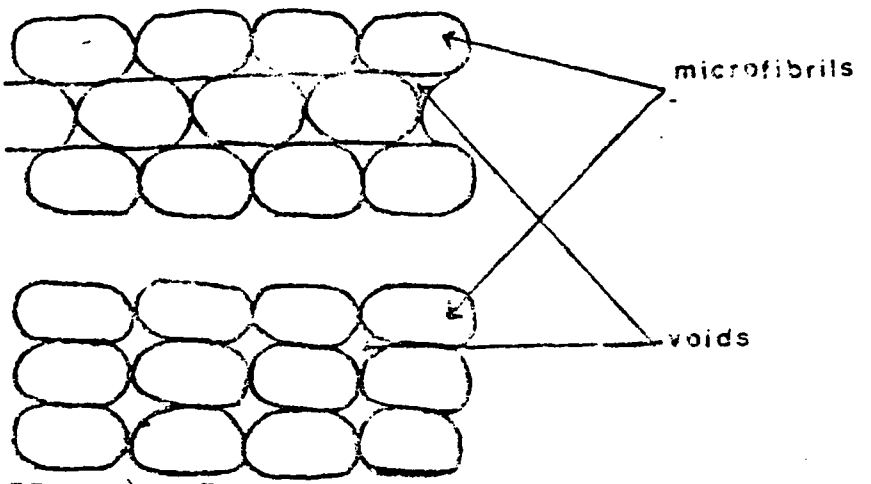

Fig. (53. a.) Proposed stacking forms of microfibrils with voids in intervals.

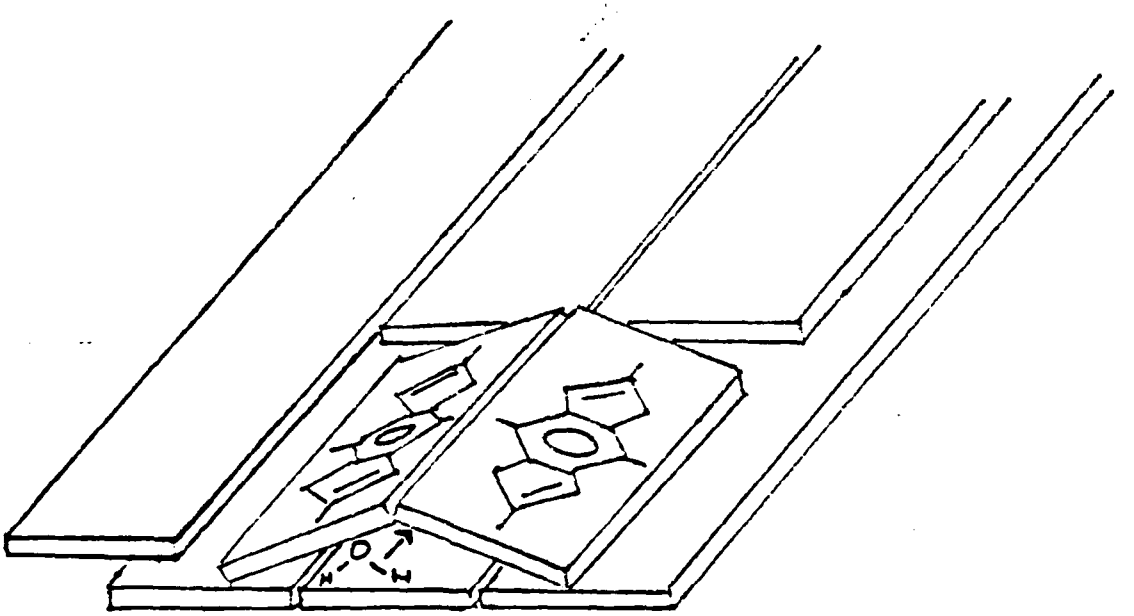

Figure (53. b.) Proposed mechanism of Parallel diffusion with rotation of chain segments.

Insert some assumed values to above equation, (See appendix E)

$$\lambda \sim 1.235\ \text{Å}, \qquad \varepsilon^* \sim 1645\ \text{Jmol}^{-1}$$

$$\rho^* \sim 4.8\ \text{Å}, \qquad \nu_0 = 10^{12}\ \text{sec}^{-1}$$

it gives the result $D_{//} \sim 2 \times 10^{-5}\ \text{cm}^2/\text{s}$ or the order $\sim 10^{-5}\ \text{cm}^2/\text{s}$ at temperature 300°K. If the microvoid is much bigger than a few angstroms; diffusion rate will approach to gas diffusion in air, for example, water vapor is $D \sim 0.239\ \text{cm}^2/\text{s}$ at 8°C.

The microvoids might not exist if, instead of voids, the intervals were filled with less ordered matrix. In this case, $D_{//}$ could be only a few times greater than $D_{\perp}$. Actually the present available PPBT samples were demonstrated to have lots of microvoids of large sizes: (163 ± 10 Å 135 ± 11 Å for heat treated film and 49.1 ± 3.5 Å x 34.7 ± 2.5 Å for heat treated fiber) as mentioned in section one in this chapter. Despite this fact, it is still interesting to extend the theoretical approach.

To simplify the question, we assume the PPBT is 100% crystalline. Then diffusion occurs only when the diffusant can penetrate into the crystal. Under this assumption, the approach in section 2. of this chapter can be applied to the calculation of the ratio $D_{//}/D_{\perp}$. The proposed parallel

diffusion mechanism is displayed in Figure (53.b.). Recall from equations (44) and (45), the A value should be the same for both cases. Thus

$$D_{//} / D_{\perp} = \bar{L}_{//}^2 / \bar{L}_{\perp}^2 \exp(-(\Delta E_{//} - \Delta E_{\perp})/RT)$$

$\bar{L}_{\perp}$ is between 3.5 and 6.1 Å and $\bar{L}_{//}$ is half of the value 12.35 Å, because the rotating segment will be either the phenyl group or the benzobisthiazole group.

Assume $\bar{L}_{\perp}$ is 3.5 Å, $\bar{L}_{//}$ is 6.18 Å,

if $\Delta E_{//} - \Delta E_{\perp} = -4$ kcal/mol,

then $D_{//} / D_{\perp} \sim 2.67 \times 10^3$.

If $\Delta E_{//} - \Delta E_{\perp} = 0$ kcal/mol,

then $D_{//} / D_{\perp} \sim 3.1$.

From above, it is easy to see that $D_{//} / D_{\perp}$ is mainly dependent on the difference between $\Delta E_{//}$ and $\Delta E_{\perp}$.

Before ending this chapter, I would like to point out that the viscosity-diameter of a diffusant is usually large. For example, O_2 has a d-value 3.5 Å.[21] Therefore, it is impossible to accommodate a diffusant without further bending after rotation. The discussion in section 2. of this chapter was based on molecular shape. Also, the protonated PPBT will have some tilt angle on its chain segments, which is not shown on our Figure (53.b.) and our discussion has not dealt with that for the purpose of

simplicity. Finally, in the case of steric hindrance between chain segments, the arrangement might not parallel as Figure (53.b.) and (33) as shown. If this is the case, the model presented here would require only slight modifications.

Chapter V CONCLUSION

It is proposed that the existence of microcavities in PPBT, lead to the measured diffusion rates which were smaller than the true values. The evidence for the micro-void model are: 1. There is an abnormally high heat of sorption (solution). 2. There is a lower water solubility when exposed to water in air than when exposed after being in a vacuum. 3. The diffusion rates are concentration dependent. These phenomenon fully consistent with the dual sorption theory.

The expected high activation energies were not found. This is thought to be due to the rotation or partial rotation of chain segments on the mer. Statistical mechanical model of Pace etc. is a powerful tool for predicting activation energy with its direct calculation using non-adjustable parameters. It would be worthwhile to make detailed theoretical calculations if enough precise data were available.

The sigmoid shape of sorption and desorption curves and negative value of $\log D_0$ in the case of water diffusion are typical of polymers below their glass transition temperature. Actually the PPBT is in crystalline state.

The diffusion rates of H_2O in salt doped PPBT are linearly proportional to q/r. This effect is consistent

with the idea that the cations act as traping sites by attracting water with an electrical field.

The evidence that doping salt is deposited mainly in microvoids are: 1. D at q/r = 0 has the value close to that of pure PPBT measured subsequently to being in the vacuum chamber. 2. The sorption coefficients of H_2O in $Co(NO_3)_2$ and in $Ni(NO_3)_2$ doped PPBT are approximately equal to the value measured of pure PPBT in the vacuum chamber method. Interactions between doping salt and PPBT are not conclusive but significant changes in the diffusion curves and solubilities are obvious after a long time with the salt in polymer.

REFERENCES

1. Barker, R. E. Jr., Tsai, R. C., and R. A. Willeney, J. Polymer Sci, Polym Symp. 63, 109 (1978).

2. Thomas, E. L., Farris, R. J., and Hsu, S. L., Technical Report, AFWAL-TR-80-4045, 2, May (1980).

3. Barker, R. E., Jr., and Chen, D. Y., Electrical Conduction of Anisotropic Poly (Paraphenylene-Benzobisthiazole), Submitted for Publication.

4. Malhotra, M. L., Reynolds, C. L. Jr., and Barker, R. E. Jr., The Journal of Chemical Physics, Vol. 60, No. 10, 15, May (1974).

5. Crank, J., and Park, S., Diffusion in Polymers, Academic Press, N. Y. (1968).

6. Frisch, J. L., J. Phys. Chem., Wash. 61, 93 (1957).

7. Garrett, T. A., M. Sc. Thesis, University of Wales, (1965).

8. Baughan, E. C., Trans, Faraday Soc., 44, 495 (1948).

9. Carpenter, A. S., and Twiss, D. E., Ind. Engng Chem., Analyt, Edn. 12, 99 (1940).

10. Barker, R. E. Jr., Journal of Polymer Science, Vol. 58, 553-570 (1962).

11. Hermans, J. J., J. Colloid Sci., 2, 387 (1947).

12. Reisfeld, R., Glasner, A., and Honigbaum, A., The Journal of Chemical Physics, Vol 42, No 6, 15, 1892, March (1965).

13. Crank, J., Mathematics of Diffusion, Oxford University Press, (1956).

14. Prager, S., and Long, F. A., J. Am. Chem. Soc., 73, 4072 (1951).

15. Blyholder, G., and Prager, S., J. Phys. Chem., 64, 702 (1960).

16. Van Amerongen, G. J., Rubb. Chem. Technol., 37, 1065 (1964).

17. Michaels, A. S., and Bixler, H. J., J. Polym. Sci., 50, 393 (1961).

18. Barker, R. E. Jr., Tsai, R. C., and Willency, R. A., Journal of Polymer Science, Polymer Symposium, 63, 109-129 (1978).

19. Michaels, A. S., Vieth, W. R., and Barrie, J. A., J. Appl. Phys., 34, 13 (1963).

20. DiBenedetto, A. T., and Paul, D. R., J. Polymer Sci., A, 2, 1001 (1964).

21. Pace, R. J., and Datyner, A., Journal of Polymer Science, Polymer Physics, Vol. 17, 437-476 (1979).

22. Pace, R. J., and Datyner, A., Polymer Engineering and Science, Vol. 20, No 1, 51, Mid-January (1980).

23. Cohen, M. H., and Turnvull, D., J. Chem. Phys., 31, 1164 (1959).

24. Barrer, R. M., J. Phys. Chem., Wash., 61, 178 (1957).

25. Glasstone, S., Laidler, K. H., and Eyring, H., Theory of Rate Process, McGraw-Hill, N.Y., 516 (1941).

26. Hopfenberg, H. B., Permeability of Plastic Films and Coatings to Gases, Vapors, and Liquids, Plenum Press, N. Y., 49 (1974).

27. Barker, R. E. Jr., Pure and Appl. Chem., Pergmon Press, 46, 157, (1976).

28. Barker, R. E., and Sharbaugh, A. H., J. Polym. Sci., C10, 139 (1965).

29. Schultz, J. M., Polymer Materials Science, Prentice-Hall, Inc., N. J., (1974).

30. Price, B. J., American Laboratory, 66, August (1981).

31. Benson, S. A., Severson, A. L., and Beckering, W., 120, American Laboratory, 120, November (1980).

32. Meyer, G. M., American Laboratory, 120, November 1980.

33. Trent, R. L., Energy Dispersive X-ray Spectroscopic Analysis of Thin Crystalline Films, Thesis, University of Virginia, 47, (1972).

34. Drummond, W. E., and Stewart, W. D., American Laboratory, 72, November, (1980).

35. DRTEC 7000 Series Si(Li) X-ray Detector Operating and Service Manual, (1970).

36. Instruction Manual #3124-1 for 200-1 Cahn Electrobalance.

37. Farris, R. J., R&D Status for March 1, 1981 - May 31, 1981. Mechanical Properties vs. Morphology of Ordered Polymers, Contract No. F33615-78-C-5175.

38. Fujita, H., Text Res. J. 22, 195, 282, 823, (1952).

39. Newns, A. C., Trans. Faraday Soc., 52, 1533. (1956).

40. King, G., Trans Faraday Soc., 41, 325, (1945).

41. Long, F. A., and Thompson, L. J., J. Polym. Sci., 15, 413, (1955).

42. Takamatsu, T., Hashiyama, M., and Eisenberg, A., Journal of Applied Polymer Science, Vol. 24, 2199-2220, (1979).

43. Purcell, K. F., and Kotz, J. C., Inorganic Chemistry, 1977, 793.

44. Tsai, R. C., Permeation in Macromolecular Systems, Thesis, University of Virginia, 11, August, (1973).

45. J. Composite Materials, Vol. 10, 21.

46. Small, P. A., J. Appl. Chem., 3, 71, (1953).

APPENDIX A. ERROR FUNCTION SOLUTION TO DIFFUSION EQUATION

The equation of linear flow mass is

$$D\partial^2 C/\partial x^2 = \partial C/\partial t \tag{79}$$

Consider the expression

$$C = t^{-\frac{1}{2}} e^{-x^2/4Dt} \tag{80}$$

Since

$$\partial C/\partial t = -(1/2t^{3/2})e^{-x^2/4Dt} + (x^2/4Dt^{5/2})e^{-x^2/4Dt}$$

and

$$\partial^2 C/\partial x^2 = -(1/2Dt^{3/2})e^{-x^2/4Dt} + (x^2/4D^2t^{5/2})e^{-x^2/4Dt}$$

It follows that equation (80) is a particular solution of euqation (79).

Clearly, further solutions of equation (79) are obtained by differentialing, or in some cases by intergrating, equation (80) with respect to either x or t. So, that equation (79) is satisfied by

$$\int_0^x t^{-\frac{1}{2}} e^{-x^2/4Dt} dx = 2D^{\frac{1}{2}} \int_0^{x/2(Dt)^{\frac{1}{2}}} e^{-\zeta^2} d\zeta$$

The notation

$$\text{erf } x = (2/\sqrt{\pi}) \int_0^x e^{-\zeta^2} d\zeta$$

will always be used here, so we have just shown that

$$A \text{ erf}(x/2\sqrt{Dt})$$

where A is an arbitrary constant, is a solution of equation (79).

Because $D\partial^2 C/\partial x^2 = \partial C/\partial t$ is a second order partial differential equation in x, the solution can be expressed as

$$C(x,t) = A \text{ erf}(x/2\sqrt{Dt}) + 1x + m \qquad (81)$$

Now, the boundary conditions are introduced to the equation as below:

$$C(x,t) = C_s, \qquad x = 0 \text{ for all } t,$$

$$C(x,t) = C_i, \qquad x > 0, \; t = 0.$$

According to the boundary conditions above, when t = 0, x= 0, C(x,t) is a constant. So, the constant 1 should be equal to zero, then equation (81) becomes

$$c(x,t) = A \text{ erf}(x/2\sqrt{Dt}) + m \qquad (82)$$

Because

$$\text{erf}(0) = 0, \qquad \text{erf}(\infty) = 1$$

by applying the boundary conditions to equation (82), we have

$$m = C_s$$

$$A + m = C_i$$

Consequently

$$A = C_i - C_s$$

Therefore

$$C(x,t) = (C_i - C_s)\text{erf}(x/2\sqrt{Dt}) + C_s$$

$$= C_i \text{ erf}(x/2\sqrt{Dt}) + C_s(1 - \text{erf}(x/2\sqrt{Dt})$$

$$= C_i \text{ erf}(x/2\sqrt{Dt}) + C_s \text{ erfc}(x/2\sqrt{Dt})$$

APPENDIX B THE SOLUTION TO DIFFUSION EQUATION WITH INHOMOGENEOUS BOUNDARY CONDITIONS

The boundary conditions are as below:[44]

$$C(x,t) = C_1 \quad \text{at } x = 0, \text{ all } t > 0$$

$$C(x,t) = C_2 \quad \text{at } x = b, \text{ all } t > 0 \tag{83}$$

$$C(x,t) = C_0 \quad \text{at } 0 < x < b, \text{ at } t = 0$$

where b is the thickness of polymer membrane, C_1 and C_2 are the concentrations of gases just inside the polymer surfaces and C_0 is the initial concentration of diffusant, assumed uniformly distributed.

In order to solve the equation, one new concentration variable U(x,t) is introduced, i.e.

$$U(x,t) = C(x,t) + \Omega(x)$$

$\Omega(x)$ is a first order linear function of x, because the equation $\partial^2\Omega(x)/\partial x^2 = 0$ must be satisfied for our purpose of solving the equation. It is defined as $\Omega(x) = \alpha x + \beta$. Now, the new boundary conditions are set as:

$$U(x,t) = 0, \text{ at } x = 0 \text{ for all } t$$

$$U(x,t) = 0, \text{ at } x = b \text{ for } t = 0 \tag{84}$$

$$U(x,t) = C_0 + \Omega(x), \text{ at } 0 < x < b, \text{ at } t = 0$$

Fick's second law becomes:

$$\partial U(x,t)/\partial t = D((\partial^2 U(x,t)/\partial x^2) + (\partial^2 \Omega(x)/\partial x^2))$$

$$= D(\partial^2 U(x,t)/\partial x^2)$$

Here $U(x,t) = C(x,t) + \Omega(x)$ must satisfy the boundary condition (84). That is

$$\text{at } x = 0,\ C_1 + \beta = 0, \text{ then } \beta = -C_1$$

$$\text{at } x = b,\ C_2 + \alpha b + \beta = 0, \text{ then } \alpha = (C_1 - C_2)/b$$

Therefore,

$$U(x,t) = C(x,t) + ((C_1 - C_2)/b)x - C_1$$

i.e.

$$C(x,t) = U(x,t) + C_1 - ((C_1 - C_2)/b)x \tag{85}$$

We begin our attack on the problem by attempting to find solutions of the diffusion equation that are of the special form

$$U(x,t) = X(x)T(t) \tag{86}$$

We impose the requirements

$$X(0) = 0,\ X(b) = 0$$

in order that these "product solutions" will also satisfy the boundary conditions

$$U(0,t) = U(b,t) = 0 \tag{87}$$

If the diffusion equation has a solution of the form (86), then we must have

$$X(x)T'(t) = DX''(x)T(t)$$

or upon dividing through by $DX(x)T(t)$

$$X''(x)/X(x) = -T'(t)/DT(t)$$

The left hand side of this equation is independent of t while the right is independent of x. Therefore, both members must be equal to a constant, which we denote by $-\lambda$, thus

$$X''(x)/X(x) = -T'(t)/DT(t) = -\lambda$$

and so the function X and T must be solutions of the ordinary differential equations

$$X'' + \lambda x = 0, \quad T' + \lambda DT = 0$$

respectively. Conversely, if X and T are solutions of the corresponding equations for the same value of λ, then the product $U(x,t) = X(x)T(t)$ is a solution of the diffusion equation because

$$\begin{aligned} U_t(x,t) - DU_{xx}(x,t) &= X(x)T'(t) - DX''(x)T(t) \\ &= X(x)(-\lambda DT(t)) - D(-\lambda X(x))T(t) \\ &= 0 \end{aligned}$$

The requirements for X, namely

$$X'' + \lambda X = 0, \quad X(0) = 0, \quad X(b) = 0$$

constitute an eigen value problem. The eigen values are

$$\lambda_n = (n\pi/b)^2 \qquad n = 1,2,3,...$$

The corresponding eigenfunctions (non trivial solutions) are

$$X_n = \sin(n\pi x/b) \qquad n = 1,2,3,...$$

For $\lambda = \lambda_n$, we have $T' + \lambda_n t = 0$. A solution is

$$\begin{aligned} T_n(t) &= \exp(-\lambda_n Dt) \\ &= \exp(-n^2\pi^2 Dt/b^2) \end{aligned}$$

Each of the product functions

$$U_n(x,t) = \exp(-n^2\pi^2 Dt/b^2)\sin(n\pi x/b), \qquad n = 1,2,3,...$$

is a solution of the diffusion equation and satisfies the boundary conditions (87). If the constant C_n are such that the series

$$u(x,t) = \sum_{n=1}^{\infty} C_n U_n(x,t)$$

$$= \sum_{n=1}^{\infty} C_n \exp(-n^2\pi^2 Dt/b^2)\sin(n\pi x/b) \qquad (88)$$

converges and can be differentiated termwise a sufficient number of times with respect to x and t, then this series also represents a solution of the differential equation that satisfies the homogeneous boundary conditions (87).

However, the constants C_n must be chosen, if possible, in such a way that the series (88) satisfies the non-homogeneous boundary condition

$$U(x,0) = f(x), \qquad 0 < x < b$$

Thus, we require that

$$U(x,0) = \sum_{n=1}^{\infty} C_n \sin(n\pi x/b)$$

$$= f(x) \qquad 0 < x < b$$

But the C_n must be the nth coefficient in the Fouriersine series for f, that is

$$C_n = (2/b)\int_0^b f(x)\sin(n\pi x/b)\,dx \tag{89}$$

Here, $f(x) = C_0 + \Omega(x)$

$$= C_0 - C_1 + ((C_1 - C_2)/b)x$$

can be used to find C_n.

From equation (89), we have

$$C_n = (2/b)\int_0^b (C_0 - C_1 + ((C_1 - C_2)/b)x)\sin(n\pi x/b)\,dx$$

$$= (2/b)\int_0^b (C_0 - C_1)\sin(n\pi x/b)\,dx$$

$$+ (2/b)\int_0^b ((C_1 - C_2)/b)x\sin(n\pi x/b)\,dx.$$

From tables, we find

$$\int \sin x\,dx = -\cos x + C$$

$$\int x\sin x\,dx = \sin x - x\cos x + C.$$

Then we have

$$C_n = -(2/n\pi)(C_0 - C_1)\cos(n\pi x/b)\Big|_0^b$$

$$+ (2(C_1 - C_2)/(n\pi)^2)(\sin(n\pi x/b)\Big|_0^b - (n\pi x/b)\cos(n\pi x/b)\Big|_0^b)$$

$$C_n = (2/n\pi)(C_2(-1)^n - C_1) + (2C_0/n\pi)(1 - (-1)^n).$$

The second term above exists, only for n odd. So we can define it as $4C_0/(2n + 1)$, $n = 0,1,2,\ldots$. Then U is the form

$$U(x,t) = (2/\pi)\sum_{n=1}^{\infty}((-1)^n(C_2 - C_1)/n)\sin(n\pi x/b)\exp(-((n\pi)^2/$$

$$b^2)Dt) + (4C_0/\pi)\sum_{n=0}^{\infty}(\sin(((2n+1)/b)\pi x)/$$

$$(2n + 1))\exp(-((2n + 1)^2\pi^2/b^2)Dt)$$

Therefore

$$C(x,t) = C_1 + ((C_2 - C_1)/bx$$

$$+ (2/\pi)\sum_{n=1}^{\infty}((-1)^n C_2 - C_1)/n)\sin(n\pi x/b)e^{-((n\pi)^2/b^2)Dt}$$

$$+ (4C_0/\pi)\sum_{n=0}^{\infty}(\sin((2n + 1)/b)\pi x)/(2n + 1)$$

$$\exp(-(2n + 1)^2\pi^2/b^2)Dt) \qquad (90)$$

The quantity of gas molecules through the membrane to the downstream of the chamber per second is then $dQ/dt = DA(\partial C/\partial x)_{x=0}$ where Q is the total amount of diffusant collected in the downstream reservoir, D is the diffusion coefficient and A is the effective cross section of the membrane normal to the flow direction x.

The total amount of gas collected downstream up to time t is

$$Q_t = AD\int_0^t (\partial C/\partial x)_{x=0} dt$$

$$Q_t/AD = \int_0^t ((C_2 - C_1)/b) + (1/b) \sum_{n=1}^{\infty} ((-1)^n C_2 - C_1) e^{-(n\pi/b)^2 Dt}$$

$$+ (4C_0/b) \sum_{n=0}^{\infty} e^{-((2n+1)^2/b^2)\pi^2)Dt}) dt$$

$$= ((C_2-C_1)/b)t - (2b/D\pi^2) \sum_{n=1}^{\infty} (((-1)^n C_2 - C_1)/n^2$$

$$(1 - e^{-(n\pi/b)^2 Dt}) - (4C_0 b/b\pi^2) \sum_{n=0}^{\infty}$$

$$(1/(2n+1)^2)(1 - e^{-(((2n+1)^2\pi^2)/b^2)Dt}) \qquad (91)$$

Experimental conditions in this work are that both C_0 and C_1 are zero, i.e. the membrane is initially evacuated to zero concentration and the concentration at the face through which diffusing gas molecule emerges is maintained effectively at zero concentration.

Therefore equation (91) becomes

$$Q_t/AD = (C_2/b)t - (2b/D\pi^2) \sum_{n=1}^{\infty} (-1)^n C_2/n^2$$

$$+ (2b/D\pi^2) \sum_{n=1}^{\infty} ((-1)^n C_2/n^2) e^{-D(n\pi)^2 t/b^2}$$

Since

$$\sum_{n=1}^{\infty} (-1)^n/n^2 = \pi^2/12$$

$$Q_t/AC_2b = Dt/b^2 + (2/\pi^2)(\pi^2/12)$$

$$- (2/\pi^2) \sum_{n=1}^{\infty} ((-1)^n/n^2) e^{-D(n\pi/b)^2 t}$$

as t approaches ∞, the exponential term approaches zero, and a linear approximation results,

$$Q_t/A \simeq (C_2D/b)(t - b^2/6D)$$

The intercept of the line Q_t/A vs t with the t axis is called the "time lag."

$$\text{i.e. } \tau = b^2/6D$$

Therefore

$$D = b^2/6\tau$$

If C_0 and C_2 have nonvanishing values, the relation is

$$D = b^2(C_2 + 2C_1 - 3C_0)/6\tau(C_2 - C_1).$$

APPENDIX C MASS UPTAKE FOR UNIFORM SURFACE CONCENTRATION

The boundary conditions are below:

$$C(x,t) = C_1, \quad \text{at } x = 0, \quad \text{all } t > 0$$

$$C(x,t) = C_1, \quad \text{at } x = b, \quad \text{all } t > 0 \tag{92}$$

$$C(x,t) = C_0, \quad \text{at } 0 < x < b, \quad \text{all } t = 0$$

The only difference of these boundary conditions to equation (83) of Appendix B is $C(x,t) = C_1$ at $x = b$. So, the equation (90) of Appendix B can be directly applied to here by changing C_2 to C_1.

We can obtain

$$C(x,t) = C_1 + (2/\pi) \sum_{n=1}^{\infty} (((-1)^n C_1 - C_1)/n) \sin(n\pi x/b)$$

$$e^{-((n\pi)^2/b^2 Dt)} + (4C_0/\pi) \sum_{n=0}^{\infty}$$

$$(\sin(\frac{2n+1}{b})\pi x/(2n+1)) e^{(-((2n+1)^2\pi^2/b^2)Dt)}$$

The second term in above equation can exist only n is odd number. The equation changes to

$$C(x,t) = C_1 + (4/\pi)(C_0 - C_1)\sum_{n=0}^{\infty}(\sin((2n+1)/b)\pi x)/(2n+1)$$

$$\exp(-((2n+1)^2\pi^2/b^2)Dt)$$

by changing n to 2n+1 in the second term and combining with the third term. After rearrangement, the equation becomes

$$(C - C_0)/(C_1 - C_0) = 1 - (4/\pi)\sum_{n=0}^{\infty}(1/(2n+1))$$

$$\exp(-((2n+1)^2\pi^2/b^2)Dt)\sin((2n+1)/b)\pi x \qquad (93)$$

We define it as the amount of diffusant has diffused into the film at time t, and Q as the amount of diffusant at infinite time.

Because $Q = \int_0^b C(x,t)dx$,

equation (93) can be simply integrated on each side to get

$$Q_\infty/(C_1-C_0) = 1 - (4/\pi)\sum_{0}^{\infty}(1/(2n+1))\exp(-((2n+1)^2/b^2)\pi^2Dt)$$

$$\int_0^b \sin((2n+1)/b)\pi x dx \qquad (94)$$

Solve $\int_0^b \sin((2n+1)/b)\pi x\, dx$,

we can get $2b/(2n+1)\pi$

Put this back to equation (94), we obtained

$$Q_t/Q_\infty = 1 - \sum_{n=0}^{\infty}(8/(2n+1)^2\pi^2)\exp(-D((2n+1)^2\pi^2)/b^2)t.$$

APPENDIX D CORRECTION OF EDGE EFFECTS[45]

For a semi-infinite solid ($h > 0$) the boundary conditions become

$$C = C_i,\ 0 < x < \infty,\ t \leq 0$$

$$C = C_m,\ x = 0,\ t > 0$$

So,

$$(C - C_i)/(C_m - C_i) = 1 - \mathrm{erf}(x/2\sqrt{D_x t}) \tag{95}$$

and the weight of moisture which enters or leaves through an area A in time t is

$$m = \int_0^t -AD_x(\partial C/\partial x)_{x=0}\,dt \tag{96}$$

Equation (95) and (96) give

$$m = 2A(C_m - C_i)\sqrt{D_x t/\pi} \tag{97}$$

In the early stages of the process of interaction of the different sides might be neglected and equation (97) can be applied to each side independently. Thus the total weight of entering moisture is

$$m = 4(C_m - C_i)(nl\sqrt{D_x} + nh\sqrt{D_y} + hl\sqrt{D_z})\sqrt{t/\pi}$$

Where D_x, D_y, D_z are the diffusivities in the x, y, z, directions.

Because $C_i = 0$, $W_d = \rho ghnl$, the mass uptake will be

$$M = ((W - W_d)/W_d) \times 100 = (m/W_d) \times 100$$

$$= (4C_m/\rho gh)(\sqrt{D_x} + (h/l)\sqrt{D_y} + (h/n)\sqrt{D_z})\sqrt{t/\pi}$$

$C_m/\rho g$ is the maximum moisture content as in the equation shown below.

$$M_m = ((W_m - W_d)/W_d) \times 100$$

$$= ((m_m/hnl)/(W_d/hnl)) \times 100$$

$$= C_m/\rho g$$

So,

$$M = (4M_m/h\sqrt{\pi})(\sqrt{D_x} + (h/l)\sqrt{D_y} + (h/n)\sqrt{D_z})\sqrt{t}$$

For the linear part in the beginning of a diffusion curve, it can be expressed as

$$M = (4M_m/h)\sqrt{t/\pi}\sqrt{D}$$

then

$$D = D_x(1 + (h/l)\sqrt{D_y/D_x} + (h/n)\sqrt{D_z/D_x})^2 \qquad (98)$$

If the material is homogeneous, $D_x = D_y = D_z$ we obtain

$$D = D_x(1 + (h/l) + (h/n))^2 \tag{99}$$

APPENDIX E ESTIMATION OF PARAMETERS

We assume 10 centers per monomer unit in PPBT, then λ equals 1.235 Å. For ρ^* we choose 4.8 Å which is the average of 6.1 Å and 3.5 Å (two transverse distances between chains). According to Small's[46] suggestion that the cohesive energy density should be an additive property for molecules, similar to the molar refraction or the parachor. δ^2 of PPBT can be estimated as below:

Molecular weight for PPBT monomer: 267

Density: 1.6

1	phenylene (p)	658
1	phenylene (m)	658
2	C ≡ N	820
2	Ring, 5-membered	110
2	Sulfide	450
	ΣG	3146

$\delta = d\Sigma G/M = 1.6 \times 3146/267 = 18.9$

$\delta^2 = 355.4$ cal/cm^3 = 1487J/cm^3

$m^* = 267/10 = 26.7$ dalton

Insert above values into equation

$\varepsilon^* = \lambda^2 m^* \rho^*/(3.88(\text{density})\rho^*)$

We obtain $\varepsilon^* = 1645$J/mole.

Because a molecule ordinarily vibrates about its equilibrium position at a frequency of 10^{12} to 10^{13} vibrations per second, we assume $\nu_0 = 10^{12}$ sec^{-1}. Then

$$\chi = \varepsilon^* \rho^* / \lambda^2 = 1645 \times 4.8 \times 10^{-8} / (1.235 \times 10^{-8})^2$$

$$= 5.177 \times 10^{11} \text{ Jcm/mole}$$

$$D = \nu_0 (RT)^2 / \chi^2 \quad \text{at } 300°K$$

$$= 10^{12} (8.314 \times 300)^2 / (5.177 \times 10^{11})^2$$

$$= 2.32 \times 10^{-5} \text{ cm}^2/\text{s}$$

DISTRIBUTION LIST

Copy No.	
1 - 6	U.S. Air Force Office of Scientific Research Bolling Air Force Base Washington, D.C. 20332 Attention: Mr. Donald R. Ulrich Building 410 NC
7 - 8	E. H. Pancake Clark Hall
9 - 10	R. E. Barker, Jr.
11	W-S. Huang
12	K. R. Lawless
13	SEAS Publications Files

JO# 6625:lsl

UNIVERSITY OF VIRGINIA
School of Engineering and Applied Science

The University of Virginia's School of Engineering and Applied Science has an undergraduate enrollment of approximately 1,450 students with a graduate enrollment of approximately 500. There are 125 faculty members, a majority of whom conduct research in addition to teaching.

Research is an integral part of the educational program and interests parallel academic specialties. These range from the classical engineering departments of Chemical, Civil, Electrical, and Mechanical and Aerospace to departments of Biomedical Engineering, Engineering Science and Systems, Materials Science, Nuclear Engineering and Engineering Physics, and Applied Mathematics and Computer Science. In addition to these departments, there are interdepartmental groups in the areas of Automatic Controls and Applied Mechanics. All departments offer the doctorate; the Biomedical and Materials Science Departments grant only graduate degrees.

The School of Engineering and Applied Science is an integral part of the University (approximately 1,500 full-time faculty with a total enrollment of about 16,000 full-time students), which also has professional schools of Architecture, Law, Medicine, Commerce, Business Administration, and Education. In addition, the College of Arts and Sciences houses departments of Mathematics, Physics, Chemistry and others relevant to the engineering research program. This University community provides opportunities for interdisciplinary work in pursuit of the basic goals of education, research, and public service.

END

FILMED

1-86

DTIC